THE UNIVERSITY
of EDINBURGH

Isomerisation of Palladium π-Allyl Complexes

Ruth Elizabeth Dooley

Doctor of Philosophy

University of Edinburgh

2015

Author's Declaration

I declare that the work in this thesis was carried out with the regulations of the University of Edinburgh. This work is original, except where indicated by reference in the text, and no part has been submitted for any other academic award. Any views expressed in the dissertation are those of the author.

Signed:

Date:

Acknowledgements

Firstly I would like to thank Professor Guy Lloyd-Jones for his help, advice, and patience throughout this work. My thanks also go to Dr Craig Butts for his support and guidance over the first couple of years.

I would also like to acknowledge all past and present members of the Lloyd-Jones group for their valuable input, and for helping to make the last few years an enjoyable experience; Dr Gareth Owen-Smith, Dr Sophie Purser, Dr Alvaro Gordillo, Dr Vincent Brunet, Dr Louise Evans, Dr Alastair Lennox, Dr Liam Ball, Dr Bertram Ong, Dr Daugirdas Racys, Dr Carl Poree, Dr Rob Cox, Dr Alex Creswell, Dr Marc Reid, Joe Tate, Nick Taylor, Jorge Gonzalez Gonzalez, Paul Cox, Tom Corrie, Matt Robinson and Katherine Geogheghan.

I would also like to thank the University of Bristol and University of Edinburgh for funding, and the many people who helped in the smooth running of the department. An extra special thank you belongs to Juraj Bella and Lorna Murray for teaching me how to maintain an NMR spectrometer!

Finally, I would like to my family; Kate, Tony, Andrew, Helen, Esther, Nicola, and Jonathan for their constant support over the final few months.

Lay Summary

Synthetic organic compounds are widely used in the pharmaceutical and agrochemical industries to name a couple of examples. Many of these chemicals are made up of two non-superimposable compounds, of which the chemical and physical properties are identical and they only differ in that they are mirror images. They are known as chiral, and each individual compound is an enantiomer.

Usually when we make a chiral compound, we will make its enantiomer at an identical rate, and as its physical properties are identical, we can't separate them. One case where chiral compounds are found with a high purity for a single enantiomer is in nature. All the enzymes, proteins, carbohydrates in your body exist as a single enantiomer, and so as your left hand does not fit in your right glove, the two enantiomers interact differently with the body. In some cases this is not a problem, for example one enantiomer of ibuprofen is inactive, but in many cases this can cause issues, for example in thalidomide, where one enantiomer is an effective treatment of morning sickness and the other inhibits cell growth. Therefore, to manufacture a drug, we generally need an efficient route to making a single enantiomer.

The palladium catalysed asymmetric allylic alkylation is a carbon-carbon bond forming reaction where we can achieve selectivity for a single enantiomer. We do this by binding a single enantiomer of a chiral organic compound to the palladium to create a 'chiral pocket' for the reaction to take place inside. This particular reaction however, is plagued by unpredictable and sometimes low selectivity. This thesis describes a method to determine why the selectivity for a single enantiomer is poor and with the view of finding a way in which we can improve it. To do this we have used isotopic labelling, where we use palladium and hydrogen of a different mass to track the atoms through the process, and we have utilised techniques such as mass spectroscopy and nuclear magnetic resonance (NMR) spectroscopy to follow the processes.

NMR spectroscopy is a technique whereby we put a nucleus such as hydrogen into a large magnetic field. Hydrogen can act as a small magnet, and so it will be energetically favourable to align with the magnetic field. We then put a small amount of energy in to excite the nucleus and record the signal it emits as it relaxes. The energy of the signal tells us a lot of information about the nucleus and the surrounding environment, and also, if recorded carefully, the number of nuclei in that specific environment; i.e. it is a quantitative technique. The second part of this thesis describes the investigation into the timing and power of the energy we put in, and the effect of these parameters on the accuracy of the data recorded.

Abstract

The palladium-catalysed asymmetric allylic alkylation is a mild and versatile bond forming reaction between a nucleophile and allylic electrophile. The wide scope of nucleophiles used, and the high regio- and stereoselectivity obtainable renders this transformation an important technique in enantioselective synthesis.

The mechanism is known to go via a key palladium π-allyl intermediate, followed by nucleophilic addition occurring at the terminal allylic carbon. Both the formation of the palladium π-allyl, and the nucleophilic addition to generate the alkylated product and palladium(0) proceed with high levels of inversion of stereochemistry, and both provide an opportunity for the induction of stereochemistry. However in the case of ligand controlled nucleophilic addition memory effects have been observed. The epimerisation of the palladium π-allyl before nucleophilic attack is key to achieving high levels of selectivity when racemic starting materials and chiral ligands are employed. Previous work in the Lloyd-Jones group has determined that prolonging the lifetime of the palladium π-allyl species, either by the use of weakly coordinating counter ions or slow addition of the nucleophile reduces this memory effect, however increasing the rate of epimerisation would have a result in a similar effect.

One of the mechanisms resulting in the epimerisation of the palladium π-allyl species is mediated by palladium(0), however the details of the mechanism are not well understood. We describe the synthesis of a diastereotopic palladium cyclohexenyl ester and labelled the complex with ^{108}palladium and d_3 at the cyclohexenyl ester. Using simultaneous ^{31}P NMR and mass spectrometry, we have acquired strong evidence against mechanisms involving a single electron transfer, as proposed by Stille, of formation of a dinuclear palladium(I) species followed by an inversion event, and we have gained evidence supporting the direct nucleophilic addition of the palladium(0), resulting in inversion of stereochemistry. The differences in rates of nucleophilic attack involving monodentate and bidentate phosphine ligands on both the palladium *I*-cyclohexenyl ester have also been explored.

Throughout the mechanistic investigation, it was noted that the ^{31}P NMR spectroscopy experiment used gave non-quantitative results, and in fact the differences in quantification of the species varied with the spectrometer used. We also describe our investigations into where these differences arise from and an optimum set of parameters for quantitative ^{31}P NMR spectroscopy. The conclusions are also applicable to other heternuclear NMR spectroscopic experiments.

Table of Contents

Abbreviations

δ	Chemical shift
°C	Degrees Celsius
Ac	Acetyl
BAr'F	Tetrakis[3,5-bis(trifluoromethyl)phenyl]borate
BINAP	2,2-bis(diphenylphosphino)-1,1-binapthyl
BINAPO	1,1-bi-2-napthylbis(diphenyl)phosphinite
d_1	Relaxation delay
dba	Dibenzylildene acetone
DCM	Dichloromethane
DPPE	diphenylphosphino ethane
ee	Enantiomeric excess
Eq.	Equivalents
ESI	Electrospray ionisation
ESI-MS	Electrospray ionisation – mass spectrometry
Et_2O	Diethyl ether
EtOAc	Ethyl acetate
EtOH	Ethanol
g	Gram
HMDS	Bis(trimethylsilyl)amine
HSQC	Heteronuclear single quantum coherence spectroscopy
Hz	Hertz
IBX	2-iodoxybenzoic acid
J	Coupling constant

k	Rate constant
K	Equilibrium constant
KHMDS	Potassium bis(trimethylsilyl)amide
M	Molar (moles per litre)
Me	Methyl
MeCN	Acetonitrile
mg	Milligram(s)
MHz	Megahertz
mL	Millilitre(s)
mol	Mole(s)
mol%	Mole percent
MS	Mass spectrometry
m/z	Mass-to-charge ratio
NaBAr'F	Sodium tetrakis[3,5-bis(trifluoromethyl)phenyl]borate
nOe	Nuclear Overhauser Effect
MeOH	Methanol
NMO	N-Methylmorpholine N-oxide
NMR	Nuclear Magnetic Resonace
Nu	Nucleophile
PCC	Pyridinium chlorochromate
Ph	Phenyl
ppm	parts per million
rt	Room temperature
SANS	Small angle neutron scattering
T_1	Spin-lattice relaxation

T_2	Spin-spin relaxation
TEMPO	(2,2,6,6-Tetramethylpiperidin-1-yl)oxyl
Tf	Triflate
THF	Tetrahydrofuran
TLC	Thin layer chromatography
TLS	Turnover limiting step
TPAP	Tetrapropylammonium perruthenate
TSL	Trost standard ligand

1 Introduction

1.1 Allylic Alkylation

In 1965, Tsuji and co-workers reported the addition of enolate and malonate nucleophiles to η^3-allyl palladium chloride dimer, **1** to yield alkylated products. This methodology provided a new palladium mediated carbon-carbon bond forming reaction.[1] In 1970, Atkins and co-workers reported an *in situ* formation of the η^3-allylpalladium complex from palladium acetylacetonate, triphenylphosphine and allylic alcohols and esters, subsequent nucleophilic attack with amine or acetylacetone nucleophiles affords the corresponding allylated product, **7**, Scheme 1.[2] In 1973, Trost and co-workers demonstrated that, in the presence of chiral ligands, 1,3-dimethyl-η^3-allylpalladium chloride, **8**, underwent asymmetric attack by the diethyl sodium malonate nucleophile to generate the alkylation product in 24% *ee*.[3] The true potential of the reaction was not realised until 1977, when Trost demonstrated that *cis*-3-acetoxy-5-methoxycarbonylcyclohexene, **10**, underwent alkylation by sodium methyl phenylsulfonyl acetate in the presence of substoichiometric amounts of $(PPh_3)_4Pd$ and chiral ligands, to provide *(R,R)*-**11** in high yields and moderate *ee'*s.

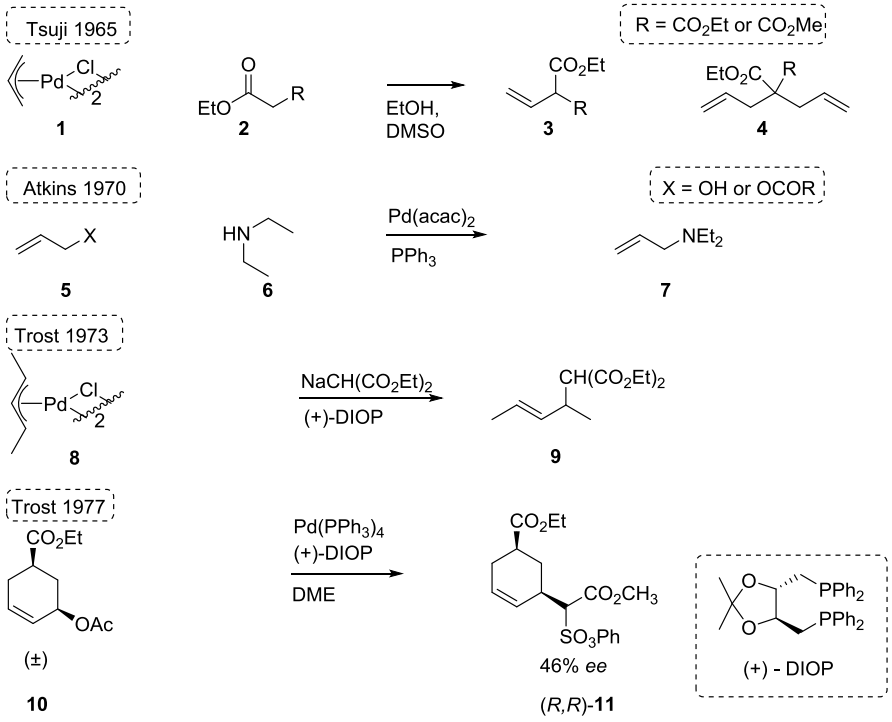

Scheme 1: Palladium mediated alkylation reactions

The mild reaction conditions, remarkable selectivity and potential for stereochemical induction has created wide interest in this methodology. The asymmetric allylic alkylation is of particular interest due to the ability to form bonds to multiple types of atoms, such as C-

C, C-N, C-O, C-S and C-H, and the scope of electrophiles and nucleophiles has been extensively explored. The multiple opportunities for the induction of asymmetry, such as the use of chiral electrophiles or the differentiation of the entantiotopic faces of the prochiral π-allylpalladium complexes, will be discussed in more detail in the proceeding sections.

1.2 Mechanism

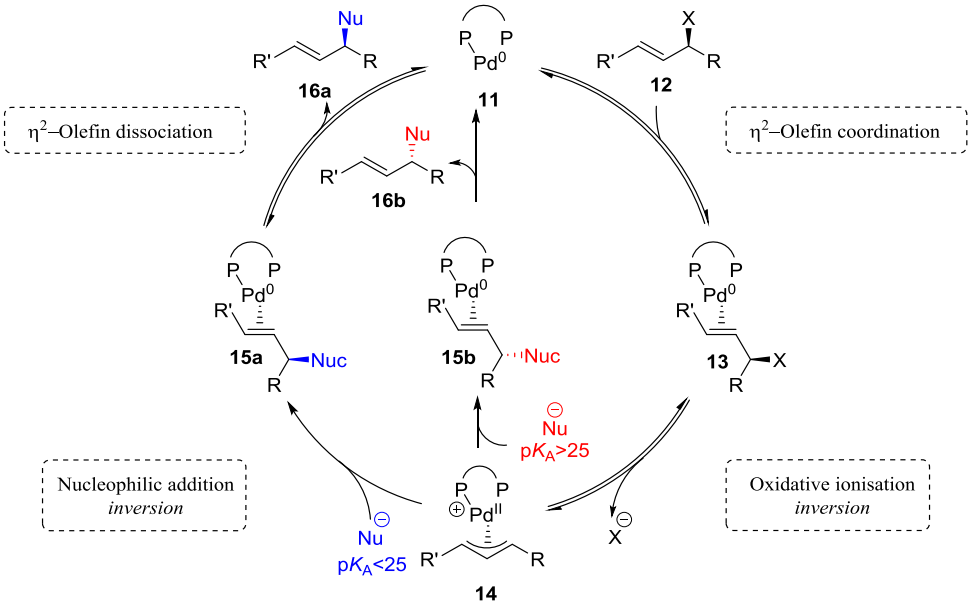

Figure 1: Mechanism of palladium catalysted allylic alkylation. Blue: soft nucleophiles, inversion of stereochemistry. Red: Hard nucleophiles, retention of stereochemistry.

The basic catalytic cycle consists of a η^2-complexation of the olefin to the palladium(0) to yield **13**, followed by oxidative ionisation to yield the key, η^3-allylic palladium(II) intermediate **14**. Nucleophilic attack and olefin dissociations yield the alkylated product **16** and regenerates the palladium(0), thus closing the catalytic cycle. The initial π-complexation of the olefin is reversible; the metal can interconvert between the two π-faces of the olefin. The oxidative ionisation of allylic esters, carbonates and phosphates proceeds with S_N2-like displacement of the nucleofuge, resulting in inversion of stereochemistry.[4] In the nucleophilic addition step, the addition of soft nucleophiles can also be considered as an S_N2-type displacement proceeding with inversion,[5] resulting in an overall retention of stereochemistry throughout the cycle, **16a**, Figure 1. In contrast, when hard nucleophiles are employed, such as aryl- and vinylzinc halides or aryl- and vinyl stannanes, the second step proceeds with retention, resulting in an overall inversion of stereochemistry, **16b**, Figure 1.[4b] This change of

stereochemical outcome is thought to be due to prior coordination of the nucleophile to the palladium, followed by a *syn* reductive elimination of palladium.

Bosnich and co-workers studied the progress of the reaction by ^{31}P NMR and found the π-allyl palladium complex to be the main component of the reaction mixture, rather than the L_2Pd species.[6] They also found the catalytic reaction to be first-order in both nucleophile and catalyst, and zero order with respect to the allyl substrate.[7] These observations are consistent with the nucleophilic addition being the turnover limiting step of the catalytic cycle, and the η^3-allylpalladium complex **14** being the resting state of the catalyst. This mechanism is not consistent with all observations, particularly the presence of a memory effect with some substrates. Lloyd-Jones and co-workers proposed a new mechanism to account for these observations, the details of which will be discussed in later sections.

1.3 The π-Allyl Palladium Intermediate

Many π-allylpalladium(II) complexes are stable in both solution and solid state, their structures have been extensively studied using ^1H and ^{31}P NMR, X-ray crystallography, and their chemical reactivity explored.[8] The π-allylpalladium is a square planar, 16-electron complex with two ligand coordination sites and the η^3 bound allyl unit. X-ray structures indicated the coordinated allyl is positioned at an angle, with the allyl termini facing the palladium. This renders *anti*- substitution unfavourable due to an interaction of the ligands on the palladium with the allyl terminus, however both the *syn* and *anti*-isomers are attainable.[9]

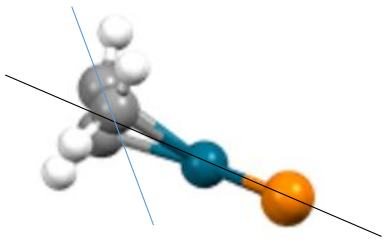

Figure 2: Crystal structure of $[Pd(C_3H_5)(BINAP)](CF_3SO_3)\cdot CH_2Cl_2$. Blue: Pd, Orange: P, Grey: C, White: H. The Pd – P plane highlighted in black is not perpendicular to the C-C-C plane highlighted in Blue. Ligands and counter ion have been omitted for clarity.[10]

Many mechanisms have been proposed that result in the apparent isomerisation of these intermediates in terms of allyl rotation, *syn-anti* exchange or epimerisation at the palladium-

allyl centre. The extent to which each mechanism is operating is determined by the steric hindrance at the allyl, the electronics and sterics of the ligands, and the nature of the counter ion.

1.3.1 η^3-η^1-η^3 Isomerisation

The η^3-bound π-allylpalladium complexes are in equilibrium with the η^1-derivative, the rate of interconversion is increased by more coordinating counter ions such as halides.[11] The consequences of the η^3-η^1- η^3 isomerisation depend on the substitution at the allyl termini, as well as whether the Pd-C or C-C bond rotates. Faller *et al* has found that the rates of the various isomerisation processes are influenced by the substitution at the allyl termini.[12]

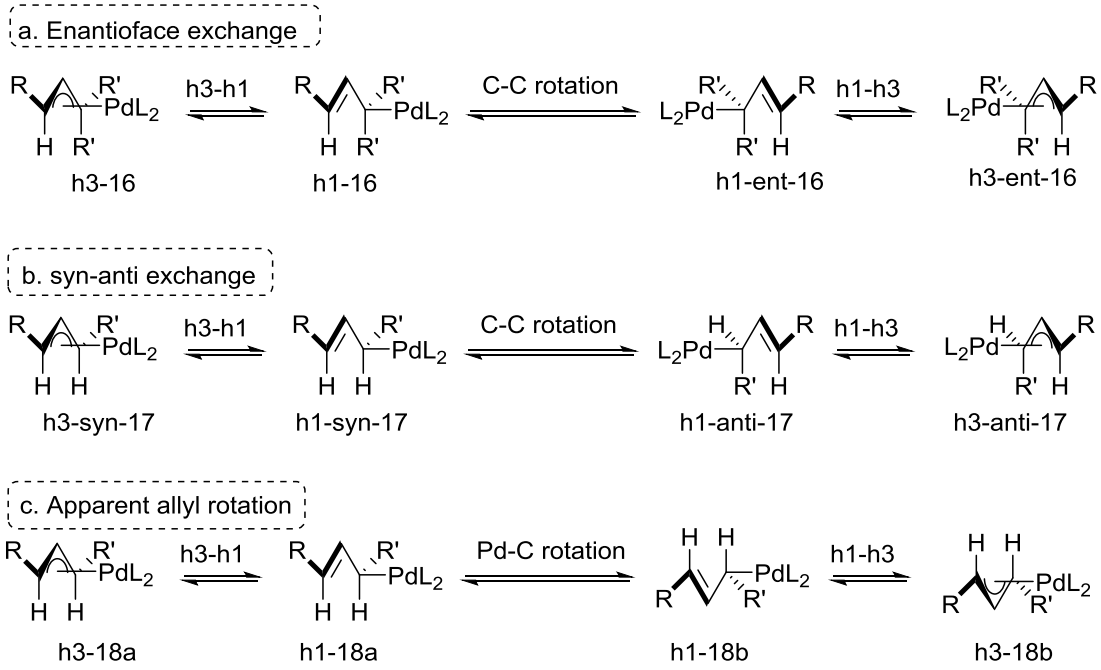

Scheme 2: Mechanisms of isomerisation via an η^1-allylpalladium complex

There are three possible outcomes for the η^3-η^1 isomerisation depending on the substitution about the allyl and which bond rotates. The first example is a 1,1,3-tri substituted allyl where the substituents at one terminus are the same, Scheme 2a. η^3-η^1 isomerisation of η^3-**16** provides η^1-**16**, a rotation by 180° about the carbon-carbon σ-bond, to give η^1-ent-**16**, and η^1-η^3 isomerisation results η^3-ent-**16**. This mechanism of isomerisation has been utilised by Burckhardt and co-workers in the amination of 1,3-diphenylprop-2-enylethyl carbonate, **19**, where the addition of fluoride anions increases the rate of isomerisation, thereby enhancing the stereoselectively, i.e. the reaction is under Curtin-Hammett control.[11c]

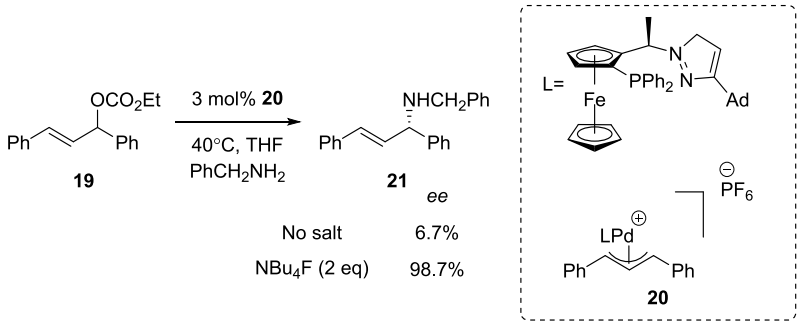

Scheme 3: Addition of coordinating salts increases the rate of isomerisation by an η¹-complex, increasing the ee.

The second example is a 1,2-di substituted allyl, Scheme 2b. η^3-η^1 isomerisation of η^3-*syn*-**17** provides η^1-*syn*-**17**, where one of the substituents at the palladium allyl terminus is hydrogen. A carbon-carbon bond rotation provides η^1-*anti*-**17**, and η^1-η^3 isomerisation results in η^3-*anti*-**17**. This isomerisation determines whether the resulting olefin has *E* or *Z* geometry, nucleophilic addition to η^3-*syn*-**17** will give an *E* alkylation, however η^3-*anti*-**17** with provide the *Z* isomer. The *syn* isomer is generally favoured in solution as the geometry reduces 1,3-allylic strain, and steric interactions between the allyl terminus and ligands on palladium are required to favour the *anti*-isomer, however if the rate of nucleophilic addition is high, the *syn*-*anti* isomerisation is less able to compete, thereby allowing clean conversion to the corresponding products, as demonstrated by Kazmaier and co-workers.[13]

The third example, Scheme 2c is analogous to the previous example, however instead of C-C bond rotation, if the Pd-C bond were to rotate, upon isomerisation back to the η^3-complex we would form η^3-**18b**, an apparent allyl rotation.

1.3.2 Ligand Dissociation

An alternative mechanism that can explain apparent π-allyl rotation is ligand dissociation, followed by a palladium nitrogen bond rotation.[14] Bäckvall and co-workers used the bidentate nitrogen ligand 2,2'-bipyrimidine to provide evidence for the ligand dissociation. Four discrete signals corresponding to H^4, $H^{4'}$, H^6 and $H^{6'}$ are visible by proton NMR at low temperatures; these signals coalesce as the temperature is raised, indicating all four protons are in exchange. This exchange of signals cannot be explained by a simple pseudorotation mechanism, and can only be achieved by partial dissociation and internal rotation of the two pyrimidyl rings with respect to each other; providing unequivocal evidence for ligand dissociation.

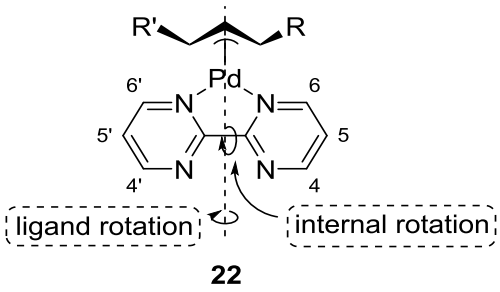

Figure 3: The unsymmetrical bipyrimidyl π-allyl complex used by Bäckvall to confirm ligand dissociation

1.3.3 Pseudorotation of a Pentacoordinate Palladium Intermediate

The rate of allyl rotation (i.e. *syn-syn* to *anti-anti* isomerisation) is increased in the presence of coordinating anions. Akermark and co-workers employed variable temperature and saturation transfer ^{1}H NMR experiments to demonstrate a mechanism that did not involve ligand dissociation. This effect was attributed to the pseudorotation of a pentacoordinate intermediate, promoted by coordinating counterions. When tetrafluoroborate was used as a counterion and a source of silver added to remove all the chloride ions from solution, the rate of allyl rotation was significantly slowed, and the coalescence temperature observed by ^{1}H NMR increased from 200K to 270K. [15]

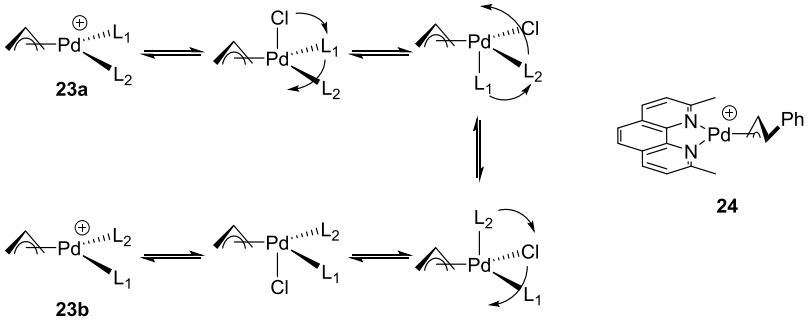

Figure 4: Pseudorotation of a generic pentacoordinate palladium complex

The observation that chloride ions increases the rate of apparent allyl rotation was also reported by Faller[12] in the η^{1}-mechanism. However, Akermark found that the *syn-anti* isomerisation was not observed by saturation transfer experiments of complex **24**, even with the chloride anion present. This observation suggests that, as well as the mechanism proceeding via the η^{1}-complex, there is an additional mechanism responsible for allyl rotation present in these systems.

1.3.4 Nucleophilic Attack of Palladium(0)

The isomerisation of π-allylpalladium complexes facilitated by palladium(0) was first proposed by Tsuji and Bosnich in 1984[16] and 1985[7] respectively. Bäckvall and co-workers studied the palladium(0) mediated isomerisation in more detail to provide more mechanistic details. The addition of $(PPh_3)_4Pd$ to the diastereomerically pure (methoxycarbonyl-cyclohexenyl)palladium(II) complex **26** results in the *cis-trans* isomerisation of the allyl, the rate of which was followed by ^{31}P and ^{1}H NMR. The rate of isomerisation was fitted to a second order equilibrium kinetic profile, first-order in both the palladium(II) complex, and nominally the $(PPh_3)_4Pd$. An excess of phosphine was shown to inhibit the isomerisation, as did the use of the bidentate phosphine dppe. The isomerisation was shown to occur at relatively high rates in THF, chloroform, acetone or acetonitrile, and more slowly in benzene.

The isomerisation was proposed to proceed via nucleophilic displacement of palladium(0) by a bis or tris-ligated palladium(0) species, occurring at the rear face of the allyl, and hence proceeding with inversion. Bäckvall suggested that the addition of triphenylphosphine shifts the equilibrium of ligation of the palladium(0) towards more heavily ligated species, however no suggestion was offered for the inhibiting effect of dppe.[17] Triflate was employed as a counterion to minimise isomerisation *via* the mechanisms discussed in the previous section.

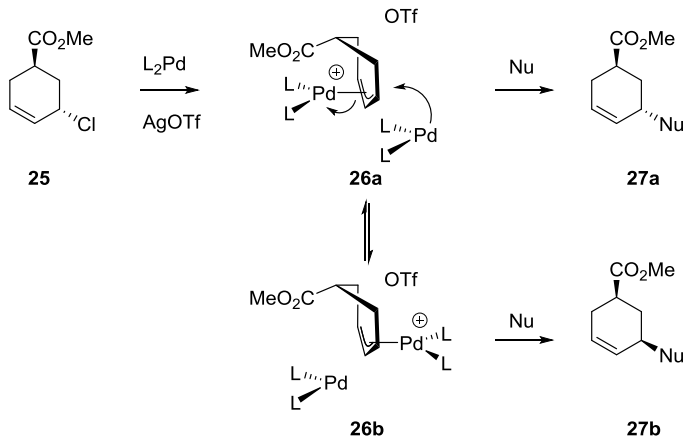

Scheme 4: Palladium(0) catalysed isomerisation

1.4 Methods of Asymmetric Induction

Both the oxidative ionisation and the nucleophilic addition steps proceed with inversion of stereochemistry with high levels of selectivity. The vast majority of the literature employs

chiral ligands, anions or nucleophiles to induce selectivity from two rapidly epimerising isomeric palladium(II) allyl intermediates.

1.4.1 Ionisation of an Enantiotopic Allylic Substrate

This method of enantiocontrol retains the stereospecificity of a chiral allyl unit throughout the mechanism. Fiaud and co-workers utilised this approach with the allylic alkylation of *trans*-4-t-butyl-1-vinylcyclohexyl benzoates, **28**, where the enantiomeric excess of the product is determined by the stereochemistry of the resulting olefin.[18] They found an effect of both solvent and nucleofuge on the resulting geometry. Ethereal solvents such as dimethyl ether, and electron donating benzoates provided the best enantioselectivites, with *para*-methoxybenzoate giving 90% ee in dioxane.

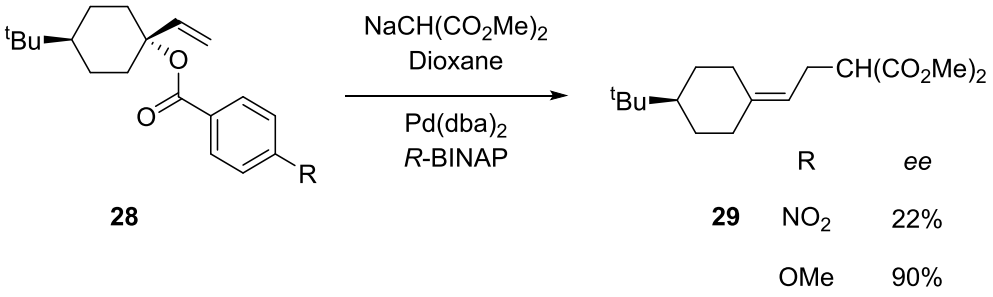

Figure 5: Leaving groups with electron donating groups in the para position give higher ee's than electron withdrawing groups.

Pfaltz and co-workers demonstrated this technique with the alkylation of enantiomerically enriched 1-tolyl-3-phenyl allylic acetate, **30**.[19] Differentiation between the two ends of the allyl distinguishes between regioselective nucleophilic attack and enantiofacial exchange of the palladium allyl. The enantiomeric excess of the resulting olefin provides an indication of the level of enantiofacial exchange of the palladium π-allyl intermediate, while the regiochemistry is determined by of the site of nucleophilic substitution. The regioselectivity was determined by the enantiomer of ligand **33** used. Even when triphenylphosphine was employed as a ligand and the regioselectivity was close to 1:1, no degradation in *ee* was observed indicating there was no enantiofacial exchange of the π-allylpalladium intermediate.

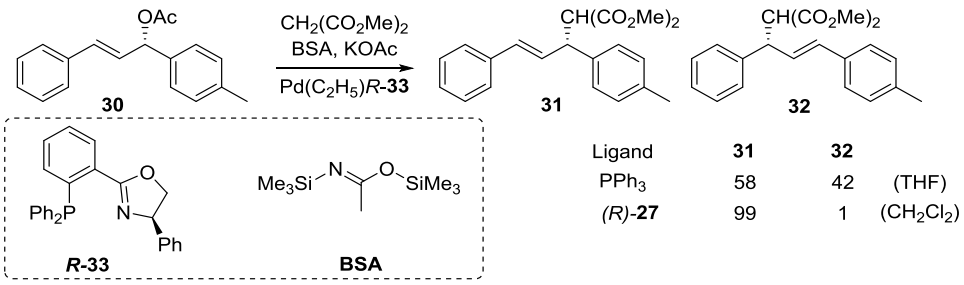

Scheme 5: Mechanisitic evidence against enantiofacial exchange of palladium π-allyl intermediates.

1.4.2 Differentiation of leaving groups of a C2 symmetric allyl

When the bis-carbamate, **34** is subjected to asymmetric allylic alkylation conditions with a non-racemic catalyst, differentiation between the two enantiotopic leaving groups provides an asymmetric palladium π-allyl complex. An intermolecular nucleophilic cyclisation occurs to yield the cyclised products, **35**. Trost and co-workers screened the ligand series based on the 2-(diphenylphosphino)benzoic acid (DPPBA) moiety with both amide and ester backbones. The more rigid amide backbones generally gave higher *ee*'s with the ligand (**36**) giving (+)-**35** in 94% yield and 88% *ee*. Overall, the DPPBA ligand series afforded higher enantioselectives than the other ligands tried such as BINAPO or DIOP.[20]

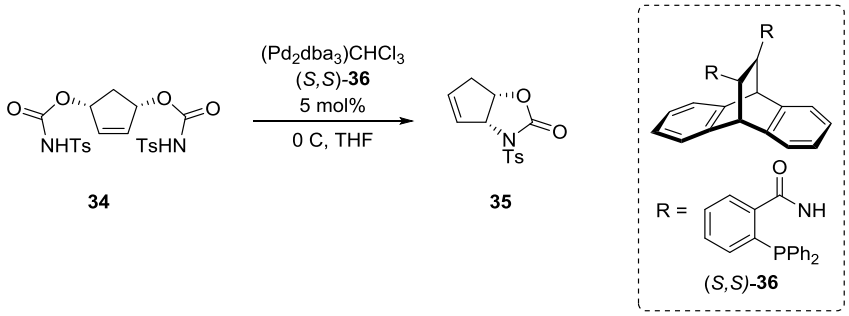

Scheme 6: Discrimination of the enantiotopic leaving groups with chiral ligands.

It was found that the addition of an equivalent of triethylamine increased the *ee* to <99%, albeit with a slight decrease of yield 84%. It is proposed that this is due to an increase in the rate of nucleophilic addition by deprotonation of the second tosylamide, decreasing the competitive ion return pathway to regenerate the starting material.[21]

1.4.3 Desymmeterisation of *meso*-π-Allyl Complexes

The accepted mechanism detailed in section 2, Figure 1 suggests that each enantiomer of a racemic allyl such as **37** should provide a common *meso*-π-allyl palladium intermediate, and by the differentiation of the prochiral faces of the allyl with chiral ligands, racemic substrates

can be converted to enantio-enriched products. Indeed, employing the 1,3-diphenylallyl acetate, **37**, $Pd_2(dba)_3CHCl_3$ and (*S*)-BINAP, the alkylation product was obtained in 73% yield and 92% *ee*.[22] However it was observed that the nature of the incoming nucleophile greatly influenced the *ee* obtained, with the greatest *ee*'s observed when the malonate nucleophile was slowly released *in situ* by the base activated (*N,O*-bis-(trimethylsilyl)acetamide) BSA. The low concentration of base is maintained by the release of acetate ions following the oxidative ionisation of the substrate.[23]

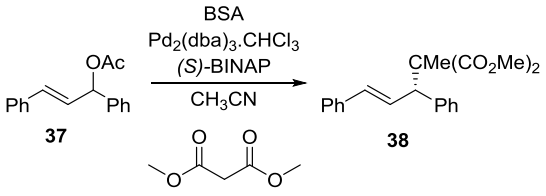

Scheme 7: Dynamic kinetic resolution of 1,3-diphenylallyl acetate

This is the most common method of inducing asymmetry in allylic alkylation; it includes the kinetic dynamic resolution of racemic allyl substrates.[24] The Trost standard ligand (TSL) series has enjoyed great success and achieved high enantioselectivities with substrates that have proven challenging with other ligand sets.[20a, 25]

1.4.4 Discrimination of Enantiotopic Faces of a Prochiral Nucleophile

In all of the examples described so far, stereoselectivity has been achieved by discriminating between two faces of a prochiral allyl unit, however Trost and co-workers have demonstrated that the discrimination of the faces of a prochiral nucleophile can afford high *ee*'s. One such example is the asymmetric allylic alkylation of the oxindole **39** with allyl palladium chloride dimer, allyl acetate and base in DME. Use of ligand *(R,R)*-**36** from the TSL series, and triethylamine as a substoichiometric base allowed for the generation of the quaternary carbon centre in 66% yield and 78% *ee*.[26] In a similar example, Williams and co-workers demonstrated a double stereodifferentiation in the alkylation of phosphonate **42** and 1,3-diphenylallyl acetate. The alkylated product was obtained in good enantioselectivity and diastereoselectivity, Scheme 8.[27]

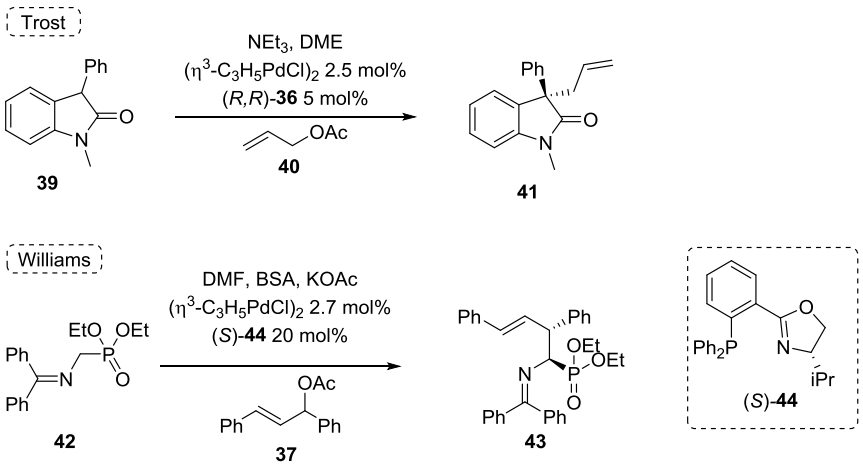

Scheme 8:Asymmetric induction with a prochiral nucleophile

1.4.5 Alkylation with Unstabilised Nucleophiles

Alkylation with hard nucleophiles has been far less well studied and with less success than soft nucleophiles. The nucleophilic addition step is thought to proceed *via* complexation of the nucleophile to palladium, and subsequent reductive elimination, rather than by direct attack at the cationic allylpalladium(II) species as with the soft nucleophiles. As the enantiodiscriminating step is thought to take place within the coordination sphere of palladium, it would be reasonable to assume that achieving high enantioselectivies would be easier with hard nucleophiles, however there are far fewer highly selective examples of alkylation with hard nucleophile.[28]

Lithium enolates can engender high stereoselectivities with ligands such as the Trost standard ligand; the reaction times are decreased and the yields and selectivities increased by a stoichiometric tin additive, Scheme 9.[29] The decarboxylative alkylation of allyl enolates, **48**, simultaneously developed by Trost[30] and Stoltz[31] negates the need for stoichiometric tin additives, but still provides high selectivities and minimal formation of the decarboxylative side product **49**.

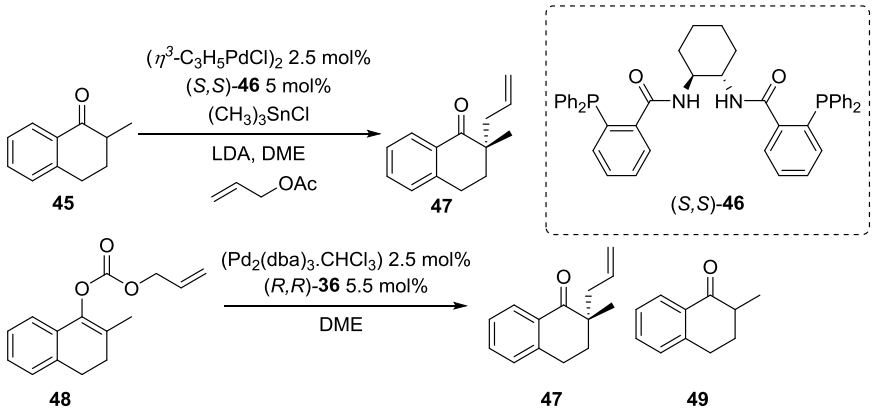

Scheme 9: Asymmetric allylic alkylation with enolates

More recently, Trost demonstrated the use of $BF_3{\cdot}OEt_2$ to "soften" a lithiated 2-methylpyridine, to give high yields and *ee*'s, these behave as soft nucleophiles, and react by addition to the allylic ligand, rather than attack at palladium and reductive elimination, Scheme 10.[28]

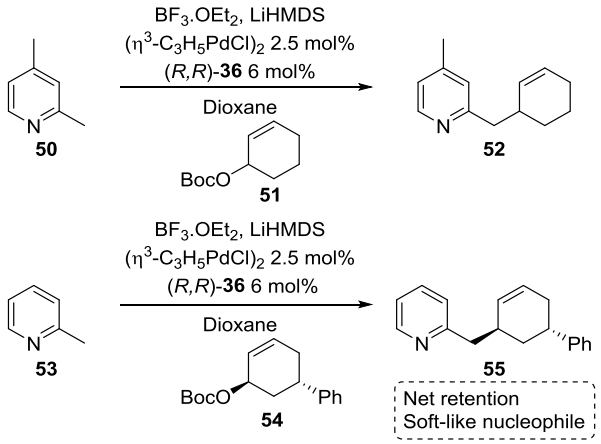

Scheme 10: Asymmeteric allylic alkylation with hard nucleophiles and a $BF_3.OEt_2$ additive

1.5 Memory Effects

The mechanism described in section 1.2, Figure 1, predicts that when a racemic substrate such as **56** is used, a *meso*-π-allylpalladium intermediate is generated; therefore the enantiomeric enrichment of the product should be independent of the enrichment of the substrate. When **56** (55% *ee)* is subjected to Pd((*R,R*)-**46**), an *ee* of 47% was obtained, however when the same substrate was subjected to the same conditions with the opposite enantiomer of the ligand Pd((S,S)-**46**), an *ee* of just 33% was obtained.[32] If the mechanism does proceed *via* a *meso*-π-allylpalladium intermediate the enantiomeric excess obtained

should be equal and opposite for the stereoisomeric ligand. As this is not the case, it can be said that some form of 'memory effect' of the substrate used exists.

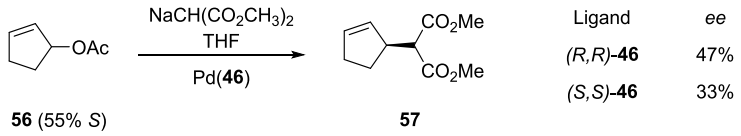

Scheme 11: Memory effects in the asymmetric allylic alkylation

To identify the origin of these memory effects, Lloyd-Jones and co-workers employed the racemic ^{13}C-labelled substrate **37**. The ^{13}C label differentiates the two enantiomers of the substrate, allowing for analysis of the enantiomeric excesses arising from the individual isomers of the starting material, rather than just a calculation of the global *ee* obtained. Employing BINAP as a ligand, it was found that the contribution to the enantiomeric excess from the matched substrate was much greater than the global *ee* observed, for the mismatched substrate a reversal in selectivity was observed. The addition of NaBAr'F had little effect on the *ee* of the matched substrate, but greatly increased the *ee* of the mismatched substrate.[33]

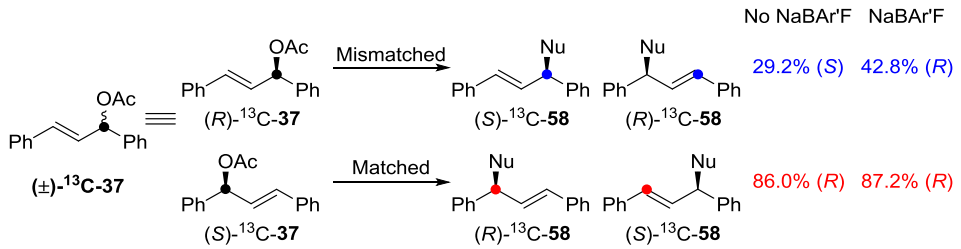

Scheme 12: Identifying the memory effects.● = ^{13}C, ligand = (S)-BINAP, Nu=CH(CO$_2$Me)$_2$

A series of stoichiometric and catalytic studies into the rates and *ee* contributions of each substrate led Lloyd-Jones and co-workers to propose a new catalytic cycle, where the resting state of the catalyst was in fact a $L_2Pd(\eta^2\text{-allyl})$ complex, in equilibrium with the $L_2Pd(\eta^3\text{-allyl})$ complex previously proposed as the resting state. The position of the equilibrium was sensitive to the coordinating ability of the leaving group, and hence the counterion. Addition of a catalytic amount of sodium BAr'F leads to ion pair metathesis generating a longer lived $L_2Pd(\eta^3\text{-allyl})$ intermediate, giving the complex more time to equilibrate, and nucleophilic attack becomes more selective, arising from an increased selectivity of the mismatched

substrate. Slow addition or release of the nucleophile also results in an increased *ee* of the mismatched substrate.

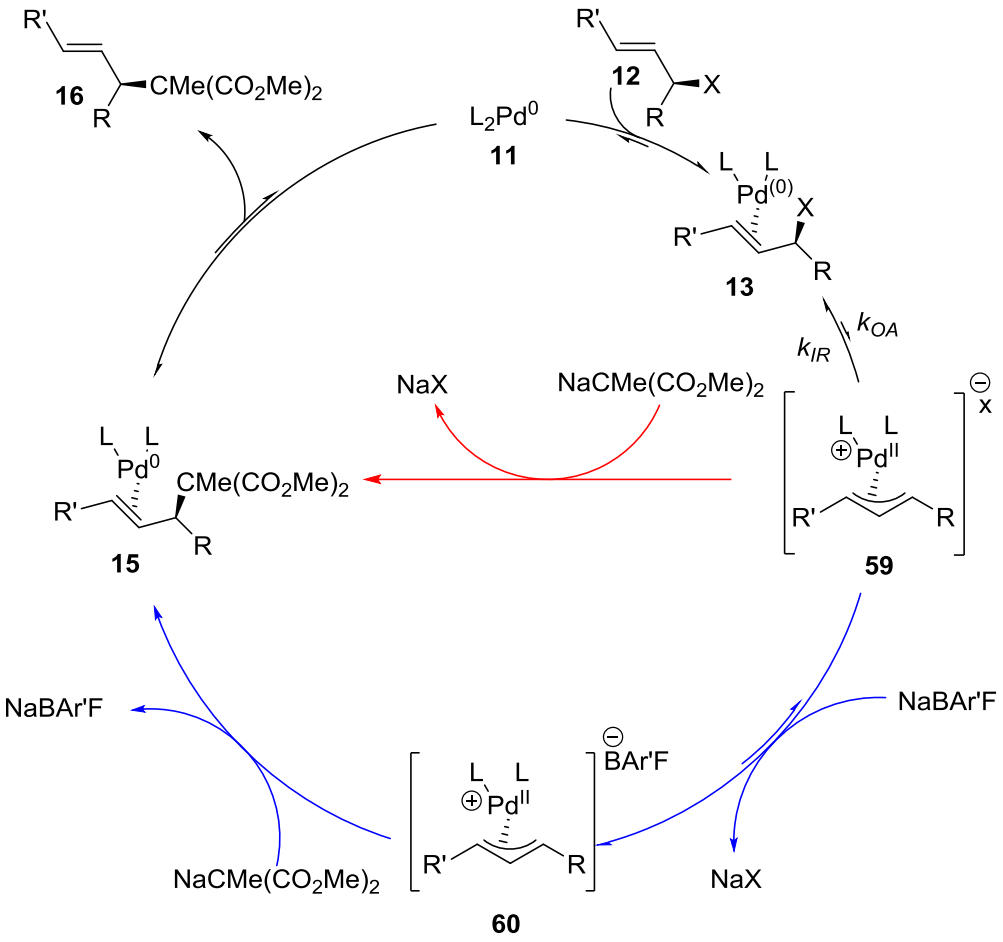

Figure 6: Revised catalytic cycle.

In the revised catalytic cycle, the η^2-olefin complex **13** is the resting state of the catalyst and the oxidative ionisation (k_{OA}) is reversible. Sodium BAr'F removes the acetate from the tight ion-pair **59** to generate **60**, prolonging the life-time of the cationic π-allylpalladium(II) intermediate allowing time for the equilibration and the nucleophilic attack becomes more selective. Secondly, as the tightly bound acetate is removed, the malonate nucleophile is no longer 'guided' in by the counterion and the memory effect is reduced, Figure 6.

1.6 The Trost Standard Ligand

1.6.1 A Working Model

A working model based around the design principles of the Trost modular ligand series has been developed by Trost *et al* to rationalise the stereochemical outcome of the asymmetric transformations. The model is based on a steric deactivation; the allyl moiety sits in a chiral pocket created by the orientation of the ligand phenyl rings, and a direct interaction between the nucleophile and the phenyl rings deactivates the undesired reaction pathway. The C2 symmetry of the ligand is retained when complexed to the metal, and the chiral space is created by the propeller-like array of phenyl rings, the absolute stereochemistry of which is transmitted from the chiral diamine through the rigid benzamide linkages. The phenyl rings can lie in one of two orientations, in the plane parallel or perpendicular to the η^3-allyl, known as 'flaps' and 'walls' respectively.

There are four possible trajectories for nucleophilic attack. It is generally accepted that the nucleophile approaches the η^3-allyl antiperiplanar to the palladium and so it is assumed the nucleophile approaches via the *exo* mode and the stereochemistry is introduced by the front two phenyl rings. The nucleophile approaching the π-allyl from the right hand side, Scheme 13, would encounter a raised flap, however a nucleophile approaching the π-allyl from the left hand side would encounter a lowered flap, providing the energy difference of the transition states.[34]

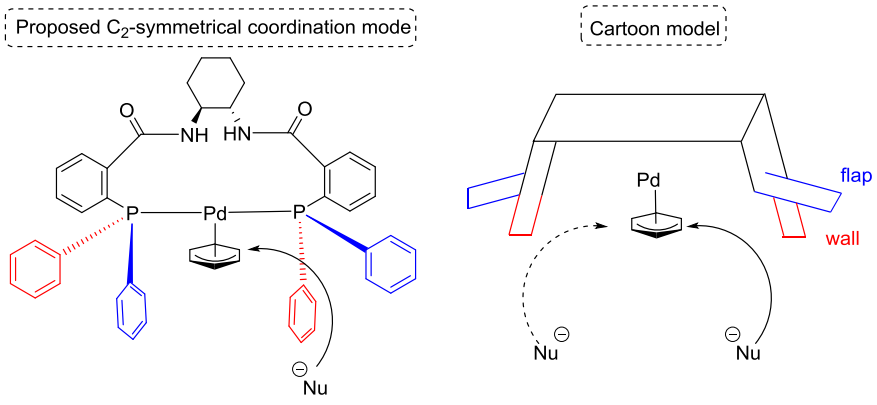

Scheme 13: The proposed C2 coordination mode of the Trost standard ligand and a cartoon model used to predict the stereochemical outcome.

This model generally works well in predicting the stereochemical outcome the asymmetric transformations, however there are a few exceptions to the rule.[34] NMR studies raised

questions as to the C2 symmetry of the palladium η^3-allyl as two distinct diastereomers were observed by ^{31}P [17b] NMR; the η^3-allyl rotamers are degenerate if the ligand is coordinated in a C2 conformation.[35]

1.6.2 The Revised Working Model

While Trost's wall-and-flap model is sufficient for predicting the outcome of the majority of the optimised reactions by the Trost Modular Ligand series, the steric deactivation model cannot fully explain all observations. Lloyd-Jones and co-workers utilised a combination of computational, ^{2}H- and ^{13}C- label-facilitated NMR and kinetic analysis to study the system in more detail.[36]

^{31}P NMR of complex **46** at low palladium concentrations revealed an AB spin system ($^{2}J_{PP}$), showing that the ligand does not display C2 symmetry once bound to the palladium. Systematic selective deuteration of the phenyl rings, the benzamide linker and the cyclohexenyl ring allowed for assignment of ^{1}H-^{1}H NOESY interactions. A key nOe interaction was found between one amide proton in the backbone and the cyclohexenyl ring, suggesting a twist in the cyclohexane diamine backbone. Positioning one NH of the backbone close to the cyclohexenyl ring allows for delivery of the incoming nucleophile, and hence a rate acceleration of the dominant pathway.

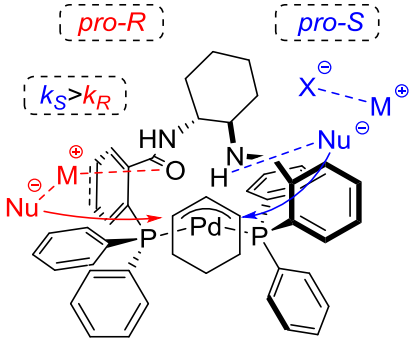

Figure 7: Revised working model.

1.6.3 Oligomerisation

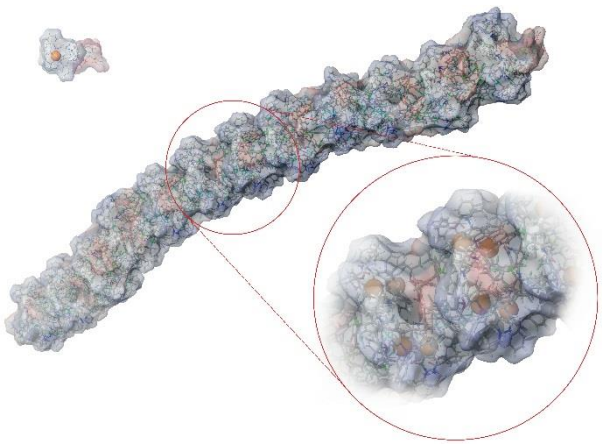

Figure 8: Oligomers of complex 46. Cyclic tetramers stack to form columns.

The mono-nuclear complex **46** is reported to be in equilibrium with other species, observable by ^{31}P NMR. The concentration dependence of these other species is consistent with aggregated or oligomeric complexes, and indeed, a combination of ^{31}P NMR, SANS, x-ray crystallography and DFT calculations has led to the proposed model in which the mono-nuclear complex is in a very fast equilibrium with a cyclic tetrameric complex with the phosphine ligands bridging two palladium cations, Figure 8.[35, 37] The cyclic tetramer de-oligomerises rapidly in solution, with a half-life of seconds. The extent of aggregation increases with concentration, decreased temperature, or increased ionic strength of the medium. Studies into the effect of aggregation on the selectivity of the catalytic system **46** furnished the conclusion that the oligomeric complex is catalytically active. However a lower, or even reversed preference for the matched substrate is observed, therefore oligomeric concentrations result in a reduction of enantioselectivity. The identity of the counterion has a dramatic impact on the monomer concentration at a given total palladium concentration. The less interactive the counterion (whether it be through size, charge distribution or hydrogen bonding) the greater the monomer concentration obtained.

1.7 Conclusions

The mechanism of the Tsuji-Trost asymmetric allylic alkylation has been extensively studied and is well understood, and the many different opportunities for asymmetric induction explored. Often high enantioselectivies are observed, however in some systems memory effects are present. These memory effects are thought to be due to the slow interconversion

of the various isomeric forms of the η^3-allyl palladium(II) intermediates. Many isomerisation mechanisms of the η^3-allyl palladium(II) intermediates are known, and the outcome is determined by the substitution pattern about the allyl termini and the mechanism dominating. The mechanism mediated by palladium(0) is less well understood, although it has been shown to occur, and results in enantiofacial exchange.

Understanding this palladium(0) mediated mechanism may allow increase in the rate of isomerisation of the η^3-allyl palladium(II) intermediate, and hence reduce the memory effect (i.e. under Curtin-Hammett conditions).

2 Results and Discussion

2.1 Mechanistic insight into the palladium(0) catalysed isomerisation of palladium(II) π-allyl complexes

2.1.1 Previous investigations

Upon addition of palladium(0) to a palladium(II) π-allyl complex, three mechanisms have been determined and are detailed here:

1. Addition of palladium(0) to the allyl moiety resulting in a S_N2-like displacement of a palladium(0)
2. Addition of palladium(0) to the palladium(II) to form a dinuclear palladium(I) species
3. Single electron transfer

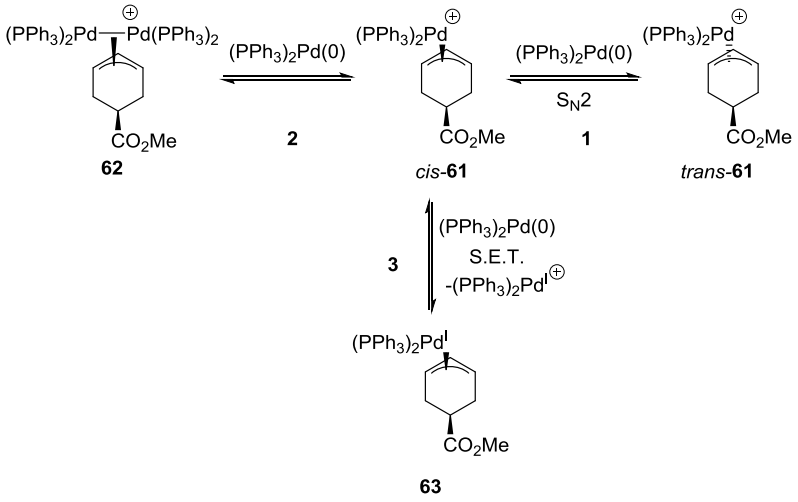

Scheme 14: Addition of palladium(0) to a palladium π-allyl complex

2.1.1.1 Addition of palladium(0) to the carbon atom of the allyl

If nucleophilic addition occurs in an S_N2-type fashion by attack of palladium(0) at a carbon of the allyl group this would result in an inversion of stereochemistry, proposed by Bäckvall in 1992.[17a] This isomerisation has also been proposed by Tsuji,[16] Bosnich[7] and Jutand.[38] Kurosawa[39] confirmed the bimetallic redox allyl transfer occurs with a mixed palladium(II)/platinum(0) system, Figure 9.

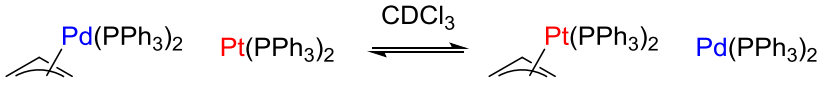

Figure 9: Kurosawa used a bimetallic Pd/Pt system to provide evidence for the allyl transfer

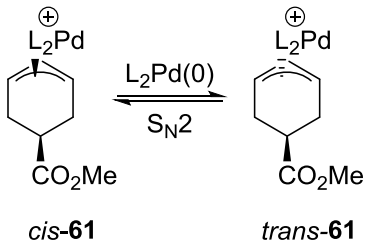

Scheme 15: Nucleophilic substitution of palladium

Bäckvall found that the reaction followed pseudo-first-order bimolecular equilibrium kinetics, which is consistent with an S_N2 mechanism, Scheme 15. It was found that the addition of excess ligand retards the reaction, comparing entries 3 and 5, Table 1; an excess of triphenylphosphine would favour the coordinatively-saturated $(PPh_3)_4Pd$, rather than the bis or tri ligated palladium species proposed to be the reactive species. This again is consistent with the nucleophilic attack of mono- or bis-ligated palladium triphenylphosphine species. Above 0°C triphenylphosphine can act as a nucleophile to the π-allyl palladium(II) complex, generating the palladium(0) to initiate the isomerisation entries 6 and 7, Table 1.

Entry	*Solvent*	*π-allyl complex/ OTf*	*Temp °C*	*Phosphine equiv*	*$(PPh_3)_4Pd$ equiv*	*T_{eq} mins*
1	$CDCl_3$	*cis*-**61**	0	PPh_3, 2	0.5	<5
2	$CDCl_3$	*trans*-**61**	0	PPh_3, 2	0.5	<5
3	$CDCl_3$	*cis*-**61**	-14	PPh_3, 2	0.5	25
4	$CDCl_3$	*trans*-**61**	-13	PPh_3, 2	0.5	20
5	$CDCl_3$	*cis*-**61**	-14	-	1	<5
6	$CDCl_3$	*cis*-**61**	-15	PPh_3, 2	-	∞
7	$CDCl_3$	*cis*-**61**	2	PPh_3, 2	-	15
8	$CDCl_3$	*cis*-**61**	20	-	-	∞
9	THF	*cis*-**61**	20	-	-	∞

Table 1: Kinetics of isomerisation of isolated palladium π-allyl complexes

For the kinetic experiments, Bäckvall used $(PPh_3)_4Pd$ as the source of palladium(0), and so the amount of active palladium species in solution was not calculated as the position of the equilibrium is not known. As a consequence the molecularity with respect to palladium(0) was not determined in this study. The effect of the dependence of palladium(0) and the effect of bidentate ligands were studied using the catalytic reaction, by monitoring the

stereoselectivity of product, *cis*- and *trans*-**66**, and remaining starting material, **64**, entries 1 and 2 Table 2.

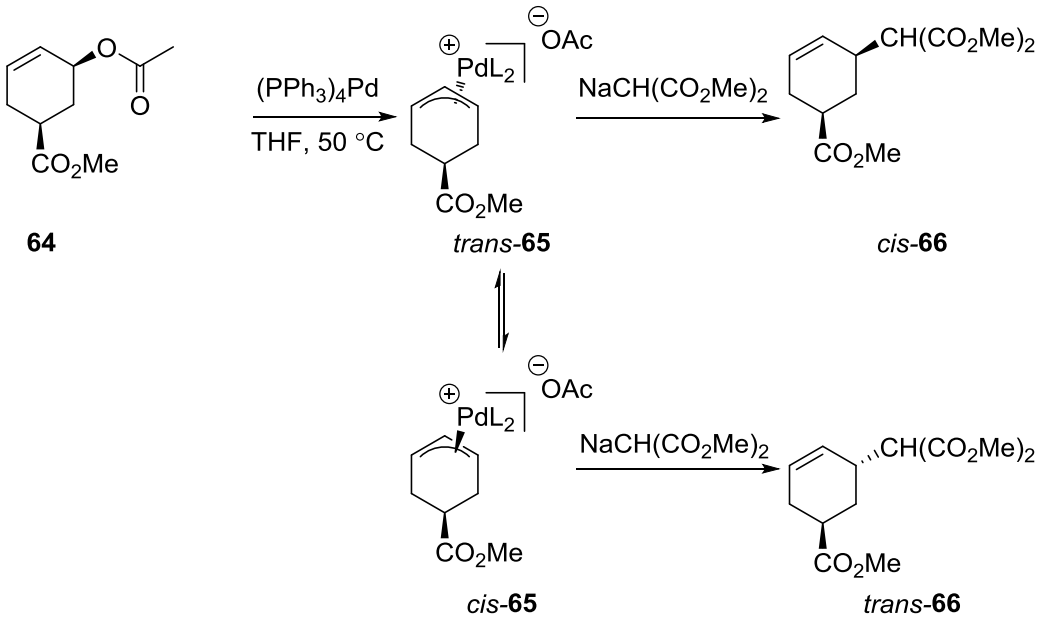

Entry	*Catalyst (mol%)*	*Time hour*	*Conversion %*	*Product Cis/trans*
1	*$(PPh_3)_4Pd$ (5)*	12	100	18.2
2	*$(PPh_3)_4Pd$ (24)*	12	100	11.3
3	*$(dppe)_2Pd$ (5)*	1	100	199

Table 2: Effect of palladium(0) concentration of the diastereoselectivity of the catalytic asymmetric allylic alkylation. All reactions were in THF at 50°C

Bäckvall also suggested that the isomerisation is retarded when bidentate ligands such as DPPE are employed, entries 1 and 3 Table 2, however this observation is based on the stereoselectivity of the product of the catalytic reaction. The increase in selectivity could simply be due to an increased rate of nucleophilic addition to the dppe π-allyl palladium complex over to the bis(PPh_3) π-allyl palladium complex, not allowing time for the epimerisation, rather than a decrease in the rate of epimerisation of the π-allyl palladium complex catalysed by palladium(0). The published data relating to this observation is limited, and the effect of the bidentate ligands on the isomerisation catalysed by palladium(0) is not explained by the proposed mechanism.

Jutand also studied the kinetics in some detail, using the cyclic allyl complex **67** where the oxidative ionisation into the allylic benzoate is reversible.[38] $(PPh_3)_4Pd$ or $[Pd(dba)_2 + 2PPh_3]$ was added in the absence of a nucleophile, and the *cis-trans* ratio of **67** was studied by ^1H NMR, Scheme 16. Jutand found a difference between the two sources of palladium, with *cis*-**67** reaching equilibrium in approximately 30 minutes with 50 mol% $(PPh_3)_4Pd$, and 1200 minutes when the same concentration of $[(dba)_2Pd + 2PPh_3]$ is used. Jutand proposes that equilibrium concentration of $(PPh_3)_2Pd$ is lower in equilibrium **A** than **B**, i.e. $K_2 > K_1$, Scheme 17. Again the molecularity in palladium(0) was not determined, and the observed rate constants are dependent on an unknown concentration of the assumed active palladium species.

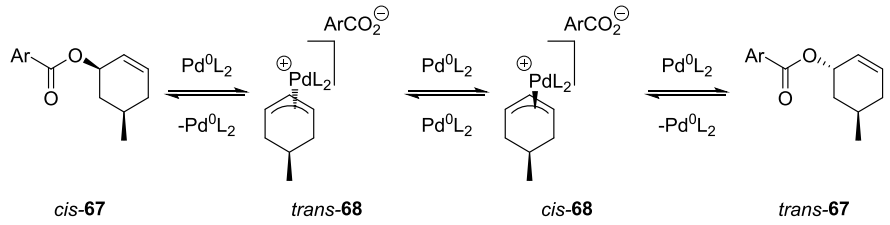

Scheme 16: Palladium(0) catalysed isomerisation of allylic carbonates via a palladium(II) intermediate.

$$Pd(dba)(PPh_3)_2 \underset{}{\overset{K_1}{\rightleftharpoons}} PdL(PPh_3)_2 + dba \quad \mathbf{A}$$

$$Pd(PPh_3)_3 \overset{K_2}{\rightleftharpoons} Pd(PPh_3)_2 + PPh_3 \quad \mathbf{B}$$

Scheme 17: Dissociation of a ligand to yield a bis(triphenylphosphine)palladium(0) species.

2.1.1.2 Addition of palladium(0) to palladium(II) to form a dinuclear palladium(I) species

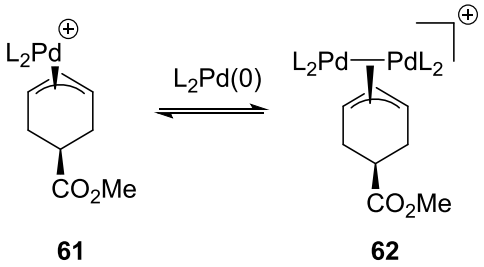

Scheme 18: Palladium(0) addition to π-allyl palladium(II) species

Addition of palladium(0) at the palladium(II) centre, as a hard nucleophile would result in a dinuclear palladium(I) species. These dinuclear complexes have been observed in asymmetric allylic alkylation reactions; Pfaltz and co-workers have observed the dinuclear complex **71** by ESI-MS and ^{31}P NMR upon the addition of malonate **70**, Scheme 19.[40] The chemistry of

palladium(I) dinuclear complexes has been studied extensively by Kurosawa, and generally have a structure similar to **72**, where X is a bridging halide or second bridging allyl ligand.[41]

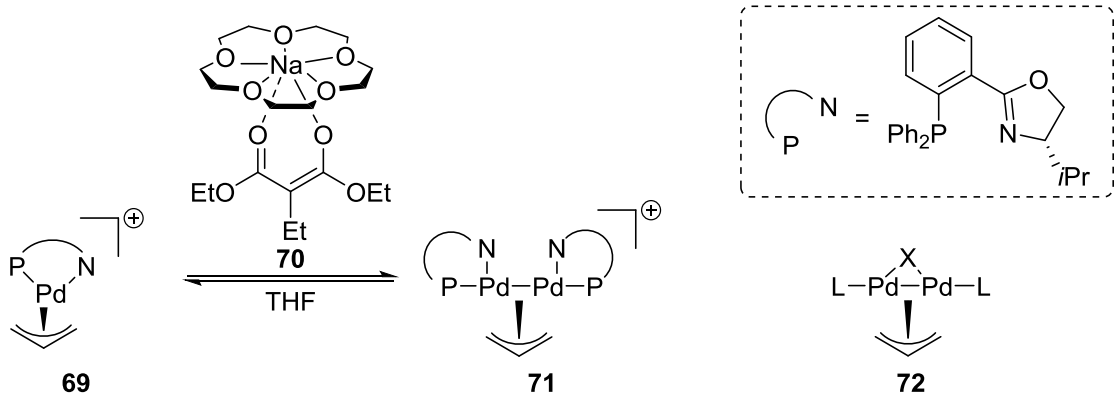

Scheme 19: Dinuclear palladium(II) species observed in the asymmetric allylic alkylation

The dinuclear species observed by Pfaltz under asymmetric allylic alkylation conditions are positively charged, with bidentate ligands on the palladium rather than a second anionic group.

2.1.1.3 Single electron transfer

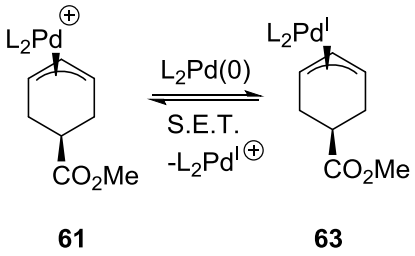

Scheme 20: Palladium(0)-catalysed S.E.T. to a π-allyl palladium(II) species

The single electron transfer to generate a rapidly inverting palladium(I) species as a mechanism of isomerisation was proposed by Kurosawa, Scheme 20.[4b] Stille proposed the single electron transfer from an alkyl halide to a palladium(0) species as a mechanism competing with the S_N2 oxidative addition of palladium(0) into benzyl halides **73**, and attributes the loss of enantiopurity of palladium(II) alkyl halides to this mechanism.[42] When X = Cl, a reduction of *ee* from 87% in **73** to 63% in **76** was observed, Scheme 21 however when X = Br, there was a much greater reduction in *ee* from 50% in **73** to 10% in **76**.

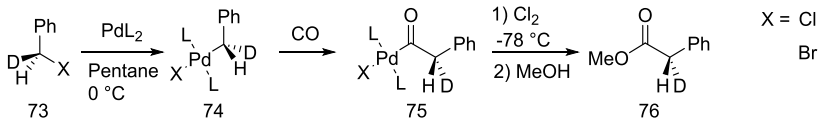

Scheme 21: Oxidative addition of palladium(0) to alkyl halides, S_N2 or S.E.T?

The S_N2 oxidative addition mechanism proceeds with inversion of stereochemistry, however if the solvent-caged radical pair, **78**, is formed, inversion of the radical followed by a collapse to the palladium(II) complex would give retention of stereochemistry, Scheme 22. The rate of S.E.T. is greater in the case of benzyl bromide than benzyl chloride,[43] and so an increase in the non-stereoselective S.E.T would result in a decrease of *ee*. Krammer and Osborn detected radicals by chemically induced dynamic nuclear polarization (CIDNP) in the oxidative addition of benzyl bromide to $(Et_3P)_3Pt$, and isopropyl iodide to $(Et_3P)_3Pd$.[44] Stille's attempts to detect the radicals in the case of the benzyl bromide **78** were unsuccessful, which is proposed to be due to the short lifetime of the benzyl radical or the presence of the paramagnetic palladium(I) species.

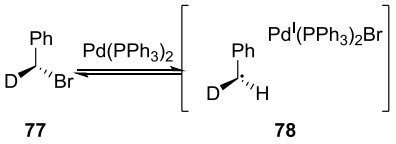

Scheme 22: Formation of a biradical cage by S.E.T.

Kurosawa proposed S.E.T. as a mechanism of isomerisation of palladium(II) π-allyl complexes, Scheme 20.[39] A S.E.T. from palladium(0) to *cis*-**61** would result in a palladium(I) cation and the palladium(I) π-allyl radical species *cis*-**63**, the latter which would be prone to stereochemical inversion, possibly *via* an allylic radical intermediate. A second S.E.T. would result in **61** with stereochemical scrambling.

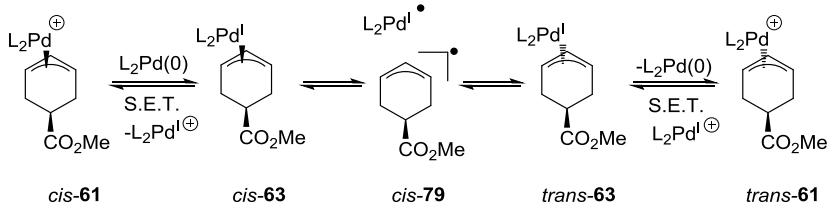

Scheme 23: S.E.T. as a mechanism for the palladium(0) catalysed stereochemical scrambling of palladium π-allyl complexes

2.1.2 Differentiating between mechanisms 1, 2 and 3

To differentiate between the three mechanisms, we chose to add an isotopic label to the L_2Pd moiety and the allyl group. If a system can be designed where the palladium(II) moiety

of a palladium π-allyl complex can be distinguished from the palladium(0) species, then incorporation of the palladium(0) species, **81** into the palladium(II) complex, **80** provides us with means to monitor the process. Considering the palladium moiety, we could label the ligand (for example PPh_3-d_{15}) however the ligand could be susceptible to exchange, Scheme 24, which would not be distinguishable from nucleophilic attack of palladium(0). To overcome this problem, monoisotopic ^{108}Pd was chosen as the isotopic label.

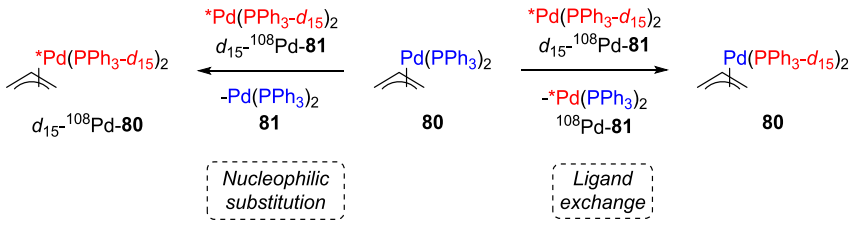

Scheme 24: Distinguishing between palladium(0) substitution and ligand exchange.

If the allyl group is also labelled, **80,** Scheme 25, addition of a substoichiometric amount of a nucleophile generates equal amounts of two palladium(0) species that are analogous to those created under the reaction conditions. In this case, formation of the crossover products indicates the breaking of the palladium-allyl bond. Initially the d_0 and d_5 allyl groups, d_5-**80** and ^{108}Pd-**80**, were chosen, however the information gained from studies of this system was limited and will be discussed in section 2.1.7.2. Instead the cyclohexenyl esters complexes **61** and d_3-^{108}Pd-**61** were chosen, due to their divergent synthesis from a common lactone **82**, Scheme 27.

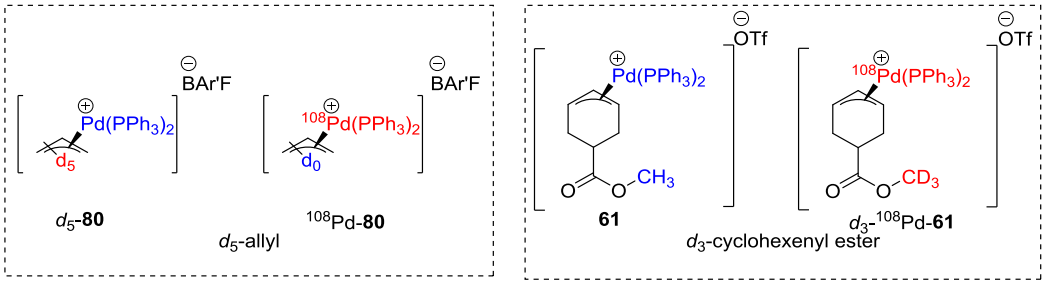

*Scheme 25: Labelled allyl group – **80** versus **61***

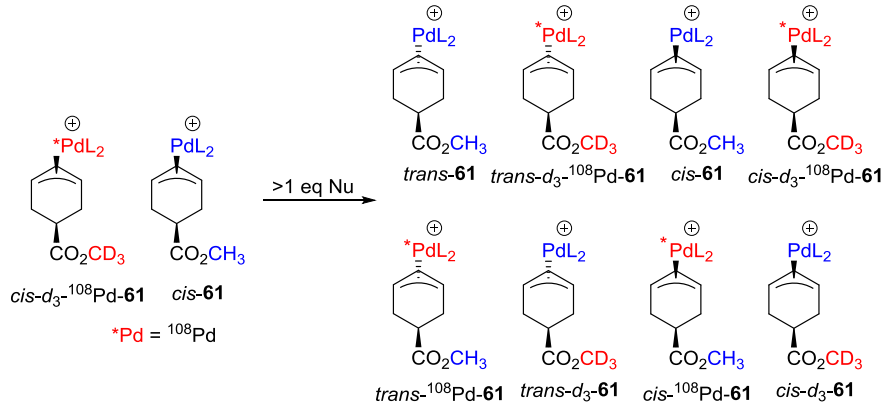

*Scheme 26: 8 possible isomers generated by isotope scrambling and cis-trans isomerisation of complex **61***

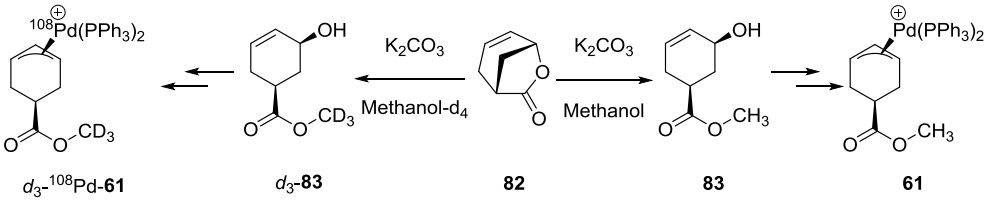

*Scheme 27: Divergent synthesis of d_3-^{108}Pd-**61** and **61** from a common lactone.*

In addition to the isotopic scrambling, the cyclohexenyl ester complex **61** is prepared as a single diastereomer, and the diastereoisomers are distinct by ^{31}P and ^{1}H NMR, which provides a method of monitoring stereochemistry of the palladium-allyl bond. Using the labelled complexes *cis*-d_3-^{108}Pd-**61** and *cis*-**61**, there are eight possible isomers, Scheme 26. Considering the reaction with palladium(0) with the diastereotopic complexes *cis*-d_3-^{108}Pd-**61** and *cis*-**61** *via* each of these three processes allows us to distinguish between them.

The method of comparing the rate of displacement of a nucleofuge by a nucleophile, the process that results in isotopic scrambling, against stereochemical inversion was inspired by the work of Hughes and co-workers in determining the mechanism of a S_N2 displacement.[45] Hughes prepared enantiomerically enriched (*R*)-2-iodooctane **84**, and a sample of sodium iodide radiolabelled at iodine, Scheme 28. The relative rate of uptake of the radioactive iodide in the iodooctane was equal to the rate of reduction of optical rotation of the iodooctane. From this result, Hughes and co-workers concluded that substitution proceeds with, and only with, inversion. This conclusion provided strong evidence for the proposed mechanism; that the nucleophile attacks from the rear face of the electrophile, resulting in inversion.

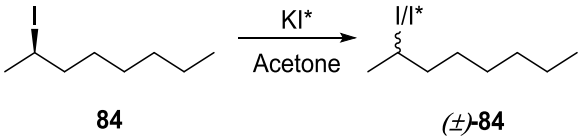

84 *(±)*-**84**

Scheme 28: The rate of uptake of radiolabelled iodine versus the rate of loss of optical activity confirmed the mechanism of the bimolecular nucleophilic subsitution.

The relative rates of isotopic scrambling and inversion of stereochemistry are predicted to be different if each of the three mechanisms proposed is dominating.

2.1.2.1 Addition of palladium(0) to the carbon atom of the allyl moiety

The S_N2 mechanism is a substitution mechanism proceeding with inversion of stereochemistry. For every Pd(0) attack, Pd(0) is liberated, which would be accompanied by exchange of the isotopic labels, and an inversion of stereochemistry, which would be observed in the formation of *trans*-**61** by ^{1}H or ^{31}P NMR.

If we consider both *cis*-*trans* isomerisation, and isotopic scrambling of **61** and d_3-^{108}Pd-**61**, there are eight possible isomers. Using the S_N2 mechanism sixteen reactions can be written to describe the isomerisation. The first eight equations involve a ^{108}Pd(II) species and an unlabelled Pd(0) species; nucleophilic attack of the Pd(II) species with the Pd(0) species would result in a palladium-allyl exchange observable by mass spectrometry. The second eight equations involve palladium species with the same isotopic abundance at palladium, e.g. a ^{108}Pd(II) and ^{108}Pd(0); this process cannot be observed by mass spectrometry. All sixteen equations involve an inversion of stereochemistry at the palladium. Assuming all rates are equal then in the case of the *cis*-*trans* isomerisation the rate would be 16*k*, and in the case of the palladium allyl exchange, 8*k* i.e. **the rate to equilibrium of the *cis*-*trans* isomers would be twice the rate to equilibrium of the palladium-allyl exchange.**

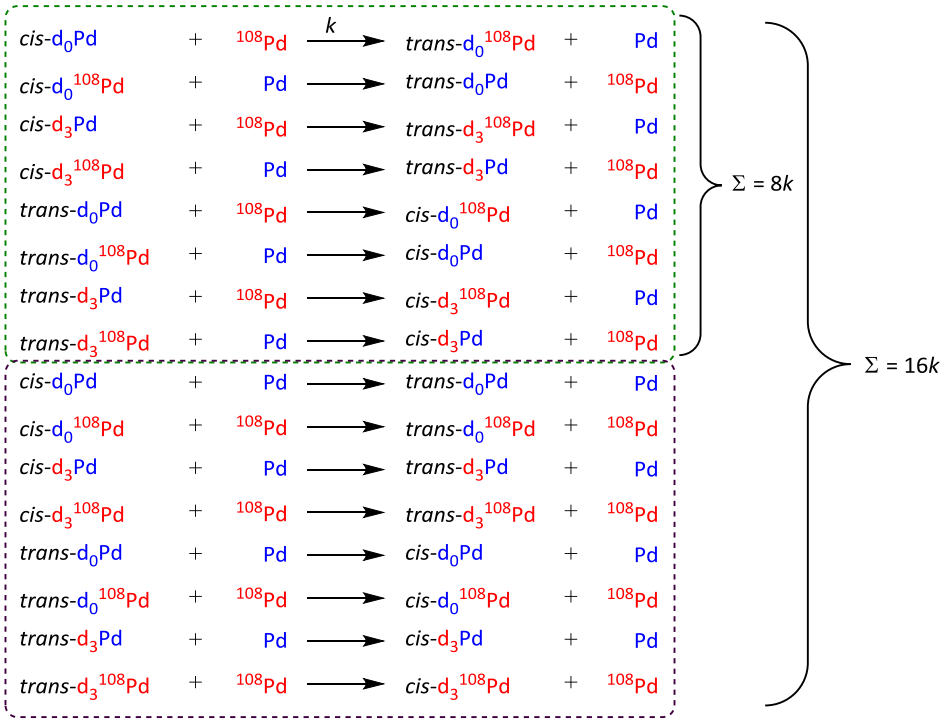

Figure 10: Mechanistic model describing the isomerisation of palladium(0) catalysed isomerisation of palladium allyl complexes. Upper: transformations involve a cis-trans isomerisation and a palladium-allyl exchange. Lower: transformations involve a cis-trans isomerisation but not a palladium-allyl exchange.

A simulation of the data using a S_N2 mechanism, as described, predicted a non-linear relationship between absolute concentrations of [*cis*-**61**]$_{total}$ vs (d_3-^{108}Pd-**61** + **61**), i.e. the complexes at t_0 distinguished by ^{31}P NMR or ESI-MS respectively, however using the integrated first-order equilibrium rate equation, a linear relationship can be obtained where, for any time *t:*

$$\frac{\ln(A_0 - A_e)}{A_t - A_e} = kt$$

$$\ln(B_0 - B_e)/(B_t - B_e) \;=\; 2 \times \ln(A_0 - A_e)/(A_t - A_e)$$

Equation 1: Intergrated rate equation for a first-order equilibrium

A = [d_3-^{108}Pd-**61** + **61**] and B = [*cis*-**61**]$_{total}$, A_0 is the initial concentration, A_e is the concentration at equilibrium and A_t is the concentration at time t.

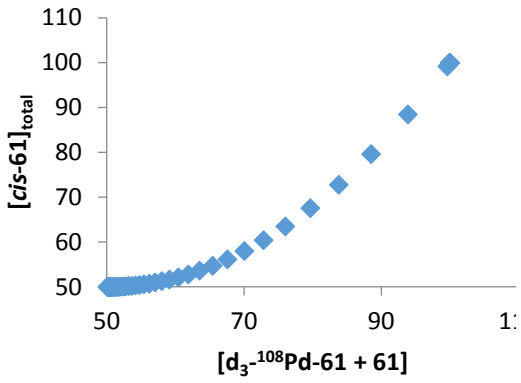

*Figure 11: Graph of absolute concentration of [cis-**61**] vs [d_3-^{108}Pd-**61** + **61**]*

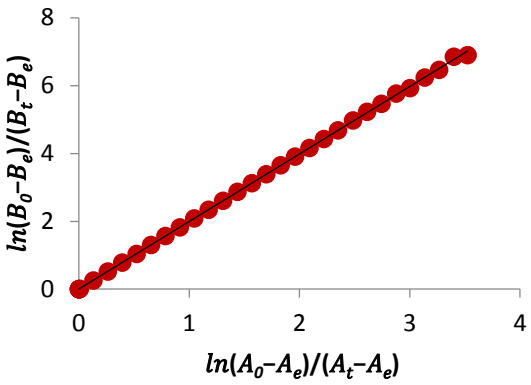

*Figure 12: Graph of integrated first-order rate equation of [cis-**61**] vs [d_3-^{108}Pd-**61** + **61**]*

If the palladium(0) attacks the palladium(II) species at the palladium centre it would form a dinuclear palladium(I) species, where both palladium centres are equivalent. If a labelled palladium(0), ^{108}Pd-**81** species were to form a dinuclear species with the unlabelled palladium(II) species **61**, the mixed dinuclear species **62** would be formed. Dissociation could occur back to the original isotopes, or an unlabelled palladium(0) **81** and labelled palladium(II), ^{108}Pd-**61** Scheme 29, i.e. **palladium-allyl mass scrambling would occur without *cis-trans* isomerisation.**

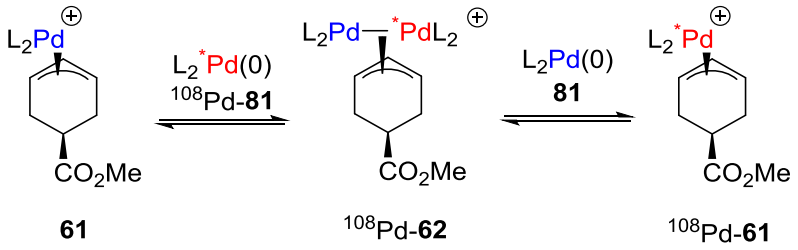

Scheme 29: Formation of a palladium(I) dinuclear species as a mechanism of isotope scrambling without stereoisomerisation

2.1.2.2 Single electron transfer

In the case of the single electron transfer mechanism there is no exchange of palladium, Scheme 30. If this mechanism is operating we would observe ***cis-trans* isomerisation without isotopic scrambling.**

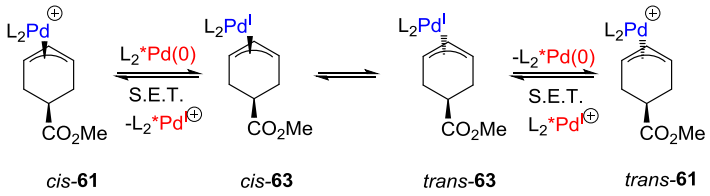

Scheme 30: S.E.T. as a mechanism for isomerisation without isotopic scrambling

2.1.3 Comparing the rates of *cis-trans* isomerisation and palladium-allyl exchange

Water was chosen as the substoichiometric nucleophile as it cleanly generates the allylic alcohol, palladium(0) species, and triflic acid. Benzene was chosen as the solvent as the isomerisation was slow enough to monitor by mass spectrometry. The sensitivity of the reaction to water concentrations, which will be discussed in more detail in section 2.1.7.3, presented a very significant challenge, however it was found that a large excess (> 10 equivalents) of dibenzylideneacetone significantly slowed the isomerisation such that its addition effectively quenched the reaction, allowing the mass spectrometry to be performed open to the atmosphere. To minimise errors in calculations of absolute rates due to differences in water concentration, the measurements were performed on one sample, and the residual water in the solvent was used as the nucleophile.

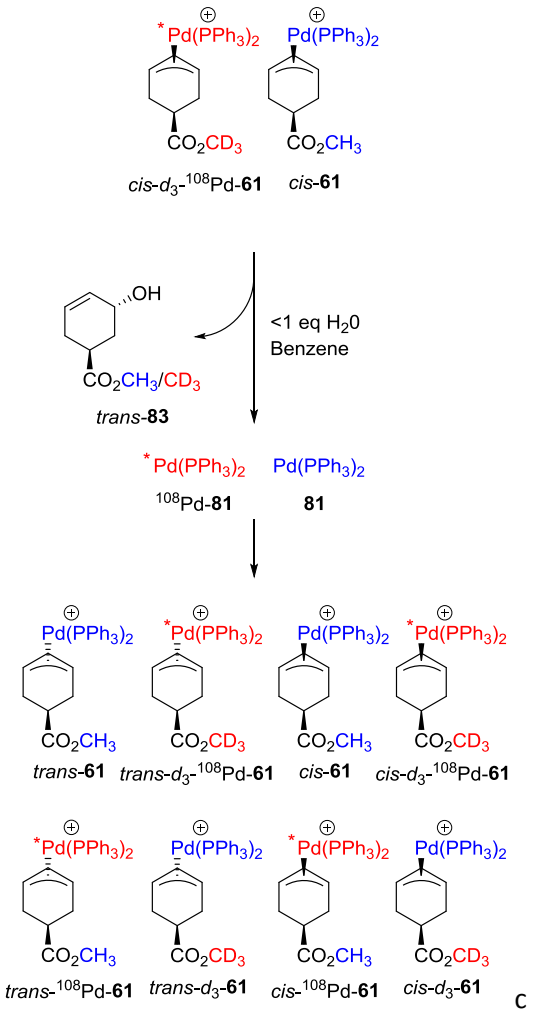

Scheme 31: Addition of water to cis-***61*** *and* cis-d_3-^{108}Pd-***61*** *in benzene*

A solution of total palladium content 5 mM in a 1: 0.997 ratio *cis*-**61** to *cis*-d_3-^{108}Pd-**61** was dissolved in benzene and transferred to a NMR tube. The sample was monitored by *in-situ* NMR, freezing to remove aliquots for ESI-MS monitoring at intervals of approximately 15 minutes. The aliquot was quenched by addition to a solution of dba in THF (see section 2.1.5.2 for dba inhibition of isomerisation). The blue data points, Figure 13, show the rate of *cis-trans* isomerisation observed by ^{31}P NMR. The scatter in the points is due to difficulties in shimming the sample once it has been frozen and thawed. A linear line of best fit was used to calculate the rate, and this value was used simulate the data points in grey, which were the data points used in the plot of rate of *cis-trans* isomerisation *versus* mass spectrometry, Figure 14, to reduce the error due to poor shimming. The orange data points, Figure 13, show the rate of isotope scrambling by mass spectrometry.

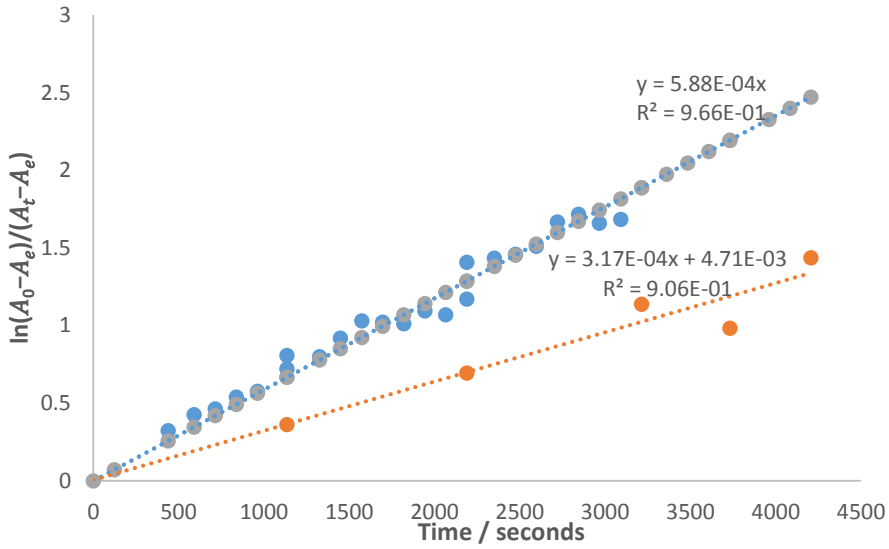

*Figure 13: Kinetics of isomerisation of **61**. Plot of ln(A$_o$-A$_e$)/(A$_t$-A$_e$) versus time. Blue:* Cis-trans *isomerisation by ^{31}P NMR. Grey: simulated data points for* cis-trans *isomerisation using* k$_{obs}$. *Orange: Palladium-allyl exchange by ESI-MS.*

Figure 14, is a graph of $\ln(B_0 - B_e)/(B_t - B_e)$ against $\ln(A_0 - A_e)/(A_t - A_e)$ for 5 independent time points where A = [d_3-^{108}Pd-**61** + **61**] and B = [*cis*-**61**]$_{total}$, A_0 is the initial concentration, A_e is the concentration at equilibrium and A_t is the concentration at time *t,* see Figure 12. The green line, Figure 14 shows the rate of *cis-trans* isomerisation is twice the rate of palladium-allyl exchange.

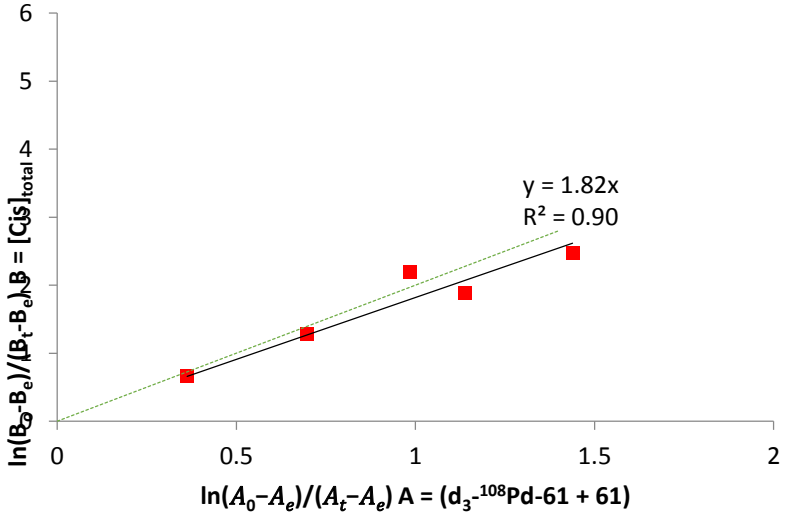

Figure 14: Rate of cis-trans *isomerisation versus isotope scrambling. Red:* Cis-trans *isomerisation versus the rate of palladium-allyl scrambling. Green: Simulated:* cis-trans *isomerisation is twice the rate of palladium-allyl exchange.*

Assuming a zero intercept, the rate of *cis-trans* isomerisation is 1.8 times the rate of palladium-allyl exchange. Within experimental error, this is consistent with the S_N2 mechanism with palladium(0) attack at carbon, resulting in inversion of stereochemistry. This also provides evidence that neither the palladium(0) attack at palladium(II) to form the palladium(I) dinuclear species, nor single electron transfer mechanisms are in operation, or if they are, they are not significantly competitive. This experiment was repeated 4 times, the reactions proceed at different rates due to small differences in water concentration. All for experiments were consistent with the conclusion that *cis-trans* isomerisation is twice the rate of palladium-allyl exchange.

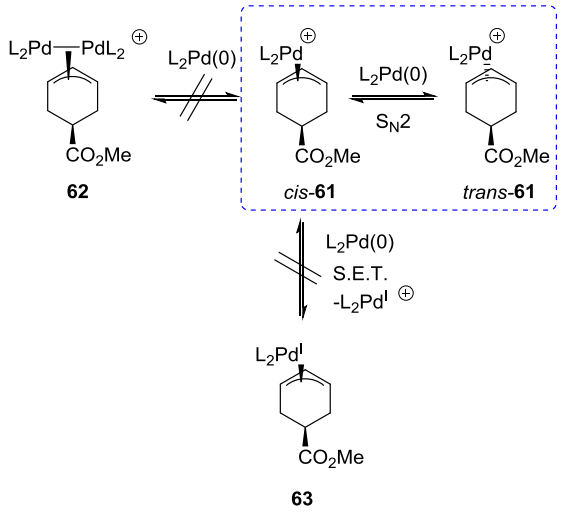

Figure 15: The S_N2 mechanism with palladium(0) attack at carbon is operating. Formation of the dinuclear Pd(I) complexes, and the S.E.T. pathway (both described above) are ruled out on the basis of the rate of cis-trans *isomerisation being twice the rate of palladium-allyl exchange.*

2.1.3.1 Deconvolution of the mass spectrometry data

The interpretation of the mass spectrometry data was complicated by the broad isotope distribution; palladium has six stable isotopes with atomic weights ranging from 102-110 and the complex has further complications arising from the large ^{13}C isotope pattern due to the 44 carbon atoms. The palladium isotope used was ^{108}Pd, the second most abundant isotope (26.46%),[46] and the allyl labelled used was the d_3-methyl ester, adding just 3 mass units. As a consequence, significant overlap of isotope envelopes was observed. Reference spectra of the **61** and d_3-^{108}Pd-**61** were collected, and the ^{108}Pd-**61** and d_3-**61** were calculated by adding or subtracting three mass units to the relevant spectra. The relative abundances of each of the four complexes were calculated by minimising the error between the calculated and experimental data. Figure 16 shows the difference between calculated and experimental

data of a typical spectrum and Figure 17 describes the change in mass spectrum over the course of a typical reaction.

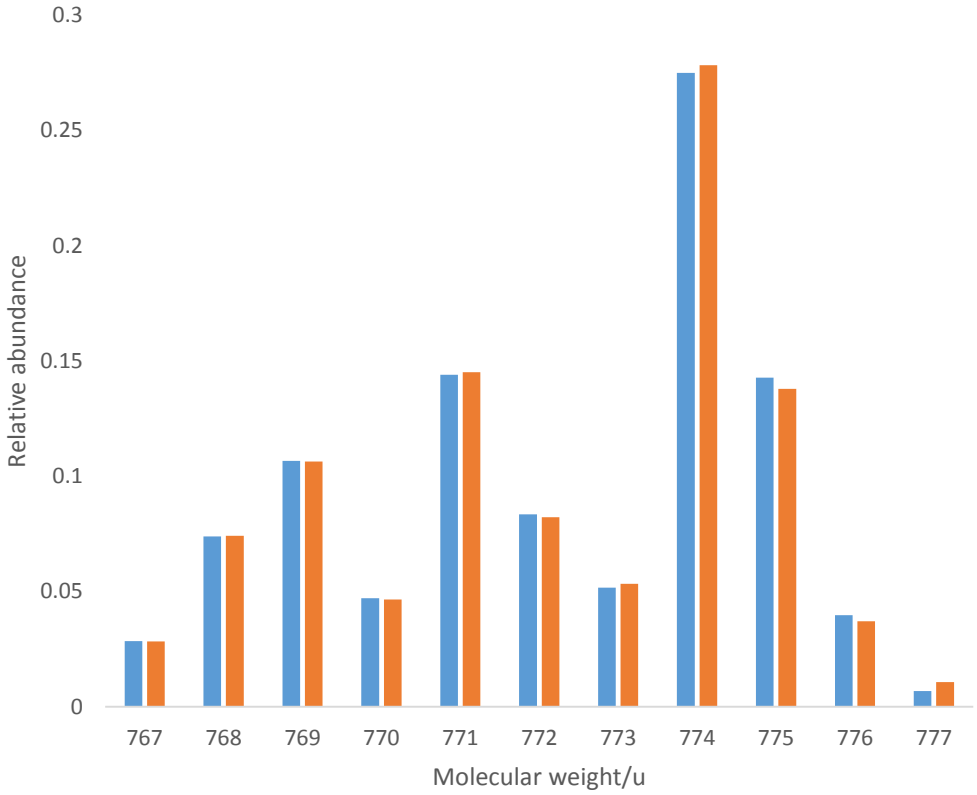

Figure 16: Plot of calculated versus experimental data for a typical mass spectrum of the reaction mixture. Blue: calculated. Orange: Experimental data

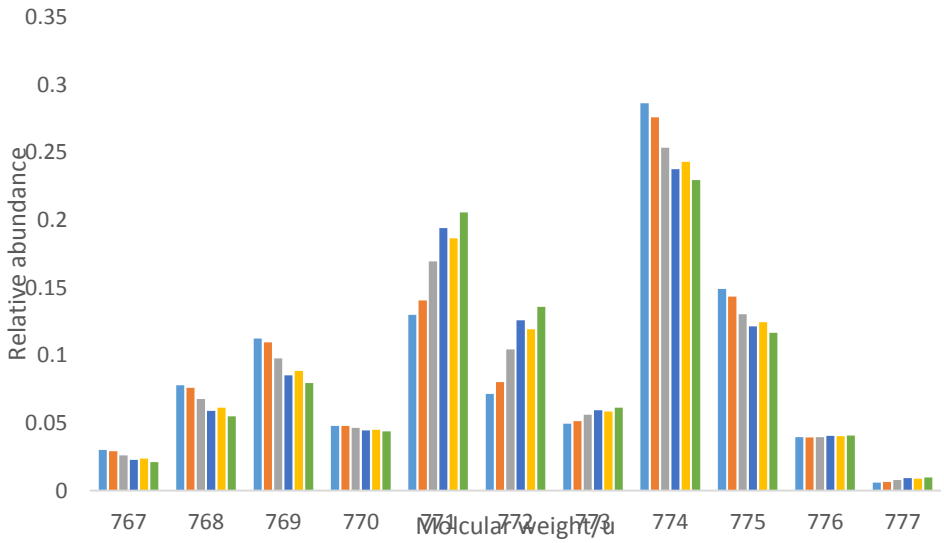

Figure 17: Plot of experimental data over the course of a reaction. Blue to green: MS time points 1-5 respectively, Figure 11, ranging from 88 - 62% total starting material concentration. Equilibrium at 50%.

2.1.4 Determining the rate equation

During the synthesis of the complexes, 2.1.7.3, we discovered that water was an efficient nucleophile and led to the isomerisation of *cis*-**61** without the addition of a source of palladium(0) or an additional nucleophile. The nucleophilic addition of water to the cyclohexenyl palladium(II) complex **61** would generate palladium(0), **81** and the corresponding cyclohexenyl alcohol, *trans*-**83**. Water was titrated into a 5 mol% solution of *cis*-**61** in dry benzene and the kinetics measured by ^{1}H NMR. Figure 18 shows the rate profiles of 0, 26 µM, 51 µM, 94 µM, and 120 µM, (green, blue, red, yellow, and orange data points respectively) of water added. Water concentrations were estimated by dilution of a water saturated solution of benzene, and diluting with dry benzene.[47]

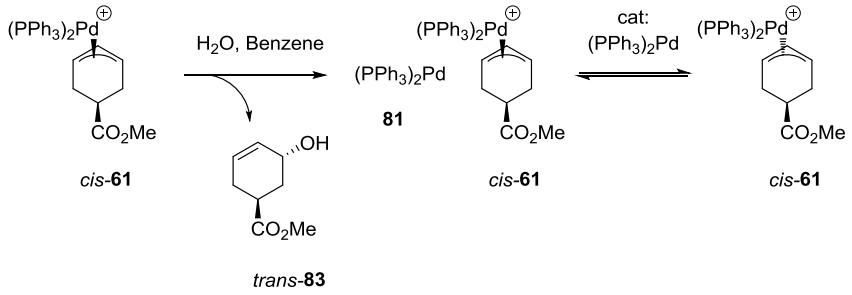

*Scheme 32: Addition of water to cis-**61** in benzene*

If the proposed mechanism is correct the nucleophilic addition of water to generate palladium(0) will be fast, and the displacement of palladium will be the rate determining step. A pseudo-first-order equilibrium profile with respect to the palladium(II) allyl, **61** would be expected, Equation 2. A first-order dependence on the concentration of palladium(0), **81** is also predicted; a linear relationship between k_{obs} and the water concentration, where $k^{obs}{}_f$ is the observed forward rate constant, $k^{obs}{}_b$ is the observed reverse rate constant. A plot of $\ln\left(\frac{A_0-A_e}{A_t-A_e}\right)$ versus *t* will give a linear relationship where the gradient = k_{obs}, Figure 18.

$$\ln\left(\frac{A_0 - A_e}{A_t - A_e}\right) = \left(k^{obs}{}_f + k^{obs}{}_b\right)t$$

$$k^{obs}{}_f + k^{obs}{}_b = k_{obs}$$

$$k_{obsf} = k_f[Pd^0] \qquad k_{obsr} = k_r[Pd^0]$$

Equation 2: Rate equation describing a pseudo-first-order equilibrium

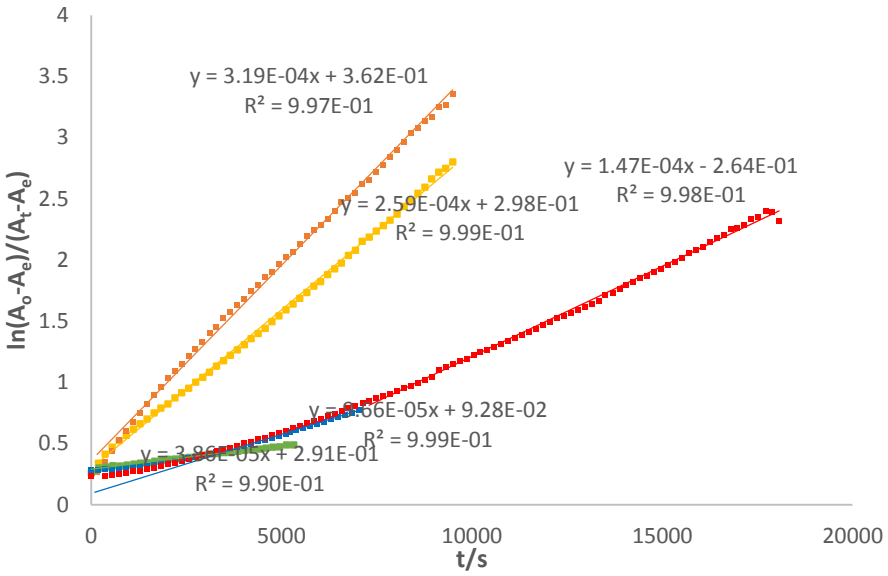

Figure 18: Kinetics of isomerisation of cis-**61**. *Green: no added water, Blue: 26µM, Red: 51µl, Yellow: 94*µl, *120 µM of water.*

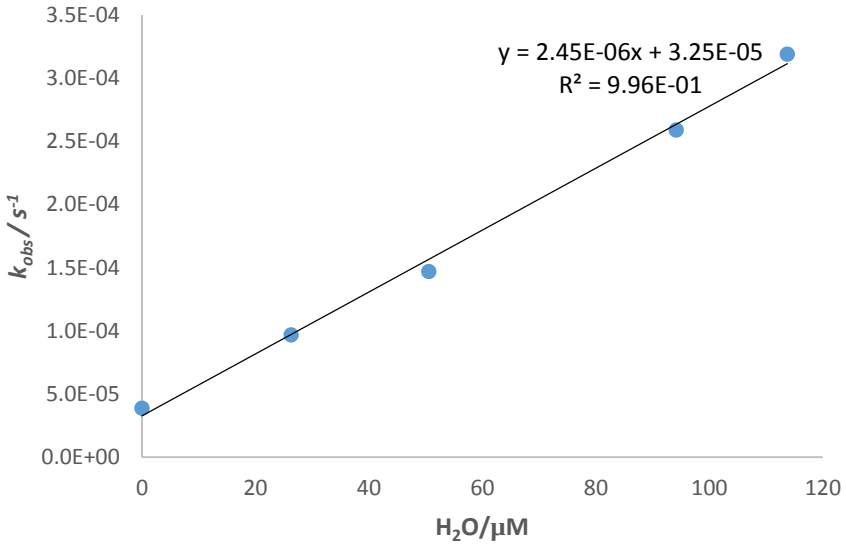

Figure 19: Psuedo first-order equilibrium, rate constant (k_{obs}) shows a first-order dependance on water. Note the background rate with no added water is due to the remaining water in the "dried" solvent, calculated as 15µM.

This is indeed what we observe, Figure 18 shows the rate determining step is first-order in palladium(II) complex **61**. The curvature evident in the early stages of the reactions at low concentrations of water is due to the rate of generation of palladium(0) being much slower at the limit of water concentration. The apparent rate constants are derived from the point where the gradient becomes linear, neglecting the initiation period. Figure 19 demonstrates the first-order dependence in water concentration. Both of these observations are also

consistent with pseudo-first-order bimolecular equilibrium, such as S_N2 mechanism catalytic in palladium(0).

So far we have shown both inversion and palladium exchange events are occurring with the same rate, consistent with a S_N2 mechanism where they occur in the same step. We have determined that the reaction is first-order with respect to both **61** and water. We are assuming the nucleophilic addition to **61** is fast with water, and is generating the palladium(0), however we have no evidence for the isomerisation being catalysed by palladium(0) and not by direct reaction of water.

2.1.5 Gaining evidence for the involvement of palladium(0)

2.1.5.1 Addition of tetrakis(triphenylphosphine) palladium(0)

If the active species is palladium(0), addition of an unlabelled source of palladium(0), such as **85**, Scheme 33, would result in the formation of the complexes *d*$_3$-**61**. Indeed this is the case, upon addition of 10 mol% of $(PPh_3)_4Pd(0)$ to a solution of *cis*-*d*$_3$-^{108}Pd-**61** in anhydrous benzene, approximately 10% of *d*$_3$-**61** was observed by mass spectrometry, and a 1: 1 mixture of the *cis* and *trans* diasteroisomers, *cis*-**61** and *trans*-**61** was observed by NMR.

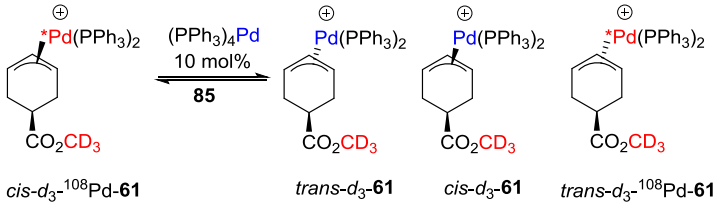

Scheme 33: Incorporation of an unlabelled palladium(0) into cis-d$_3$-^{108}Pd-***61***

This is direct evidence for the incorporation of palladium(0) into the palladium(II) π-allyl complexes, however it was too fast to monitor by either ESI-MS or NMR with 10 mol% (0.5mM) $(PPh_3)_4Pd(0)$. Unfortunately, the high concentrations of $(PPh_3)_4Pd(0)$ were required to observe the unlabelled *d*$_3$-**61** complex by ESI-MS.

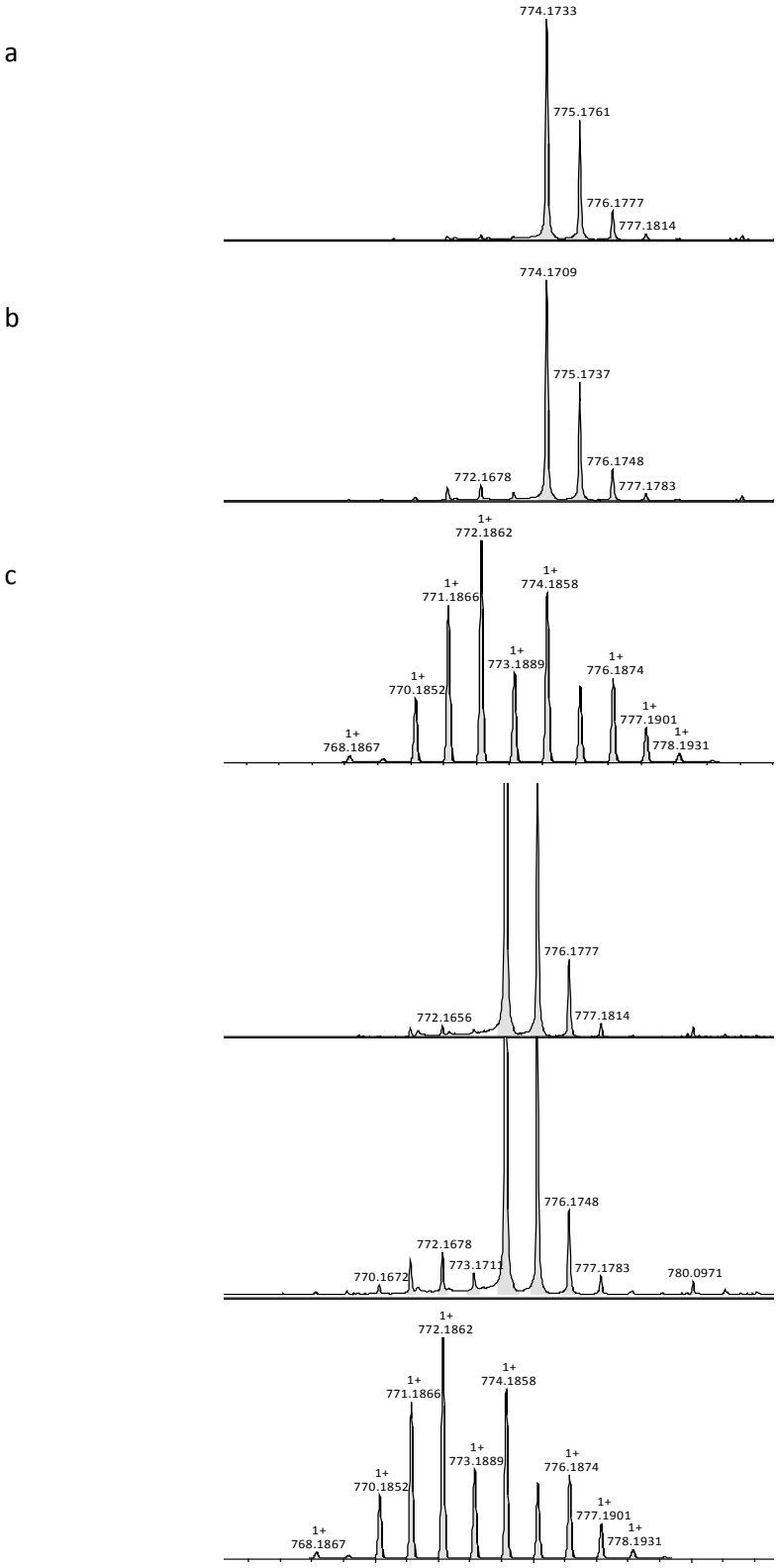

Figure 20: ESI-MS. a. d_3-^{108}Pd-***61***, *b.* d_3-^{108}Pd-***61*** *+ .* d_3-***61*** *c.* d_3-***61*** *calculated. Right: a and b zoomed in to highlight increase of peaks at 771, 772 and 773 mass units.*

Figure 20a shows the ESI-MS of d_3-^{108}Pd-**61** before the addition of $(PPh_3)_4Pd$, Figure 20b is the ESI-MS of d_3-^{108}Pd-**61** after the addition of $(PPh_3)_4Pd$, and shows an increase in relative intensity of the peaks at 771, 772 and 773 mass units. The peaks at 771 and 773 were below the detection level in the reference spectra a, 772 was observable at 1.1%. The intensities of the peaks at 771, 772 and 773 increased to 2.0%, 2.9% and 1.7%, and correspond to the ^{105}Pd, ^{106}Pd and the $^{13}C_1$-^{106}Pd peaks of the ^{108}Pd-**61** complex respectively. The calculated reference spectrum of ^{108}Pd-**61** is shown in Figure 20c.

2.1.5.2 Addition of diphenylacetylene and dibenzylideneacetone

If the active species is a low ligated palladium(0), addition of a weakly coordinating ligand should retard the isomerisation. It was found that a large excess (> 10 equivalents) of diphenylacetylene or dibenzylideneacetone (dba) added to an isomerising solution of **61** in benzene significantly slowed the isomerisation, with no significant further isomerisation observed over 40 minutes with the latter.

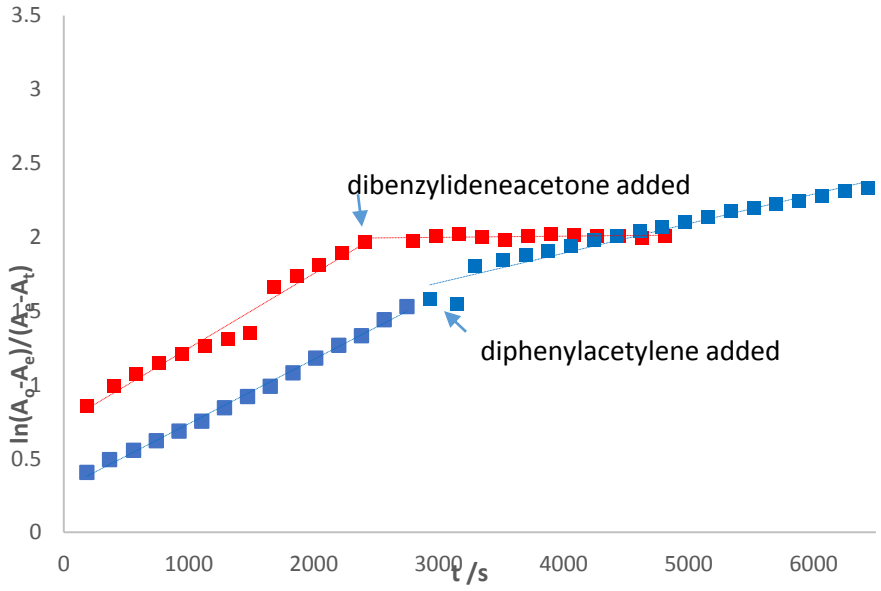

Figure 21: dibenzylideneacetone and diphenylacetylene inhibit the isomerisation of palladium allyl.

The rate of isomerisation depends on the concentration of $L_2Pd(0)$ and the addition of a ligand such as dba or diphenylacetylene generates an equilibrium, Scheme 34. The equilibrium constant of equation 1 is greater than 2, (K_1>K_2), so the concentration of $L_2Pd(0)$ is lower when dba is used resulting in a greater impedance of isomerisation. This is analogous to Jutand's findings where there was a difference between the sources of palladium(0).[38a]

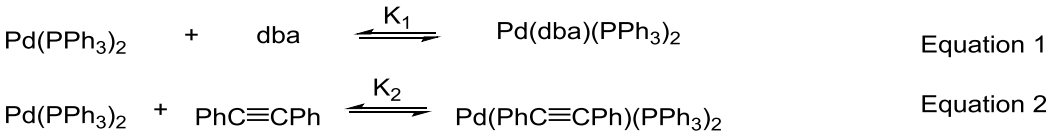

Scheme 34: Complexation of dba or diphenylacetylene to the coordinatively unsaturated $(PPh_3)_2Pd$ generates a less reactive species

2.1.5.3 Stoichiometric addition of water – identification of the organic component

If addition of water to *cis*-**61** does result in the nucleophilic addition of water to the allyl moiety, the *trans*-allylic alcohol should be observable by ^{1}H NMR. A stoichiometric addition of water to a sample of *cis*-**61** in benzene, with an excess of dba and Hünig's base was analysed by ^{1}H-^{13}C HSQC. A gradual but distinctive colour change from bright yellow, characteristic of the dba, to a deep red was observed, as well as partial conversion to the allylic alcohol. Unfortunately, the distinctive allylic peaks of the alcohol were obscured by the broad water peak under these basic conditions, and isomerisation of the *cis*-**61** was occurring as the HSQC experiment was running, and so only a mixture of the *cis*- and *trans*-alcohols was observed. Complete conversion to the allylic alcohols was observed after 12 hours at room temperature.

2.1.6 The effect of bidentate phosphine ligands

Bäckvall suggested that the palladium(0) catalysed isomerisation was slower when bidentate ligands are employed, however there is no real evidence to support this. A sample of **61** and **85** in benzene was analysed at regular intervals over two hours, again using the residual water in the solvent as a nucleophile. We expected to observe **61** isomerising at a faster rate than **85**, the relative rates would indicate a difference in the rates of isomerisation without the error in adding equal volumes of water to each sample. Unexpectedly, neither complex displayed any change in this *cis* to *trans* ratio over the 2 hour period.

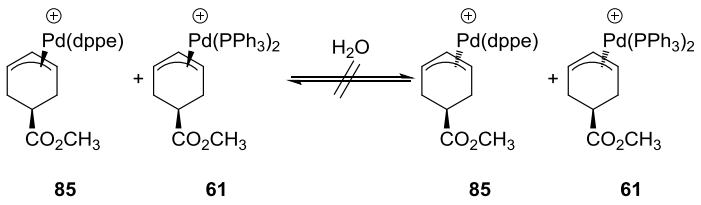

*Scheme 35: A competition study between **61** and **85**, **85** appears to inhibit the isomerisation of **61***

We propose that with bidentate ligands a different mechanism is operating; the $(PPh_3)_2Pd(0)$ is a soft nucleophile and attacks **61** at carbon, however the (dppe)Pd(0) species is a hard nucleophile and attacks at palladium to afford the dinuclear palladium(I) species. The equilibrium to form the palladium(I) dinuclear species is favourable, and acts to remove the active $(PPh_3)_2Pd$ or (dppe)Pd species from solution and inhibits the isomerisation.

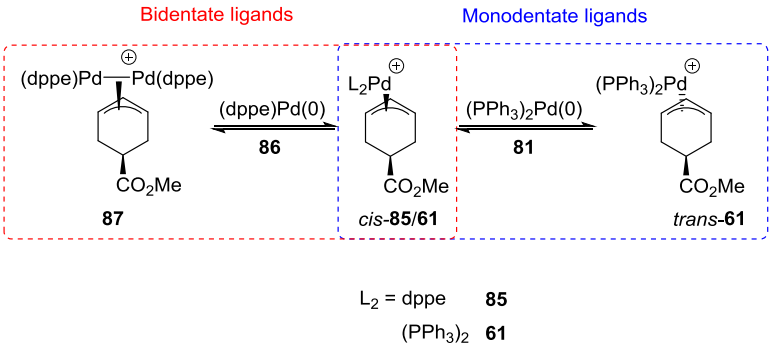

Figure 22: Monodentate ligands render the Pd(0) centre soft and the Pd(0) attack at carbon in a S_N2 mechanism. Bidentate Pd(0) complexes are harder nucleophiles and the Pd(0) attacks at palladium, forming a palladium(I) dinuclear complex

To gain evidence for this hypothesis, geometries were optimised at the BP86/BS1 level with the 6-31G** basis set on carbon, phosphorus, and hydrogen and SDD on palladium, for $(dppe)Pd^0$ **86** and $(PPh_3)_2Pd^0$ **81** (calculations performed by Dr Andrew Leach, Liverpool John-Moores University).[48]

The calculations show that for the linear $(PPh_3)_2Pd$ complex, **81** the highest occupied molecular orbital (HOMO) on palladium is the d_{z^2} orbital, and the electron density is fairly dispersed over the palladium. In the case of the (dppe)Pd complex, **86** however, the P-Pd-P angle is not 180° due to the steric constraints of the ligand backbone. This allows for σ-donation of the lone pairs into the d_{xz} orbital, however since this is an out-of-phase interaction the d_{xz} orbital is raised in energy and becomes the HOMO.[49] The non-linear orientation of the ligands also allows for more efficient orbital overlap of the d_{yz}, d_{xy}, and $d_{x^2-y^2}$ orbitals with the π-accepting orbitals on the ligands, allowing for greater π-backbonding. In the d_{xz} orbital the electron density is much more localised and so becomes a harder nucleophile. It could also be envisaged that the d_{xz} orbital would form a more efficient overlap with the d-orbitals on the palladium than the soft d_{z^2} orbital.

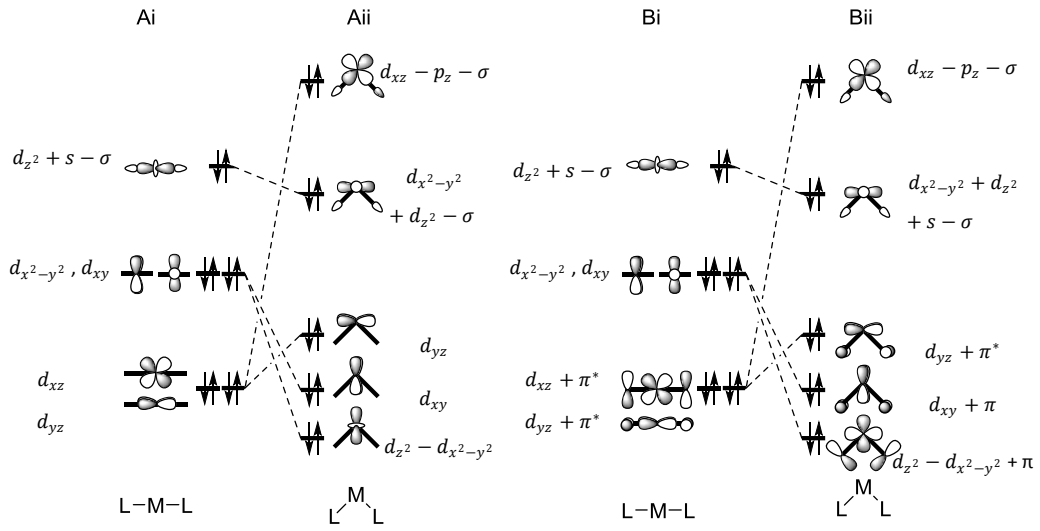

Figure 23: Simplified Walsh diagram. Ai: L_2M linear. Aii: L_2M with 90° bite angle. A) with π-backbonding not considered. B) π-backbonding considered.

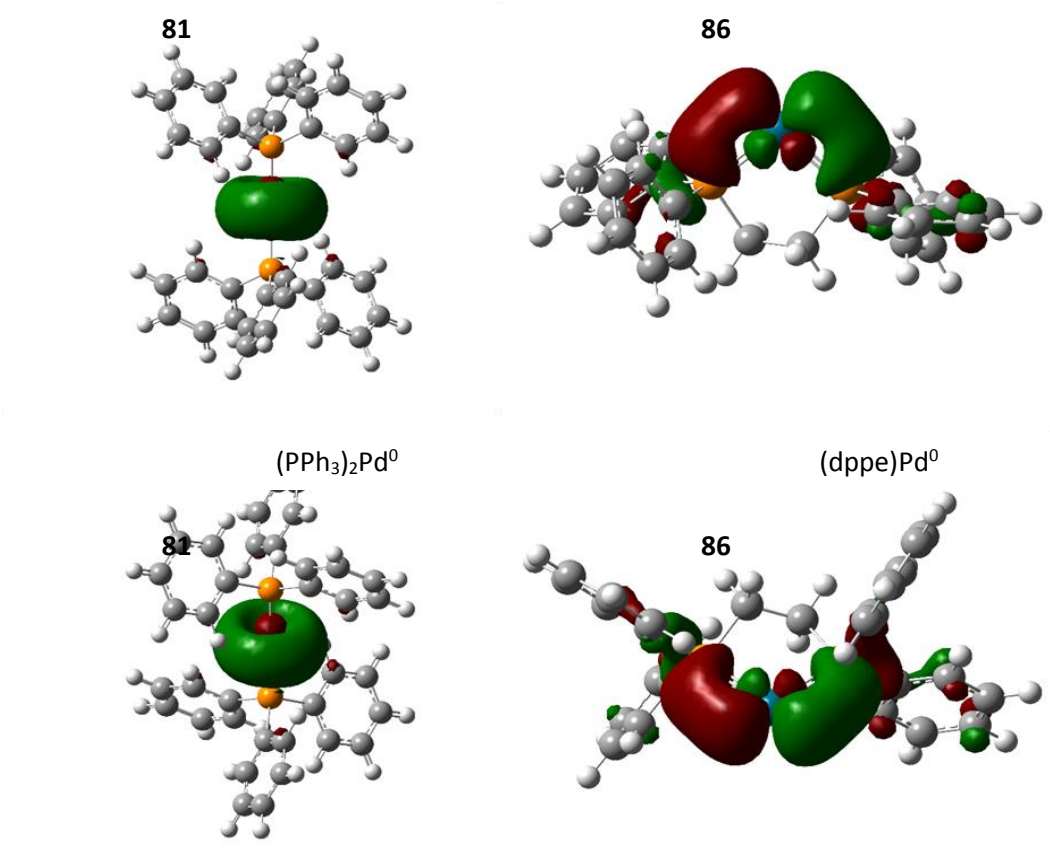

Figure 24: Optimised geometries for $(PPh_3)_2Pd$ and (dppe)Pd with calculated HOMO shown. Calculations performed by Dr Andrew Leach. Blue: Palladium, Orange: Phosphorus, Grey: Carbon, White: Proton.

The P-Pd-P angle in the optimised (dppe)Pd complex is 99°, where as in the $(PPh_3)_2Pd$ P-Pd-P angle is 180 °. The π-backbonding into the ligand is visible in the optimised (dppe)Pd(0) complex in the elongation of the palladium orbitals towards the phosphorus centres, and also by the partial electron density on the phenyl ring, neither of which are significant in the $(PPh_3)_2Pd$ complex.

2.1.7 Initial studies and synthesis of labelled materials

For the initial studies, the isomerisation of ^{108}Pd-**80** and d_5-**80** complexes was determined by mass spectrometry. The d_5-allyl was chosen to provide a large mass shift, with the expectation that the deconvolution of the resulting spectra would be simpler, and a substoichiometric amount of sodium malonate was added to generate a small amount of both labelled and natural abundance palladium(0). In this system the isotope scrambling by ESI-MS can be monitored as described before, but we could not study the stereochemistry.

2.1.7.1 Synthesis of the bis(triphenylphosphine) palladium allyl complexes

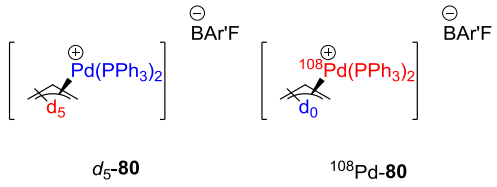

Scheme 36: d_5 **80** and ^{108}Pd-**80**

^{108}Palladium was available as metallic beads which, upon dissolution in aqua regia affords ^{108}palladium dichloride in a quantitative yield, Figure 25. Treatment of the palladium dichloride with allyl chloride and sodium chloride in water provides the π-allyl ^{108}palladium chloride dimer **89**, an ion exchange with sodium BAr'F in dichloromethane and acetonitrile yields the bis(acetonitrile) allyl ^{108}palladium chloride complex **90**, and the slow addition two equivalents of triphenylphosphine yields the desired bis(triphenylphosphine) allyl ^{108}palladium BAr'F ^{108}Pd-**80**. Crystallisation by vapour diffusion with tetrahydrofuran and pentane affords off-white needle-like crystals.

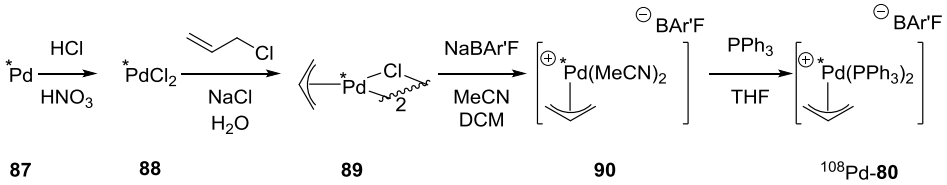

*Figure 25: Synthesis of ^{108}Pd-**80**. * = ^{108}Pd*

The synthesis of the bis(triphenylphosphine) d_5-allyl palladium BAr'F d_5-**80** was less trivial. Treatment of d_6-ethylene glycol with benzoyl chloride in the presence of potassium carbonate and catalytic dimethyltin dichloride affords the d_4-ethylene glycol monobenzoate **91**.[50] The oxidation step was more challenging and a variety of oxidation conditions were attempted (including IBX, Swern oxidation, PCC, Manganese dioxide, TEMPO and bleach, Collins reagent, sodium periodate, and TPAP/NMO). The final conditions employed were TEMPO in dichloromethane with iodobenzene diacetate as the stoichiometric oxidant. It was found that the presence of 20 mol% pinacol improved conversion of **92**.

Wittig olefination of the d_3-2-oxo ethyl benzoate with d_3-methyltriphenylphosphonium iodide and potassium hexamethyldisilazide in tetrahydrofuran generates the d_5-allyl benzoate **93**, although a deterioration of deuterium incorporation was observed, possibly due to protonation by excess hexamethyldisilazide present in the base.

The d_5-allylpalladium(II) chloride dimer was synthesised by an *in-situ* hydrolysis of the allyl benzoate with sodium hydroxide in ethanol water, followed by addition of HCl and THF. Addition of lithium chloride to palladium dichloride in water affords the lithium tetachloropalladate, and these two mixtures are combined before reduction of the lithium tetachloropalladate with carbon monoxide to afford the d_5-allylpalladium(II) chloride dimer. From here the synthesis of d_5-**80** is as described for the ^{108}Pd-**80**.

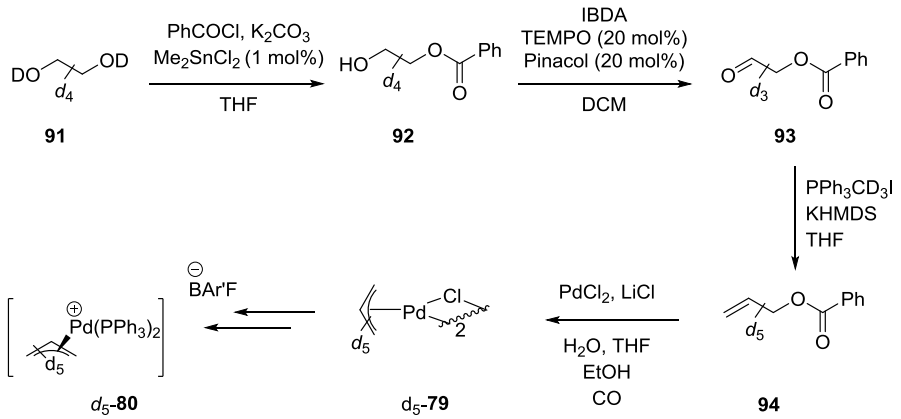

*Figure 26: Synthesis of d_5-**80***

2.1.7.2 Isomerisation of [Pd(π-allyl)(triphenylphosphine)$_2$][BAr'F]

The isotope scrambling of the bis(triphenylphosphine) π-allyl palladium complex was studied by ESI-MS. The complex ^{108}Pd-**80** and d_5-**80** was pre-mixed in THF, in a Schlenk tube under an atmosphere of dinitrogen in a fumehood. Sodium malonate in THF (1 mol%) was added and

the mixture sampled, quenched into a 1: 1 THF: acetonitrile mixture and cooled to 0°C in an ice bath.

Deconvolution of the data was complicated by the deuterium incorporation in the d_5-allyl, we could not simply add or subtract 5 from the reference sample as we could with the palladium(II) d_3-cyclohexenyl complex **61**. However, comparison of the two main peaks, 673 and 678, give us an estimate of the extent of equilibrium, Figure 27. The pale blue and pale orange data points are the theoretical start and end relative intensities of the peaks at 673 and 678 respectively. The theoretical values were calculated assuming a 1: 1 ratio of ^{108}Pd-**80** and d_5-**80** were mixed and that the equilibrium mixture contains 25% of each complex. The blue and orange data points are the experimentally determined relatively intensities of the peaks at 673 and 678 over time.

Figure 27 shows by the first data point, as soon as the sample was mixed and before the sodium malonate was added, some isotopic scrambling has taken place. By the second data point at 1 minute the isotopic scrambling has reached a maximum, but not equilibrium. The aliquots were removed from the Schlenk tube under a flow of nitrogen, and palladium black was observed at the bottom of the Schlenk tube. It is possible that this sampling technique brought enough water from the atmosphere to reach a critical concentration of palladium(0), which could aggregate and precipitate as “palladium black”, rendering it inactive. However, despite the limitations, this experiment confirms that the isotopic scrambling is taking place in another system, and not unique to the cyclic allyl complex described in earlier.

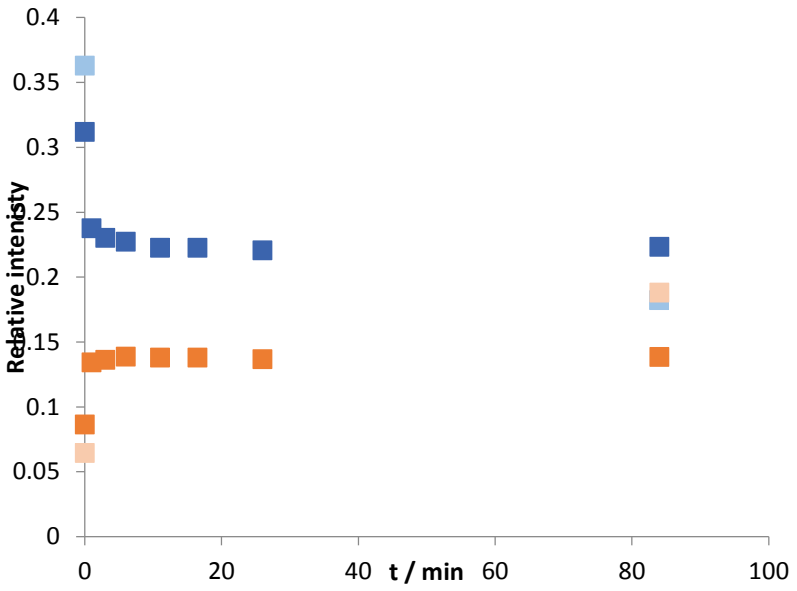

Figure 27: Comparision of peak at 673 versus peak at 678 as an indication of extent of equilibrium. Pale blue: Theoretical starting and end point, peak 673. Pale Orange: Theoretical starting and end point, peak 678. Blue: Peak 673 versus time. Orange: Peak 678 versus time.

2.1.7.3 *Synthesis of the bis(triphenylphosphine) (5-carboxyl, 1,2,3-η³-cyclohexenyl) palladium complexes*

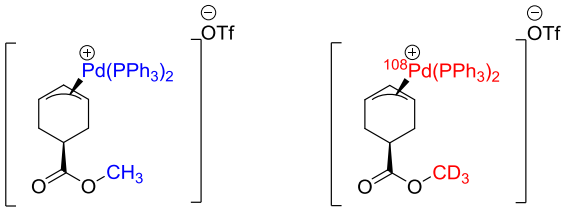

cis-**61** *cis*-d_3-^{108}Pd-**61**

As the initial attempts to follow the isomerisation of the bis(triphenylphosphine) palladium allyl **80** by mass spectroscopy were unsuccessful, the diastereotopic complex **61** used by Bäckvall and co-workers was employed to allow the process to be simultaneously studied by NMR spectroscopy. The synthesis of the methyl cis-5-hydroxycyclohex-3-enecarboxylate was simple and highly stereoselective using known methods with a few modifications. Iodolactonisation of the 3-cyclohexene-1-carboxylic acid efficiently affords the 4-iodo-6-oxabicyclo[3.2.1]octan-7-one, and elimination of hydrogen iodide with 1,8-diazabicyclo[5.4.0]undec-7-ene yields the 7-oxa-bicyclo[3.2.1]oct-2-en-6-one. Methanolysis of the lactone, mediated by potassium carbonate, affords the methyl cis-5-hydroxycyclohex-3-enecarboxylate, and replacing the methanol with d_4-methanol affords the d_3-methyl isotopologue. The allylic alcohol **83** was subjected to triphenylphosphine and N-chlorosuccinimide at 0°C to yield the *trans*-3-chloro-5-methoxyhexene with good diastereoselectivity. It was found that lower temperatures throughout the reaction and isolation maximised the diastereotopic ratio, and adding the cyclohexenyl alcohol to the pre-formed the phosphonium chloride allowed for better temperature control and so higher diastereoselectivity. An excess of N-chlorosucciniminde was added once the reaction was complete, to oxidise any remaining triphenylphosphine and simplify the purification.

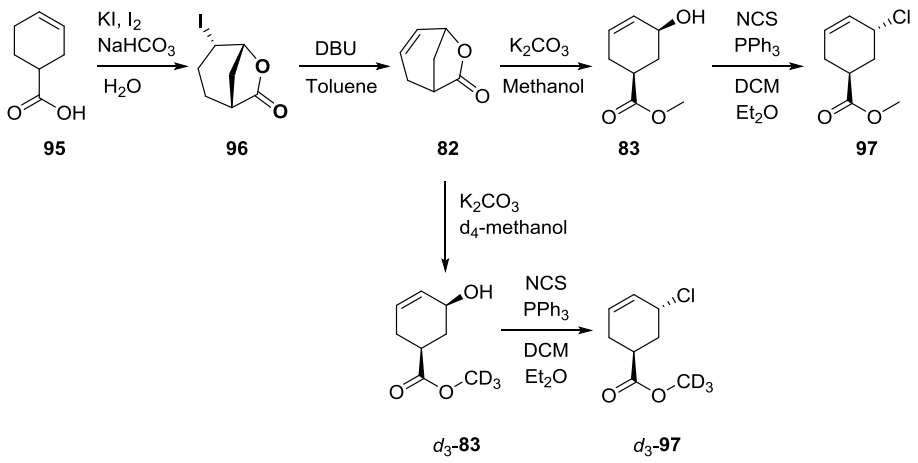

*Scheme 37: Synthesis of **97** and d_3-**97***

The palladium dimeric complex **98** was synthesised using carbon monoxide as a reductant, followed by an oxidative addition into the cyclohexenyl chloride **97,** analogous to the preparation of the labelled material described in section 2.1.7.1, however it was found that reversing the order of addition gave marginally higher yields. Chloride **97** was dissolved in a tetrahydrofuran/ethanol mixture, a balloon of carbon monoxide was fitted to the flask via a needle and septum, and the tetrachloropalladate was added as a solution in water.

An ion exchange with silver triflate in tetrahydrofuran affords the palladium(II) complex **99**. This complex was unstable at room temperature and so used immediately. Upon dissolution in toluene, and addition of a slight stoichiometric deficiency of phosphine, the bis(triphenylphosphine) (5-carboxyl, 1,2,3-η^3-cyclohexenyl) palladium triflate complex *cis*-**61** precipitated from solution. The off white powder was stored in the glovebox and used as required. The last two steps were found to be extremely sensitive to water - the isolation of **61** was effective, however upon dissolution, rapid isomerisation to a 50: 50 mixture of *cis* and *trans* isomers was observed without thorough drying of all the solvents and glassware. To prevent this, all starting materials were dried under vacuum for a minimum of 6 hours and stored in the glovebox, solvents were dried by storing over molecular sieves for a minimum of 72 hours, glassware was dried in an oven at 200 °C overnight, or in a 80 °C oven for at least 24 hours and all manipulations were carried out under nitrogen in the glovebox.

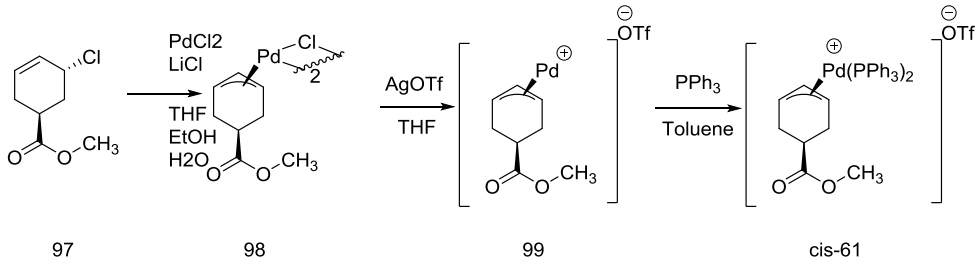

*Scheme 38: Synthesis of cis-**61***

The synthesis of the labelled complex d_3-^{108}Pd-**61** was as described above, using the d_3- **97** and $^{108}PdCl_2$

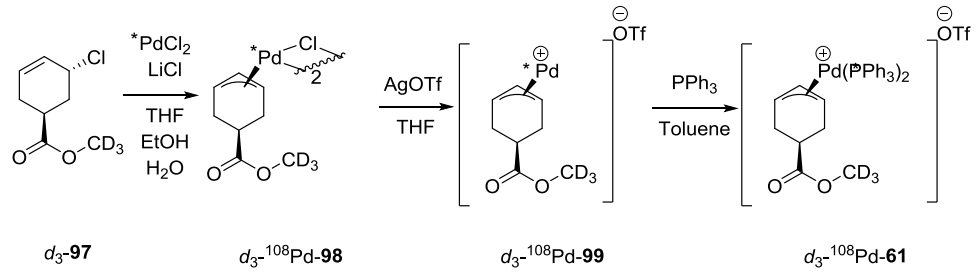

*Scheme 39: Synthesis of cis-d_3-^{108}Pd-**61**. * = ^{108}Pd*

Bäckvall's reported procedure omitted key details in the synthesis of the bidentate complexes **61** and the sensitivity of these complexes.[17a] For the kinetic experiments regarding the isomerisation of the complexes, the *in situ* generation from the palladium dimeric complex **98** was described. It was noted that the phosphine was added at low temperatures, with minimal warming to allow dissolution, and the source of Pd(0) was added at low temperatures. The isolation of the complexes was not described, nor was the synthesis of the thermally stable complex **61**, or the length of time this complex was monitored for, described in entries 8 and 9, Table 1, section 2.1.1.1.

During our initial attempts at the synthesis of *cis*-**61**, we obtained very inconsistent results. With vigorous drying of the solvents from sodium benzophenone, or storing the solvents over molecular sieves, **61** could be obtained as a 9: 1 *cis* to *trans* ratio in chloroform, with an increase in *trans*-**61** of 5% over 22 hours. A solution *cis*-**61** could not be obtained as a single diastereomer, and certainly not consistently. We found a slight excess of phosphine results in very rapid isomerisation, as does use of solvents dried insufficiently.[51]

Initially, we chose chloroform as the solvent for the kinetic experiments as most of the previous work by Bäckvall and Jutand[38] was performed in chloroform, however when adding the $(PPh_3)_4Pd(0)$ as a stock solution, the initial concentration of the $(PPh_3)_4Pd(0)$ greatly

affected the rate of isomerisation, and the isomerisation would stall. This was due to the oxidative addition of the Pd(0) to the chloroform.[52] The conditions described above, with vigorous drying and a slight stoichiometric deficiency of phosphine resulted in the precipitation of a complex that could be stored in the glovebox and used in the kinetic experiments as required.

3 Conclusions and Future work

3.1 Conclusions

The isomerisation of the palladium(II) π-allyl complexes, *via* palladium(II) or palladium(0)-mediated mechanisms, has implications in the stereoselectivity of the asymmetric allylic alkylation.[19, 53] Rapid enantiofacial exchange of the palladium(II) π-allyl intermediate allows for equilibration before nucleophilic addition when chiral ligands are employed as the method of asymmetric induction.[11c] Conversely, when chiral olefins and achiral ligands are employed, slow isomerisation of the palladium(II) π-allyl intermediate, and fast nucleophilic attack allows for high retention of enantioselectively.[17a] Many mechanisms of the isomerisation of palladium(II) π-allyl complexes *via* palladium(II) intermediates such as the rotation of palladium(II) η^1- allyl complexes,[54] ligand dissociation,[14] or pseudorotation of a pentacoordinate intermediate[15] are well known and have been extensively investigated. The palladium(0) mediated mechanism, however, has been less extensively studied and several mechanisms have been proposed.

Three possible outcomes of the addition of palladium(0) to a palladium(II) π-allyl intermediate were identified:

1. Nucleophilic attack of Pd(0) occurring at a carbon of the allyl moiety, resulting in an S_N2-like displacement of palladium and an inversion of stereochemistry, proposed by Bäckvall[17a] and Jutand.[38]
2. Pd(0) attack occurring at the Pd(II) centre, resulting in the formation of a palladium(I) dinuclear complex.[40-41] Formation of this complex would not result in isomerisation.
3. S.E.T. from Pd(0) to the Pd(II), resulting in a Pd(I) radical cation and a Pd(I) with an allylic radical. Epimerisation of the allylic radical and S.E.T. back to the Pd(I) radical cation would result in isomerisation of the palladium(II) π-allyl intermediate.[39]

Using the *cis*-d_3-^{108}Pd-**61**, and the unlabelled *cis*-**61**, we were able to compare the rate of *cis*-*trans* isomerisation of **61**, to the rate of isotopic scrambling. It was found that the rate of *cis*-*trans* isomerisation was twice the rate of isotopic scrambling, ruling out the formation of the palladium(I) dinuclear complex, mechanism **2**, and the S.E.T, mechanism **3**, and is consistent with the S_N2 mechanism, **1**. The isotopic scrambling was also confirmed with ^{108}Pd-**80** and d_3-**80** by ESI-MS, providing evidence for the Pd(0) isomerisation in another allylic system.

Titration of water to *cis*-**61**, generating a small, known amount of Pd(0) and *in-situ* NMR analysis confirmed that the process is a pseudo-first order, bimolecular equilibria. Analysis of

the concentration of *cis*-**61** and *trans*-**61** over time confirmed the process is first order in **61**. The observed rate constant, k_{obs} increased linearly with the water concentration, consistent with the nucleophilic addition of water to **61**, generating Pd(0). The pseudo-first order, bimolecular equilibrium is consistent with the S_N2 mechanism.

We were able to gain further evidence that Pd(0) is responsible for the isomerisation, rather than direct reaction of water using d_3-^{108}Pd-**61**. Addition of $(PPh_3)_4Pd(0)$ to d_5-^{108}Pd-**61** resulted in the formation of d_3-**61**, observed by ESI-MS. Furthermore, addition of a stoichiometric amount of water to **61** resulted in the formation of the cyclohexenyl alcohol, which was observed by HSQC, providing further evidence for the proposed nucleophilic addition of water to **61**, generating Pd(0).

Bäckvall found the isomerisation of **61** was slower when bidentate ligands were employed, however the published data relating to this observation is limited and it is not explained by the current mechanistic proposal. We were able to confirm that **85** does not isomerise upon the addition of water, suggesting another mechanism is also present. We propose **81** is a soft nucleophile. Computational experiments, performed by Dr Andrew Leach suggest that **81** is linear, with the dispersed d_{z^2} orbital as the HOMO, whilst the constricted backbone of the dppe in **86** forces the P-Pd-P bond angle to 99°. The anti-bonding interaction between the d_{xz} orbital and the ligands raises the energy of this orbital to the point where this more localised orbital becomes the HOMO. **81** reacts with **61** in the way soft nucleophiles react with palladium π-allyl complexes, by nucleophilic addition at a terminal carbon on the allylic moiety, displacing the palladium and resulting in isomerisation. **86** reacts with **85** as a hard nucleophile reacts with palladium π-allyl complexes, by addition to the palladium and forms a palladium(I) dinuclear species. As this is a *syn* addition, it does not result in isomerisation.

3.2 Future work

Our previous investigations suggested that nature of the ligands on the Pd(0) determine whether it reacts as a hard nucleophile in a *syn* addition to from the palladium(I) dimer, or as a soft nucleophile in an S_N2-type fashion, resulting in isomerisation. We would like to confirm this is a steric constriction effect, as described in section 2.1.6, rather than an electronic difference between the triaryl triphenylphosphine ligand and the biaryl alkyl dppe ligand. If this hypothesis is correct, a ligand such as 1,2-bis(diphenylphosphino)benzene would display similar reactivity to **85** and **86** and form the palladium(I) dinuclear species due to the constriction of the backbone, rather than displaying similar reactivity **61** and **80**. By a similar argument, the ethyldiphenylphosphine complex **100** would display similar reactivity to **61** and **80**, and undergo the S_N2-type mechanism to displace the palladium resulting in isomerisation due to the ability of the phosphine ligands to adopt a linear conformation.

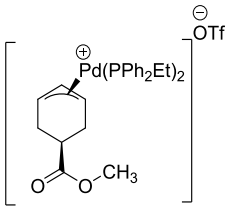

Figure 28: Cis-***100***

It would be interesting to apply the trends in reactivity we have discovered to catalytic systems. Perhaps the use of mono-dentate, chiral ligands will reduce memory effects, as the linear conformation of the ligands would allow the isomerisation to proceed *via* a palladium(0) mediated S_N2 mechanism, providing faster equilibration of the palladium π-allyl intermediate and reducing the contribution of the mis-matched substrate. On the other hand, the use of simple bidentate ligands such as dppe, or the use of a $Pd.dba_2$ pre-catalyst might retard the isomerisation and afford greater retention of stereoselectivity when chiral substrates are used.

Solvent choice may also be important, benzene was chosen as the solvent for the kinetic experiments as the isomerisation was relatively slow and allowed for monitoring by ESI-MS. Bäckvall suggested that more polar solvents lead to faster isomerisation, the relative rates in solvents more commonly used in the asymmetric allylic alkylation reactions, such as THF, DCM, or DME, may provide some useful catalytic implications as to the best solvent choice depending on the requirements of the system.

4 Heteronuclear NMR

Analysis of the initial kinetic experiments described in the previous section highlighted discrepancies in quantification of the ^{31}P NMR experiment; a nuclear Overhauser effect was observed when a decoupling pulse was applied. In this chapter, we present a short introduction to heteronuclear NMR and the methods of proton decoupling commonly used, and in the subsequent chapter, a description of our investigations and conclusions that led to the final parameter set employed throughout the kinetic experiments described in the previous section.

For simplicity we will consider the vector model. The B_O stationary field is along the z-plane; diagram a, Figure 29. There is no net transverse magnetisation at equilibrium, however there is a small preference for the spins to be aligned along with the B_O field, and so a small net magnetisation along the *z*- axis. The size of the z- magnetisation at equilibrium depends on the number of spins, the gyromagnetic ratio and the size of the applied field.

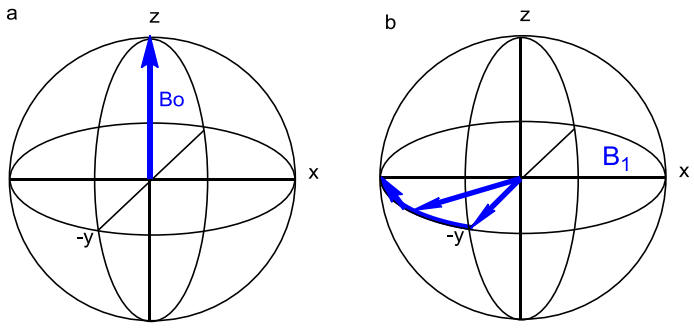

Figure 29: Visualisation of the pulse direction net magnetisation vector during a pulse sequence

Application of a radiofrequency (RF) pulse rotates the bulk magnetisation towards the -transverse plane (a 90° pulse about *x*- axis will bring the magnetisation towards –*y* axis). The spins precess about the *z*-axis; diagram b, Figure 29. The pulse applied is at the centre point of the Larmor frequency range of the nuclei we wish to excite. When the RF pulse is removed, it is the precession of the spins at the Larmor frequency that gives rise to the oscillations observed in the free induction decay (FID). Fourier transformation of the FID results in a spectrum with peaks at chemical shifts corresponding to the Larmor frequency of the individual nuclei.

The simple, single pulse, sequence consists of a relaxation time (d_1) where all spins are allowed to reach equilibrium, a RF pulse to rotate the bulk magnetisation towards the transverse plane and an acquisition time (at) where the FID is collected; Figure 30.

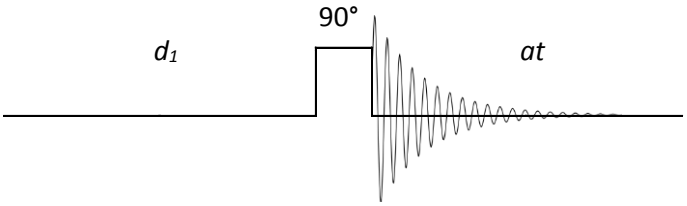

Figure 30: 1D Pulse sequence

4.1.1 Relaxation

Relaxation is the process by which the bulk magnetisation returns to the equilibrium. At equilibrium there is no net transverse magnetisation and so the spins are orientated randomly in the *xy*- plane. There is a small *z*- magnetisation at equilibrium along the direction of the B_O field. The spins aligned against the field are at a higher energy to the spins aligned with the field, and the population of the energy levels at equilibrium are predicted by the Boltzmann distribution. The return of the *z*- magnetisation to the equilibrium position is known as the *longitudinal relaxation* or the *spin-lattice relaxation*, as it is the flow of energy from the spins and the molecular motion of the surroundings (the lattice) that gives rise to this relaxation. The relaxation time constant for the z- magnetisation is described as T_1. The relaxation in the *xy*- plane is known as the *transverse relaxation* or the *spin-spin relaxation* and the relaxation time constant described as T_2.

To rotate the magnetisation back towards the *z*- axis, we require a transverse magnetic field at or near to the Larmor frequency. Appling a second RF pulse would have this effect, but this is simple spin manipulation and not natural relaxation. Oscillating fields occur naturally within the sample and act in the same way as RF pulses to relax the sample. The sources of the local fields within the sample are known as relaxation mechanisms; paramagnetic species, chemical shift anisotropy and the dipolar mechanism are a few common relaxation mechanisms.

4.1.1.1 Dipolar Relaxation Mechanism

This is the interaction of a spin with the magnetic moment of a neighbouring spin. The size of the local field due to the spin depends on a number of factors:

- The distance *r* between the two spins; the interaction falls off with $(1/r^3)$.

- The gyromagnetic ratio of the spin; spins with larger magnetic ratios have large magnetic moments and hence larger local fields.
- The orientation of the two spins with relation to the *z*- axis.

The rate at which the magnetic moment rotates depends on the Larmor frequency of the rotating nucleus, and so the overall strength of interaction of the dipoles depends on gyromagnetic ratio of both nuclei.

4.1.1.2 Chemical shift anisotropy

In a strong magnetic field, the electrons in a molecule give a small induced local field at the nuclei. The nucleus experiences the sum of the applied field and this small local field, thus shifting the Larmor frequency by an amount which depends on the size of the induced field. The size of the induced field, and hence the size of the induced chemical shift, depends on the orientation of the molecule with respect to the applied magnetic field; the chemical shift is anisotropic. In liquid samples the molecules are tumbling quickly and so we see an average chemical shift (isotropic shift), however at any one time the chemical shift is different for molecules of different orientations.

This has no effect on symmetrical molecules such as isolated atoms or molecules with tetrahedral or octahedral geometry. For unsymmetrical molecules however, the tumbling in solution causes this induced local field to oscillate. If the oscillation is close to the Larmor frequency, this oscillation can act as a relaxation mechanism.

4.1.1.3 Paramagnetic species

In the dipolar mechanism, it was the presence of other nuclear spins that is the source of oscillating local fields. Unpaired electrons also create local fields; the magnetic moment of an electron is much larger than that of a proton and so the local field generated is much larger. Unpaired electrons act as a very effective relaxation mechanism, even in low concentrations. If slow relaxation times are required the sample is usually degassed since oxygen is a paramagnetic species. If faster relaxation times are required paramagnetic relaxation agents such as chromium (III) acetylacetonate are often added to the sample to aid relaxation.

4.1.2 Cross-relaxation and nOe

The dipolar relaxation mechanism considerers the relaxation effect of a nuclear spin in close proximity to the excited spin; in this two spin system cross relaxation can occur, which gives

rise to the nuclear Overhauser effect. Considering an energy level diagram, Figure 31, we have four possible energy levels. α and β are used to represent the ground and excited states respectively. The possibly energy levels are *αα, αβ, βα* and *ββ.* At the *αα* energy level, both spins are in the ground state, *αβ* describes the energy level where spin **1** is ground state and spin **2** is in the excited state etc. If the Larmor frequency of spin **1** and **2** are equal, *αβ and βα* are degenerate*.* A dipolar interaction can lead to a transition between any of these four energy levels.

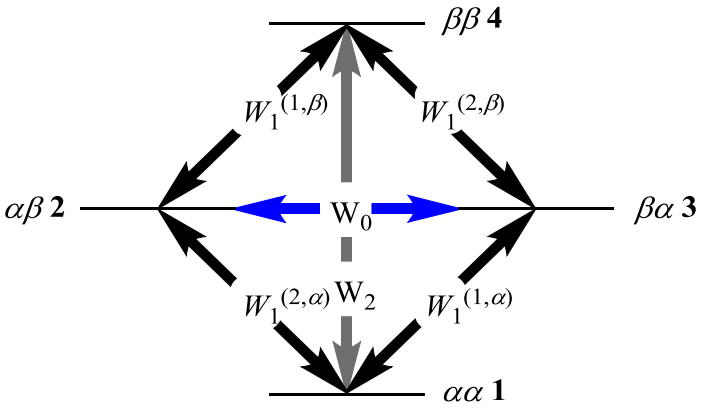

Figure 31: Energy level diagram of two spins interacting through space

Four of these transitions involve a change in quantum number of ±1, i.e. a change of one spin from *α* to *β* or *β* to α, and are known as single quantum transitions, the rate constants W_1 describe the rate of single quantum transitions. There is also one double quantum transition (rate = W_2), involving a change in spins from *αα* to *ββ* or *vice versa,* the change in quantum number is ±2 and one zero-quantum transition (rate = W_0), where the overall change in quantum numbers is 0, i.e. a transition between *αβ* and *βα*.

As the *z*- magnetisation depends on the population difference between the *α* and *β* energy levels, a transition between levels **1** and **3,** and between levels **2** and **4** will result in a change in *z*- magnetisation of spin 1, and similarly a transition between **1** and **2**, and **3** and **4** will result in a change in *z*- magnetisation of spin 2. Some of these transitions result in a transfer of *z*- magnetisation from one spin to another. This through space, relaxation mediated transfer or *z*- magnetisation is called cross relaxation, and is the process which is responsible for the nuclear Overhauser effect (nOe).

The spin receiving the magnetisation is said to have received an nOe enhancement, and the magnitude of the enhancement depends on the cross-relaxation rate constant (σ_{12}), where $\sigma_{12} \propto r^{-6}$ and r^{-6} is the distance between the two spins. The nOe enhancement falls off

rapidly with distance; for protons nOe enhancements are not usually observed from distances greater than 5 Å. Generally for small molecules σ_{12} is positive; the nOe enhancement is seen as an increase in intensity of the peak corresponding to the receive peak.[55]

$$\eta_I\{S\} = \frac{\gamma_S}{\gamma_I}\left[\frac{W_2 - W_0}{W_0 + 2W_1{}^I + W_2}\right]$$

Figure 32: Expression describing steady state nOe

4.1.3 Scalar Decoupling

Carbon-13 NMR is widely used in structural assignment of organic compounds. Scalar couplings can occur between any magnetic nuclei which are close is the bonding network. Coupling is not usually observed between neighbouring carbons due to the low abundance of carbon-13, however coupling between carbons and protons can occur and results in a more complex spectrum with reduced sensitivity.

The coupling interaction can be removed by the continuous irradiation of the protons during the data collection period with a decoupling sequence. The decoupling sequences involve a repeating series of 180 degree pulses, or composite pulses which equate to a 180 degree pulse, which rapidly inverts the spin of the interacting eliminating the direction of the local fields, the most common of which is the WALTZ-16. The simplification of the spectra is very apparent, with decoupling resulting in a single peak at each chemical shift and a greatly enhanced signal-to-noise ratio as the intensity appears as a single line rather than spread over the entire multiplet.

As the decoupling sequence is applied during the whole data acquisition time, the sample may be heated by the absorption of the RF power. The power of the RF pulse required to achieve effective decoupling, and hence the extent of sample heating, is proportional to the range of chemical shifts targeted. Protons have a relatively narrow chemical shift range and so sample heating is not usually an issue when removing coupling due to protons. The energy levels of the decoupled nuclei are no longer at equilibrium and so an nOe enhancement can occur between the decoupled and observed nuclei.

This can be beneficial, for example in the case of carbon-13 where the low abundance and low gyromagnetic ratio result in very poor sensitivity and so a nOe enhancement due to neighbouring protons increases the quality of the spectra. However, nOe enhancement leads

to a spectrum that is no longer quantitative. For quantitative, decoupled spectra the inverse-gated decoupling method was developed.

4.1.4 Decoupled heteronuclear NMR with the nuclear Overhauser effect suppressed

^{13}C NMR spectra are usually used for qualitative analysis in structural determination and so it is unusual that integration of the peaks is important, however there are occasions when accurate integrations are required (for example studying kinetic isotope effects). Any principles applied to ^{13}C NMR can also be applied to other decoupled spectra such as ^{31}P. The addition of a paramagnetic species such as di-*tert*-butyl nitroxide can provide an alternative, more efficient relaxation pathway and reduce the nOe enhancement.[56]

nOe enhancement is a relaxation mechanism and so is relatively slow to build up. The effect of the decoupling pulse in instantaneous and so the decoupled nuclei only need to be irradiated whilst the data acquired. In the inverse-gated decoupling sequence, the decoupling pulse is applied only during the acquisition time, and then equilibrium is re-established during the relaxation delay for both the observed and decoupled nuclei before the next pulse is applied, Figure 33. This method has been extensively applied to ^{13}C spectra[57] and the optimum conditions for acquiring quantitative spectra identified.[58] It is generally accepted that a scan cycle of $5T_1$ is required for complete relaxation of the nuclei before the next pulse is applied,[55a] however the length of time the decoupling pulse is applied for (i.e. the length of the acquisition time) has not been extensively scrutinised in the context of ^{31}P NMR, in the literature.

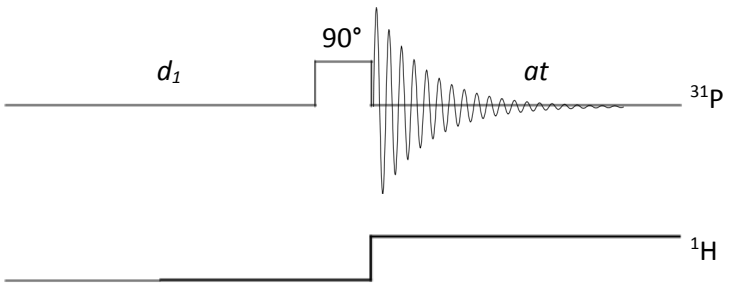

Figure 33: Inverse-gated decoupling sequence for ^{31}P NMR

5 Identification of an nOe enhancement due to decoupling in inverse-gated ^{31}phosphorus spectra.

Based on prior investigations when mixing known stoichiometries of Pd(allyl)L_2 species with other ligands, and the inconsistencies that arose from the intergration of the resulting equilibria, we designed a simple model system in which to estimate the errors in quantitative ^{31}P analysis of such complexes.

A solution of triphenylphosphine oxide (2.24 mg, 0.00805 mmol) and [Bu_4P][BAr'F] (8.96 mg, 0.00798 mmol) in degassed $CDCl_3$(0.8 ml), considering the $^{31}P\{^1H\}$ spectrum, applying the inverse gated decoupling sequence with a 1 second relaxation delay and a 0.66 second aquisition time for 32 scans gave a ratio of 1: 0.63 [Bu_4P][BAr'F]: PPh_3O. When these same parameters were applied but with no decoupling pulse applied a ratio of 1: 0.99 [Bu_4P][BAr'F]: PPh_3O was observed. Unfortunately, overlapping aromatic signals in the proton NMR make accurate calculation of integrations difficult.

A 1D ^{31}P NMR acquisition sequence begins with a relaxation delay to allow the magnetisation to reach equilibrium; at equilibrium there is no net magnetisation about the *xy*-plane but a small net magnetisation in along the *z*-axis. Application of an RF pulse about the *x*-axis brings the net magnetisation towards the -*y*-axis, the length of time this pulse is applied for determines the angle of the pulse. During the acquisition time the FID is collected; if an inverse gated decoupling sequence is used, the decoupling pulse is applied during this period. The relaxation delay allows the magnetisation to return to equilibrium before the pulse is applied again. Each three stage cycle of relaxation delay, pulse and acquisition time is referred to as a scan, and the period this takes is referred to as the cycle time.

The difference in integration between the coupled and decoupled spectra when all other parameters are identical suggests an nOe enhancement due to the decoupling pulse is increasing the intensity of one signal over the other. The inverse gated decoupling sequence is designed to suppress (nuclear Overhauser enhancement) nOe. We have two identified two mechanisms by which this amplification can occur.

i. The nOe builds up during the acquisition time due to the high density of protons about the phosphorus nuclei.

ii. Slow relaxation of the phosphorus allows for excess nOe signal to be carried through to the next scan – we have termed this the "residual nOe".

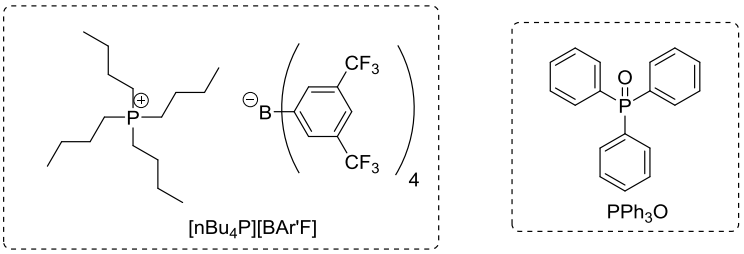

Figure 34: [nBu$_4$P][BAr'F] and PPh$_3$O

The four n-butyl groups about the phosphorus nuclei in the tetra-n-butyl phosphonium BAr'F salt provides a high density of protons held close to the nuclei. As the rate of cross-relaxation is proportional to the number of excited spins, and inversely proportion to r^6 it is reasonable to assume that tetra^{n}butyl phosphonium BAr'F would receive a greater nOe enhancement. Tetra^{n}butyl phosphonium BAr'F is tetrahedral and symmetrical – the relaxation mechanism due to chemical shift anisotropy is suppressed and so T_1 relaxation of the phosphorus nucleus is expected.

5.1 T_1 relaxation measurements by inversion recovery

The T_1 relaxation is the relaxation in the *z* plane and cannot be measured directly, to measure T_1 relaxation times we used an inversion recovery experiment. The experiment consists of the relaxation delay, a 180° inversion pulse, delay period τ, a 90° pulse and an acquisition time where the data is collected.

The 180° pulse will invert spin populations to –*z*. Over time τ, the magnetisation vector will relax back through the *x*-*y* plane towards *z*. If the delay period τ is sufficiently long $\tau_\infty >> 5T_1$ the magnetisation vector will have relaxed completely back to the *z*-axis, a 90° pulse about *x* will place the vector on the -*y*-axis and so relaxation during the FID will result in a signal with the maximum intensity observed.

If $\tau = 0$, the 90° pulse will place the magnetisation vector on the *y*-axis and so a full intensity negative signal will be observed. By increasing τ and monitoring the intensity of the signal, the intensity will increase through zero and back to full intensity by Figure 35, where M_t is the detected magnetisation, M_o is the magnetisation when $\tau = \tau_\infty = 5T_1$.

$$M_t = M_o(1 - 2e^{-\tau/T_1})$$

Figure 35: Equation describing the inversion recovery experiment

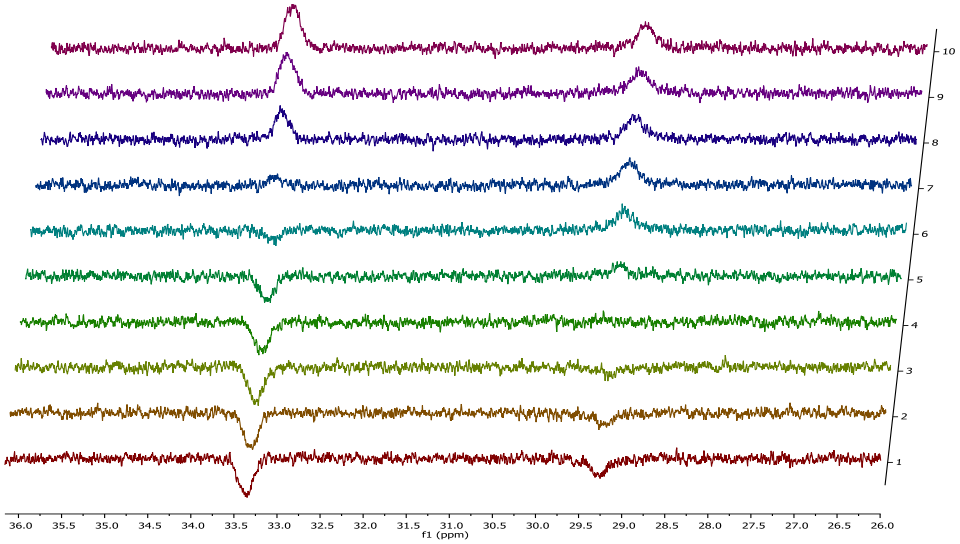

Figure 36: T_1 relaxation of [PBu_4][BAr'F] (33.5 ppm) and PPh_3O (29.3 ppm)

The T_1 ^{31}P relaxation time of [nBu_4P][BAr'F] was calculated to be 5.11 seconds, and 0.80 seconds for PPh_3O.

If the nOe builds up solely during the acquisition time (case *i*), a longer acquisition time should result in a greater nOe enhancement and hence a greater amplification of the [PBu_4][BAr'F] signal with respect to the PPh_3O signal. However, since the two species have significantly different relaxation times, simply varying the acquisition time can lead to truncation of the slow relaxing signal and hence a loss of intensity. A more precise experiment would be to apply the decoupling sequence for a time before the acquisition pulse is applied, Figure 37.

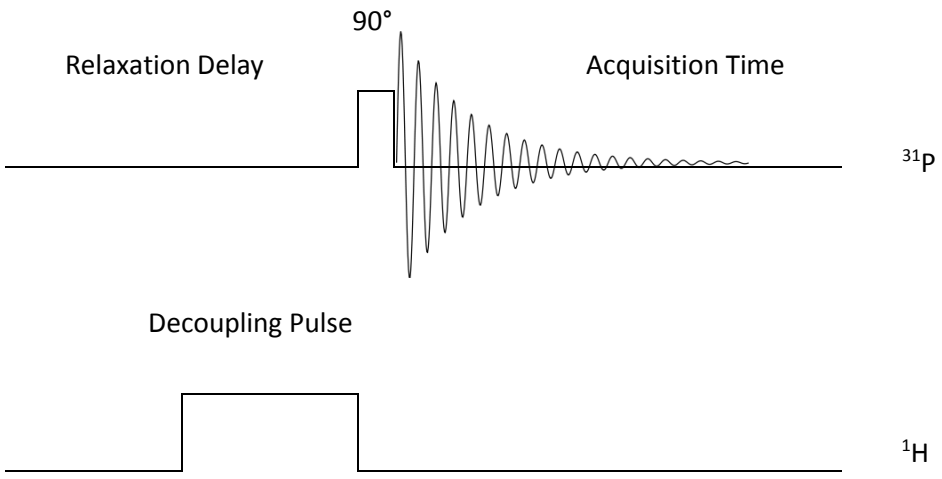

Figure 37: Introducing the decoupling pulse for a period before the pulse is applied

If case *ii* is the mechanism responsible for the nOe enhancement, there are several experiments we could do to prove this.

i. Increasing number of scans: If this mechanism were solely responsible for the enhancement a single scan experiment should provide the "true" ratio; as we increase the number of scans the nOe enhancement will gradually build until it reaches a steady value.

ii. Increasing the relaxation delay: As the relaxation delay is increased the amount of residual nOe should decrease until it reaches the true ratio.

iii. T_1 relaxation time: The ^{31}P relaxation time of the two species should be significantly different.

5.2 Increasing number of scans

For this experiment we chose a one second relaxation delay and a 0.66 second acquisition time (Figure 38, blue data points). Keeping all other parameters identical, the number of scans was increased from 1 to 1024. Here, as the number of scans is increased the intensity of the PPh_3O signal decreases with respect to the $[Bu_4P][BAr'F]$ signal, and that after approximately 16 scans a steady state is been reached. However the ratio of the signal scan experiment is still 1: 0.76 $[Bu_4P][BAr'F]$: PPh_3O; a fully quantitative experiment should give a 1: 1 ratio. We also observed that on increasing the acquisition time from 0.66 seconds to 1.32 seconds (red data points) and 2.64 seconds (green data points) increases the nOe

enhancement further; the steady state ratio of $[Bu_4P][BAr'F]$ to PPh_3O is 1: 0.46 for the 2.64 second acquisition time.

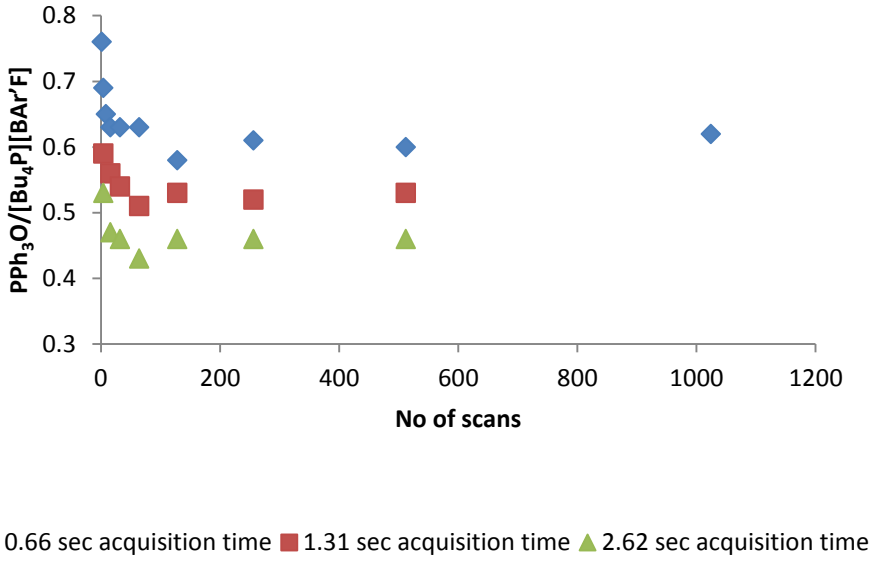

Figure 38: Effect of increasing the number of scans on the observed ratio of PPh_3O/$[Bu_4P][BAr'F]$

5.3 Increasing the relaxation delay

The parameters chosen here were a 0.66 second acquisition time and 32 scans. Keeping all other parameters identical, the relaxation delay was increased. This experiment was performed both with and without the decoupling pulse, the blue and the red data points respectively, Figure 39. As expected, when the decoupling pulse is applied the ratio tends towards a steady ratio of 1: 0.84 PBu_4BArF: PPh_3O as the relaxation delay becomes sufficiently long that there is no longer a carry through of nOe between scans, however this does not reach the expected 1: 1 ratio.

When no decoupling pulse is applied we see the ratio decrease as the relaxation delay increases. If the relaxation delay is too short the population difference between the spin states tends to zero, the system is said to be saturated and a suppression of signal is observed. As we increase the relaxation delay the intensity of the slow relaxing $[Bu_4P][BAr'F]$ increases as the system tends towards equilibrium between scans.

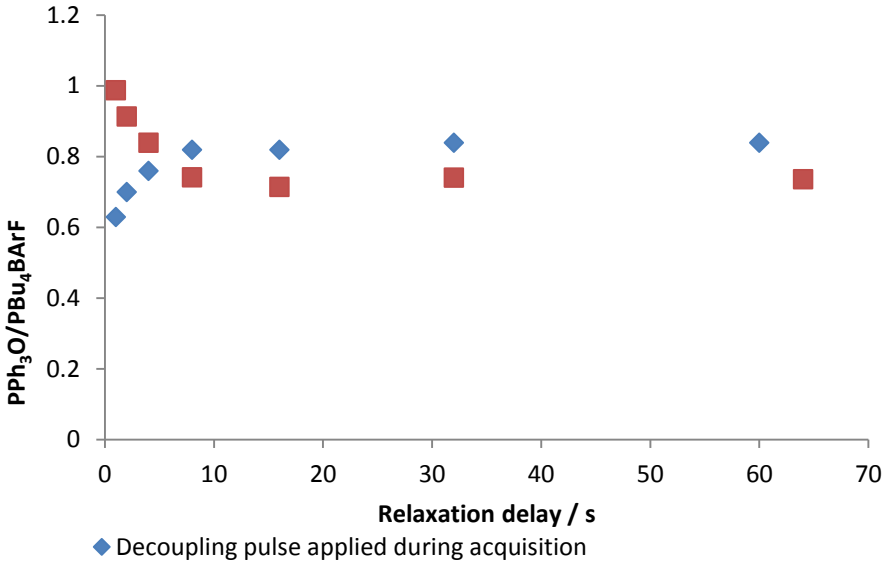

Figure 39: Effect of increasing relaxation time on the observed ratio of PPh_3O/[Bu_4P][BAr'F] in both the coupled and decoupled spectra

5.4 The effect of the time that the decoupling pulse is applied

The relaxation delay applied throughout this experiment is 16 seconds, the acquisition time is 0.66 seconds and each experiment is recorded for 32 scans. The first example is decoupled - the decoupling sequence is applied for a time period before the pulse is applied (d_1) and during the acquisition time. The time period stated is the time the decoupling pulse is applied for, so the sum of d_1 and the acquisition time, Figure 40.

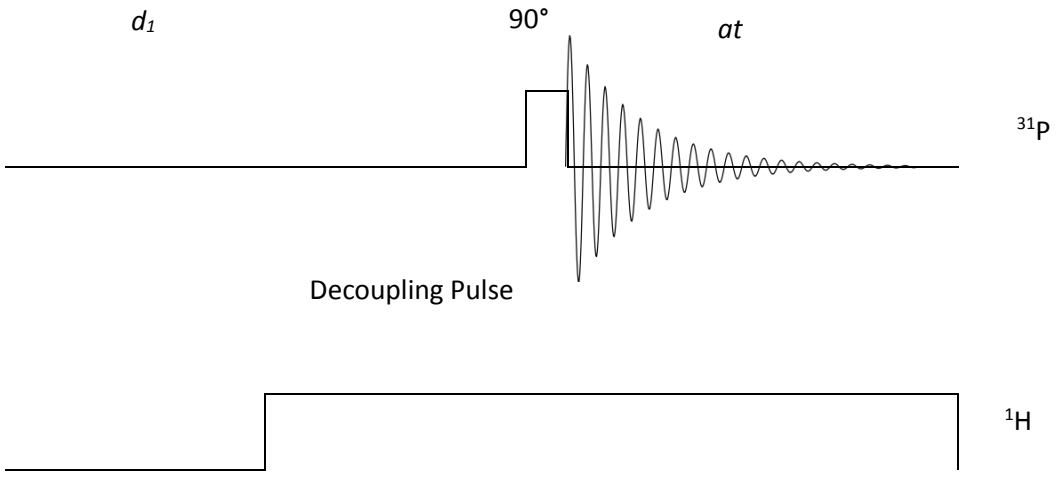

Figure 40: Introducing the decoupling pulse before and during the acquisition

The graph, Figure 41, shows a linear relationship between the time the decoupling pulse is applied for and the relative integration of the two species. If this time were extended more we would expect the system to reach saturation point and plateau.

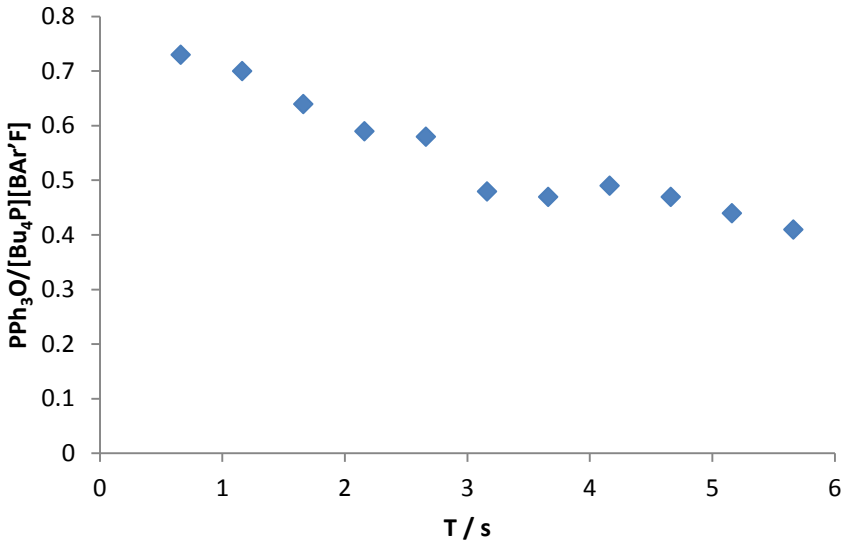

Figure 41: The effect of the time the decoupling pulse is applied for on the observed ratio of PPh3O/[Bu$_4$P][BAr'F] with the inverse gated decoupling sequence

The second example is using a 16 second relaxation delay, 32 scans and a 2.6 second acquisition time, but the decoupling sequence is only applied before the pulse (d_1) and not during the acquisition time, and the time stated is d_1, Figure 37. Here we also see a linear relationship.

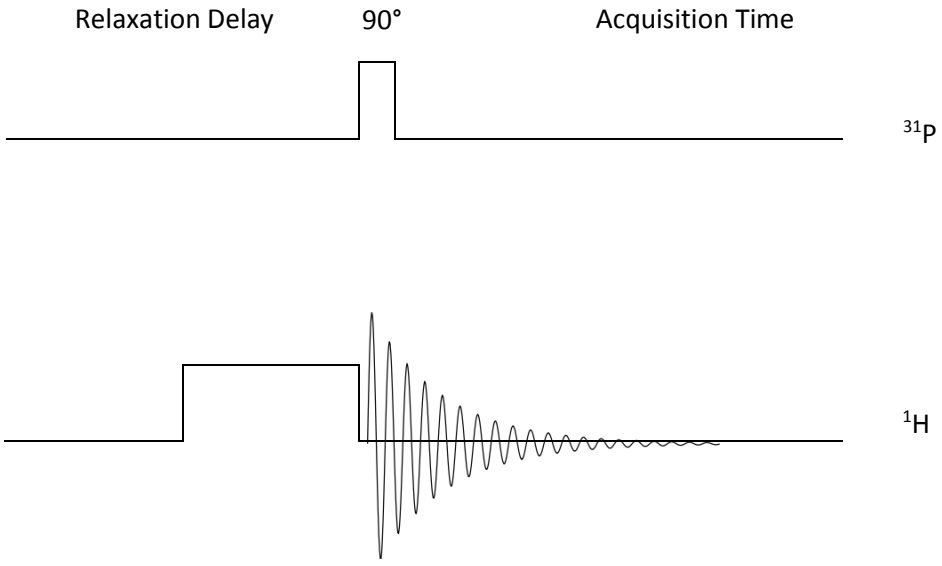

Decoupling Pulse

Figure 42: Introducing the decoupling pulse for a period before the pulse is applied

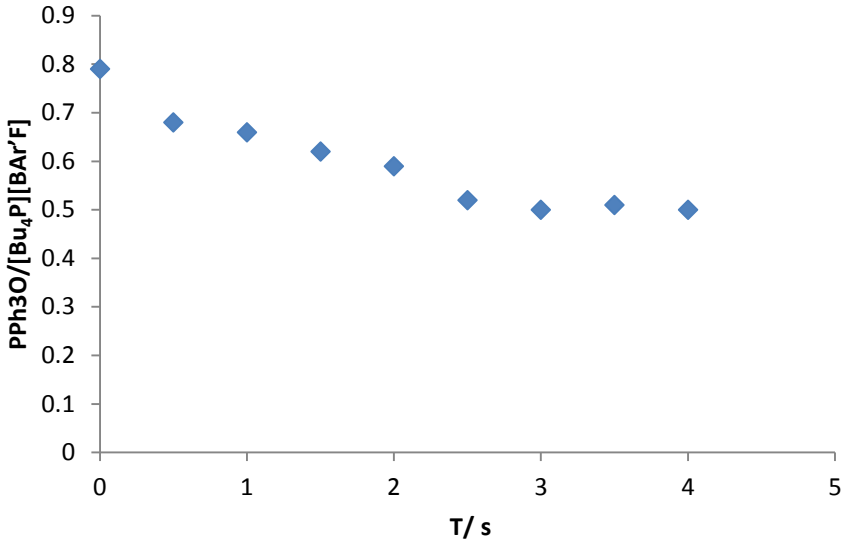

Figure 43: The effect of the time the decoupling pulse is applied for on the observed ratio of PPh3O/[Bu$_4$P][BAr'F] in the coupled system

These series of experiments suggest that the nOe is building up during the acquisition time due to the high density of protons about the phosphorus nuclei in [Bu$_4$P][BAr'F], and that if the relaxation delay is not sufficiently long then the residual nOe can be carried through from one scan to the next.

This point in the project coincided with a move to Edinburgh University, and the installation of Bruker III Ascend 400 MHz magnet fitted with a liquid nitrogen-cooled BBO cryoprobe. The experiments described from here on in were performed on a fresh sample of [Bu$_4$P][BAr'F] in $CDCl_3$. The T_1 relaxation times were repeated and calculated to 4.45 seconds and 4.51 seconds for [Bu$_4$P][BAr'F] and PPh_3O respectively, much closer than the previous calculation of 5.11 and 0.8 seconds respectively.

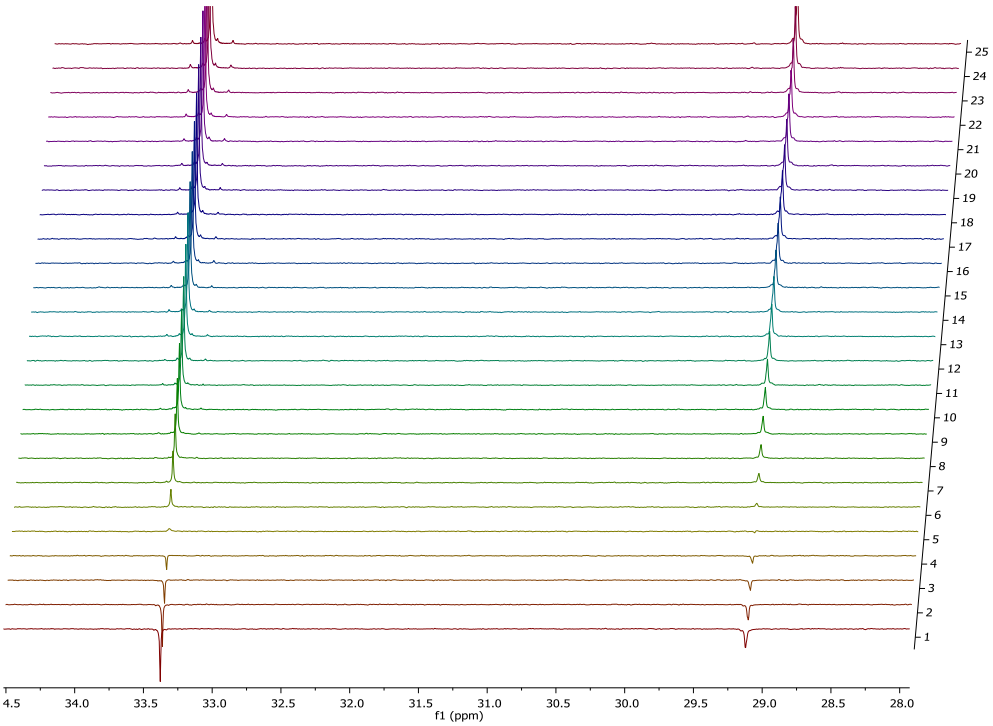

Figure 44: T_1 Experiment: [Bu_4P][BAr'F] (33.5 ppm) and PPh_3O (29.3 ppm).

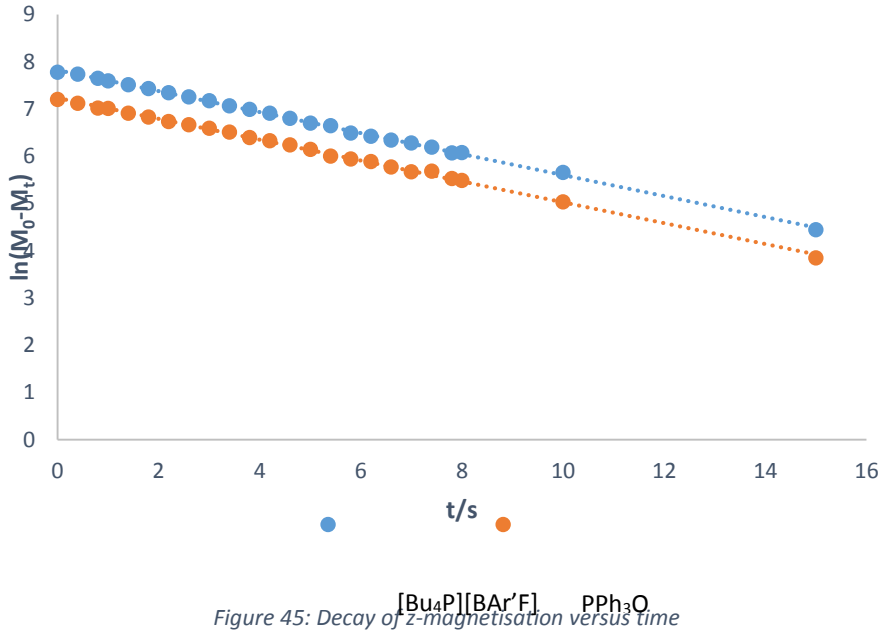

Figure 45: Decay of z-magnetisation versus time

The greater sensitivity of the cryoprobe allowed us to collect single scan experiments with variable acquisition times. If the nOe is building up during the acquisition time, the ratio of the two species should change with longer acquisitions, with the [Bu_4P][BAr'F] increasing as

the acquisition time is increases, as the $[Bu_4P][BAr'F]$ has a greater density of protons about the phosphorus than PPh_3O.

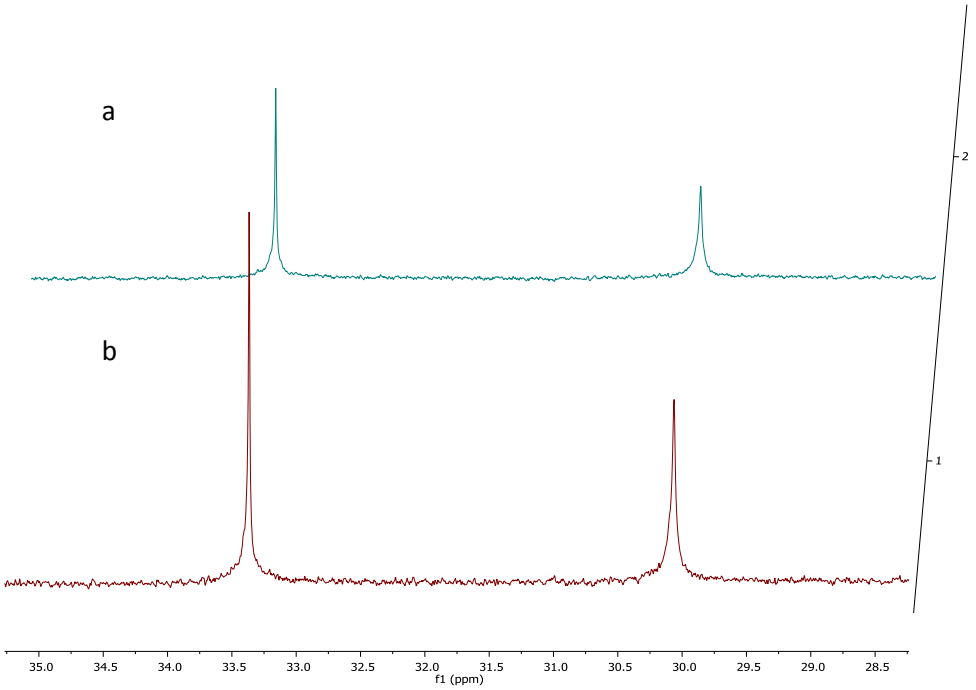

Figure 46: Single scan experiment, increasing aquisition time

Figure 46a shows the single scan $^{31}P\{^1H\}$ with inverse-gated proton decoupling, a 30° flip angle and a 0.66 second acquisition time. Figure 46b is the same spectrum with a 1.32 second acquisition time. The relative integration of $[Bu_4P][BAr'F]$ and PPh_3O of the two spectra are 1: 0.96 and 1: 1.05 respectively, equal within the error of a single scan experiment. This suggests that the nOe is not building up during the acquisition time, and through the early experiments we were simply not allowing time for the phosphorus signal to fully relax before the next acquisition. If this is the case, repeating this experiment with a greater number of scans and a longer relaxation time (approximately 5 x T_1) should give the same result.

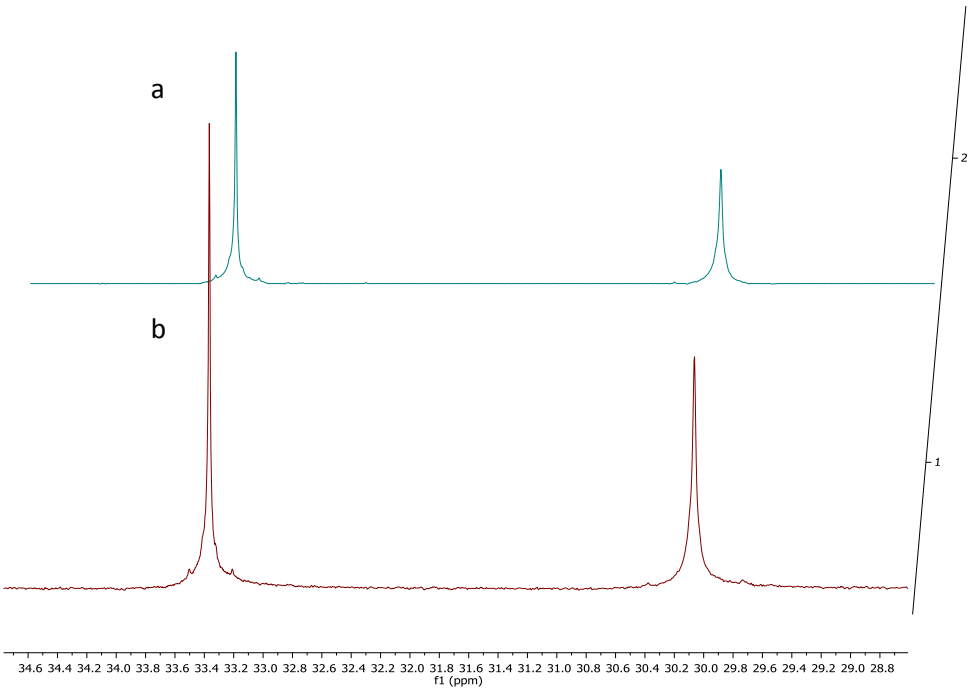

Figure 47: 32 scan experiment with long relaxation delays, increasing acquisition time

Figure 47a shows a 32 scan $^{31}P\{^{1}H\}$ with inverse-gated proton decoupling, a 30° flip angle, a 30 second relaxation delay and a 0.66 second acquisition time. Figure 47b is the same spectrum, but with a 1.32 second acquisition time. Again, the relative integration of the two spectra is equal, (1: 1.05 and 1: 1.01 respectively) indicating that the nOe during the acquisition time is not causing an enhancement of the signal, providing sufficient time is allowed between the end of acquisition and the next pulse.

If we consider the diagram of two spins interacting by dipolar relaxation, section 4.1.2, the nOe builds through the W_0 transition, and transfers the z-magnetisation from spin 1 onto spin 2 or vice versa.[55a]

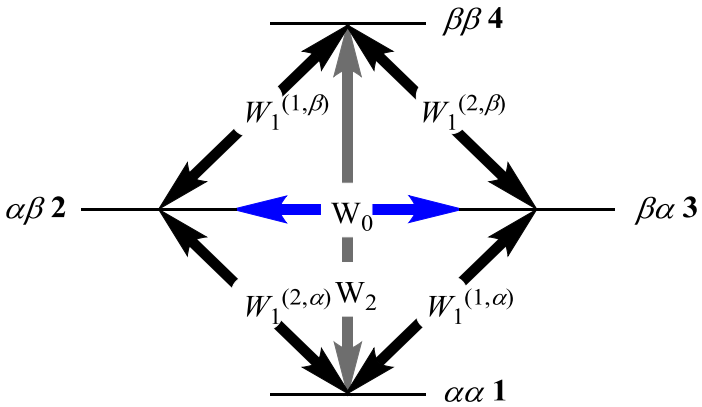

Figure 48: Energy level diagram of two spins interacting through space

The signal observed in an NMR spectrum is due to the precession of the spin about the z-axis at the Larmor frequency of the nuclei; the magnetisation requires an x or y coordinate. The z-magnetisation requires a pulse to transfer in into the xy-plane before it will be observed in a spectra, and hence, if the spin has fully relaxed before the start of the next acquisition, the nOe enhancement will not be observed.

The observation that a delay of 5 X T_1 between scans is required for acquisition of quantitative spectra is in agreement with the published literature surrounding acquisition of quantitative carbon.[58] Quantification of signals is often sacrificed in return for greater sensitivity and shorter experiment times. Heteronuclear NMR can be extremely useful for following kinetic experiments or determining conversions due to the large spectral width, reducing the signal overlap sometimes observed in ^{1}H NMR, but the relaxation times are not always considered, or at least it is not necessary to state the parameters employed when using heteronuclear NMR in a quantitative manner.[59]

To highlight the importance of consideration of the parameters in heteronuclear NMR, two spectra were collected using the one sample. Figure 49a shows the standard, 32 scan experiment on all of the University of Edinburgh NMR spectrometers, an experiment with power-gated decoupling and a two second relaxation delay, an experiment often assumed to be quantitative. Figure 47b is the quantitative spectrum described earlier, with inverse-gated decoupling and long relaxation times. The relative intensity of the $[Bu_4P][BAr'F]$ to the PPh_3O signal is 1: 0.48 and 1: 1.05 in Figures a and b respectively; the intensity of $[Bu_4P][BAr'F]$ is twice in a than it is in b.

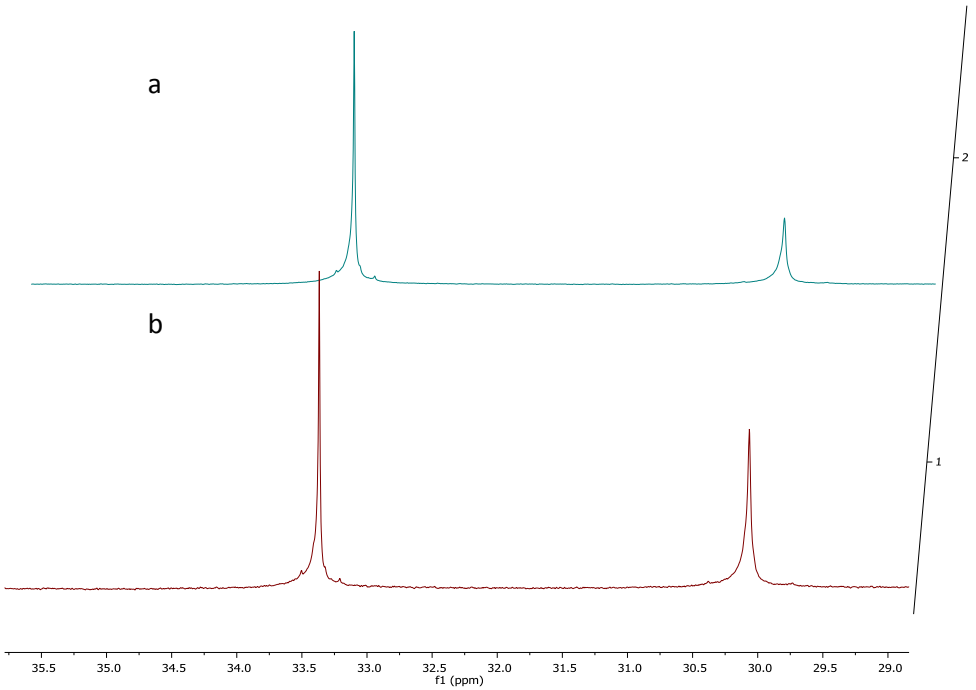

Figure 49: Quantitative experiment versus standard experiment at University of Edinburgh

Whilst it is known to NMR spectroscopists that long relaxation times (the recovery of z-magnetisation can be described as an exponential grown, therefore 5 X T_1 provides approximately 99% recovery of relaxation) and inverse-gated decoupling is required to obtain quantitative specta, this is often overlooked in return for faster experiment times and greater sensitivity.

6 Experimental

6.1 General experimental techniques

Solvents: Dry solvents were obtained from an *Anhydrous Engineering* alumina column based drying system, and further dried over molecular sieves for a minimum of 72 hours. Degassing of solvents was achieved by three freeze-thaw cycles under an atmosphere of nitrogen. Water was degassed by bubbling nitrogen through for at least 15 min prior to use. Methanol was distilled from 3Å molecular sieves under an atmosphere of nitrogen. Deuterated solvents for NMR analysis were purchased from *Cambridge Isotopes Ltd* and degassed by a series of 3 short path distillations or freeze-thaw cycles.

Techniques: Air sensitive manipulations were conducted under an atmosphere of dinitrogen using Schlenk line techniques. All glassware was dried in an oven and heated under vacuum prior to use. Air-sensitive NMR samples were prepared in a 5mm NMR tube sealed with a Youngs tap. For the kinetic experiments, NMR tubes were dried at 80 °C under vacuum for 24 h before use.

NMR analysis: NMR spectra were recorded on ECP300, *ECS300, ECS400, Varian 400*, *Varian 500* MHz, *Bruker 400MHz* or *Bruker 400MHz Prodigy cryoprobe*. NMR instruments utilising the ^{2}H signal lock from the solvent.^{1}H and ^{13}C spectra were referenced internally to the residual deuterated solvent peak and quoted in parts per million (ppm).^{31}P, ^{11}B and ^{19}F spectra were referenced externally and quoted in parts per million (ppm). Coupling constants are quoted in Hertz (Hz) to 0.5 Hz. NMR spectra were processed using *MestReNova* or *Topspin* software.

Mass spectrometry: Mass spectra were recorded by the University of Bristol or the University of Edinburgh Mass Spectrometry service. EI and CI were recorded using a *VG autospec* with an *EBE* magnetic sector. ESI was recorded using an *Applied Biosystems QStar XL* fitted with a *QqToF* analyser.

Elemental analyses were carried out by the University of Bristol Microanalytical Laboratory.

η^3-allyl palladium chloride

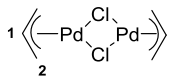

To a slurry of palladium chloride (4.51 g, 25.4 mmol, 1 eq) and sodium chloride (2.96 g, 50.7 mmol, 2 eq) in degassed water (900 ml). Allyl chloride (13.16 g, 14 ml, 172.0 mmol, 6.8 eq) was added dropwise over 20 min and the resulting slurry stirred for 48 h under an atmosphere of nitrogen to give a clear yellow solution. The mixture was extracted into CH_2Cl_2 (4 x 200 ml), dried over magnesium sulfate and dried *in vacuo* to give a yellow solid. The crude material was filtered through Celite and recrystallized from a minimum volume of CH_2Cl_2 by layering with hexane to yield the η^3-allyl palladium chloride as lemon yellow needle-like crystals, 1.8 g, 35%. **^{1}H NMR** (301 MHz, $CDCl_3$) δ 5.45 (tt, J = 12.0, 6.5 Hz, 1H, C(**1**)H), 4.10 (d, J = 6.5 Hz, 2H C(**2**)H, *syn*), 3.03 (d, J = 12.0 Hz, 2H C(**2**)H, *anti*); **^{13}C NMR** (76 MHz, $CDCl_3$) δ 111.31 (s, 1C), 63.09 (s, 2C).

All spectroscopic data is consistent with the data published in the literature.[60]

2-hydoxy-[$^{2}H_4$]-ethyl benzoate

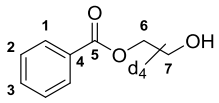

To a solution of [$^{2}H_6$]-ethylene glycol (2 ml, 35.8 mmol) in THF (200 ml) was added dimethyltin dichloride (78 mg, 0.4 mmol, 1 mol %), K_2CO_3 (9.9g, 71.6 mmol, 2 eq) and benzoyl chloride (5 ml, 43.1 mmol, 1.2 eq). The resulting suspension was stirred at room temperature for 72 h until complete consumption of the ethylene glycol was observed by TLC.

The mixture was diluted with H_2O (50 ml) and extracted into Et_2O (100 ml). The organic extract was washed with H_2O (5 x 50 ml), dried over $MgSO_4$, filtered and dried *in vacuo*. The crude material was purified by flash chromatography (hexane: ethyl acetate, 4: 1) to afford the title compound as a colourless oil. (5.17 g, 85 %). **^{1}H NMR** (400 MHz, $CDCl_3$) δ 8.05 (d, J = 7.5 Hz, 2H 2C(**1**)H), 7.57 (t, J = 7.5 1H C(**3**)H), 7.45 (t, J = 7.5 Hz, 2H, C(**2**)H), 1.85 (br s, O*H*); **^{13}C NMR** (100 MHz, $CDCl_3$) δ 167.11 (s, 1C), 133.32 (s, 1C), 129.99 (s, 1C), 129.82 (s, 2C), 128.55 (s, 2C). Carbons at 66.6 and 61.3 ppm are not observed; these carbons are quaternary and coupled to deuterium and so a longer experiment is required.

Spectroscopic data is consistent with the data published in the literature data for the unlabelled compound.[61]

2-oxy-[$^2H_3$]-ethyl benzoate

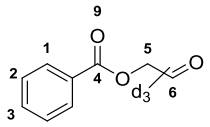

To a solution of 2-hydoxy-[$^2H_4$]-ethyl benzoate (1 g, 5.9 mmol) and pinacol (134 mg, 1.1 mmol, 20 mol %) in CH_2Cl_2 (30 ml, dry) was added iodobenzene diacetate (3.9 g, 12.1 mmol, 2 eq) and 2,2,6,6-tetramethylpiperidine-1-oxyl radical (190 mg, 1.1 mmol, 20 mol%). The suspension was stirred for 16 h before quenching with water. The organics were extracted into CH_2Cl_2 (3 x 30 ml) and dried *in vacuo* to give an orange residue. The crude material was purified by column chromatography (hexane: Et_2O, 2: 1; then toluene: Et_2O: methanol, 60: 39: 1) to give a viscous oil. The oil was distilled under reduced pressure (115 °C, 1.5 mmHg) to give the title compound (161 mg, 16%).**^{1}H NMR** (301 MHz, $CDCl_2$) δ 8.11 (dd, *J* = 8.0, 1.4 Hz, 2H, 2C(**1**)H), 7.62 (t, *J* = 7.0 Hz, 1H, C(**3**)H), 7.48 (t, *J* = 7.0 Hz, 2H, 2C(**2**)H); **^{2}H NMR** (46 MHz, $CHCl_3$ δ 9.77 (s, 1H, C(**6**)^{2}H), 4.88 (s, 2H, 2C(**5**)^{2}H); **^{13}C NMR** (101 MHz, $CDCl_3$) δ 133.79 (s, 1C), 130.09 (s, 2C), 129.00 (s, 1C), 128.70 (s, 2C). Carbons at 166.1 and 69.2 ppm are not observed; these carbons are quaternary and coupled to deuterium and so a longer experiment is required. Consistent with the published data for the unlabelled compound.[62]

[$^2H_5$]-allyl benzoate

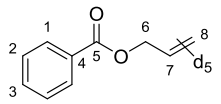

KHMDS (1.1 ml, .0.95 M, toluene, 1.05 mmol, 1.1 eq) was added dropwise to a suspension of methyl-[$^2H_3$]-triphenylphosphonium iodide (429 mg, 1.05 mmol, 1.1 eq) in THF (20 ml, anhydrous) at -20°C. Once addition was complete the bright yellow suspension was stirred at -20°C for 2 h. 2-oxy-[$^2H_3$]-ethyl benzoate (161 mg, 0.96 mmol) was added as a solution in THF (3 ml, anhydrous) and the mixture allowed to warm to room temperature and stirred for a further 3 h. The mixture was diluted with water (10 ml) and extracted with Et_2O (2 x 20 ml), dried over Mg_2SO_4, filtered and dried *in vacuo.* The crude material was purified by flash chromatography (pentane: Et_20, 20: 1) to give the title compound as a colourless oil without complete removal of solvents. (94 mg, 85%, contains THF, Et_2O, CH_2Cl_2 and HMDS). **^{1}H NMR** (400 MHz, $CDCl_3$) δ 8.07 (dd, *J* = 8.0, 1.4 Hz, 2H, 2C(**1**)H), 7.57 (t, *J* = 8.0 Hz, 1H, C(**3**)H), 7.45 (t, *J* = 8.0 Hz, 2H, 2C(**2**)H), 5.43 – 5.36 (m, 0.18H), 5.34 – 5.24 (m, 0.2H), 4.87 – 4.78 (m, 1H); **^{2}H NMR** (77 MHz, $CHCl_3$) δ 6.06 (br. s, 1H, C(**7**)^{2}H), 5.46 (br. s, 2H, 2C(**8**)^{2}H), 4.83 (br. s, 2H, 2C(**6**)^{2}H).

Consistent with the published data for the unlabelled compound.[63]

[$^2H_{10}$]-allyl palladium chloride dimer

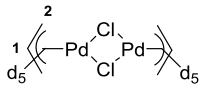

A suspension of [$^2H_5$]-allyl benzoate (94 mg, 0.56 mmol) and KOH (98 mg, 1.74 mmol, 3.1 eq) in EtOH (2 ml, degassed) and H_2O (1 ml, degassed) fitted with a cold finger and stirred at 40°C for 2 h. THF (1.5 ml, degassed) and (0.5 ml) were added and the suspension cooled to room temperature.

In a separate 3 neck round bottom flask, a suspension of palladium chloride (103 mg, 0.58 mmol, 1.04 eq) and lithium chloride (48 mg, 1.13 mmol, 2 eq) in EtOH (1.5 ml, degassed) and H_2O (1 ml, degassed) was purged with carbon monoxide and sealed causing the reaction mixture to turn black. The allyl benzoate solution was added immediately by cannula filtration and two carbon monoxide filled balloons were attached *via* a septum. After stirring for 1 h the balloons were removed and the flask opened to nitrogen and stirred for a further 20 min. The mixture was extracted with 20 ml aliquots of $CHCl_3$ until no yellow colour was evident in the washes. The combined organic extracts were dried *in vacuo* and the yellow residue dissolved in CH_2Cl_2, filtered through a pad of silica and dried under vacuum to afford the title compound as a yellow powder. (62 mg, 28 %). Crystallised by layering from CH_2Cl_2 and hexane as required. **^{2}H NMR** (77 MHz, C_6H_6) δ 5.43 (s, 1^{2}H, C(**1**)^{2}H), 4.01 (s, 1.65^{2}H, C(**2**)^{2}H, *syn*), 2.95 (s, 1.65^{2}H, C(**2**)^{2}H, *anti*). Loss of signal at C(**2**) due to H/D exchange.

Consistent with the unlabelled compound, *vide supra.*

[$^2H_5$]-allyl palladium bis(triphenylphosphine) tetrakis 3,5-bis(trifluoromethyl)phenyl borate (BAr'F)

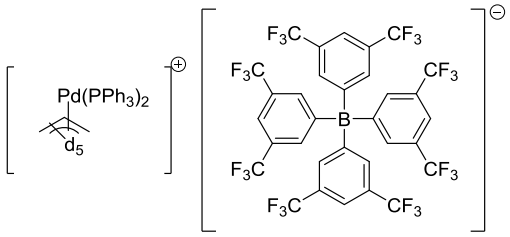

A Schlenk flask was charged with [$^2H_{10}$]-allyl palladium chloride dimer (7 mg, 0.019 mmol) and CH_2Cl_2 (0.5 ml, anhydrous, degassed). A solution of NaBAr'F (33 mg, 3.7 mmol) in CH_2Cl_2 (0.5 ml, anhydrous, degassed) and MeCN (0.25 ml, anhydrous, degassed) was added and the resulting solution stirred for 10 min, filtered through celite and dried in vacuo. The residue was triturated from hexane (10 ml) to give [$^2H_5$]-[allyl palladium bis(MeCN)]BAr'F as an off-white solid. (22.8 mg, 55%).

To a solution of [$^2H_5$]-[allyl palladium bis(MeCN)]BAr'F (22.8 mg, 0.02 mmol) in THF (5 ml, anhydrous, degassed), triphenylphosphine (10.8 mg, 0.04 mmol) in THF (5 ml, anhydrous, degassed) was added dropwise over 10 min. The solution was stirred at room temperature for 1 h and the solvents removed *in vacuo* to give an off white solid. The crude material was crystallised by vapour diffusion with THF and pentane to give the title compound a colourless, needle crystals (25 mg, 78.5 %). **^{1}H NMR** (301 MHz,d_8-THF) δ 7.80 (br. s, 8H, BAr'*H*F), 7.58 (br. s, 4H, BAr'*H*F), 7.48 – 7.40 (m, 6H, PPh*H*), 7.37 – 7.24 (m, 24H, PPh*H*), **^{31}P NMR** (122 MHz, d_8-THF) δ 24.20 (s), **MS (ESI)** *m/z* 675 (M^+ for major isotope (^{106}Pd)).[63]

^{108}Palladium chloride

^{108}Palladium metal (48 mg, 0.44 mmol) was stirred in HNO_3 (0.6 ml) and HCl (2.25 ml) until complete dissolution of the metal and a deep red colour was observed. The aqua regia was removed under reduced pressure and any remaining nitrate removed by two evaporations with HCl (1 ml). The red solid was washed with CH_2Cl_2 (1 ml) and the volatiles removed under a reduced pressure to afford the title compound as red-brown solid. (75 mg, 94%). The salt was not characterised.

Allyl ^{108}palladium chloride dimer

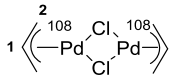

To a suspension of $^{108}PdCl_2$ (75.1 mg, 0.42 mmol) and NaCl (50 mg, 0.86 mmol, 2.04 eq) in water (15 ml, degassed) allyl chloride (235 μl, 220 mg, 2.88 mmol, 6.9 eq) was added dropwise. The resulting mixture was stirred for 14 h under an atmosphere of nitrogen to give a clear yellow solution. The mixture was extracted with 20 ml aliquots of CH_2Cl_2 until the yellow colour was no longer evident in the washes and the solvent was removed *in vacuo* to afford the title compound as a yellow solid. The crude material was recrystallised by layering with CH_2Cl_2 hexanes to give needle-like crystals as required. **^{1}H NMR** (301 MHz, $CDCl_3$) δ 5.46 (tt, *J* = 12.0, 6.5 Hz, 1H, C(**1**)H), 4.12 (dt, *J* = 6.5, 1.0 Hz, 2H, , C(**2**)H, *syn*), 3.04 (d, *J* = 12.0 Hz, 2H, , C(**2**)H, *anti*).

Consistent with the data for the unlabelled compound, *vide supra.*

Allyl ^{108}palladium bis(triphenylphosphine) tetrakis 3,5-bis(trifluoromethyl)phenyl borate (BAr'F)

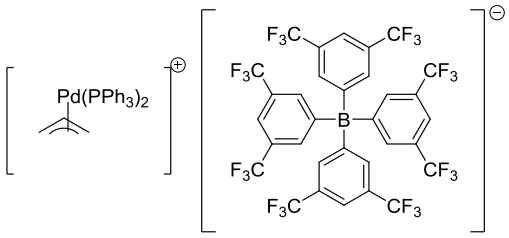

Allyl ^{108}palladium bis(triphenylphosphine) BAr'F was prepared in an analogous manner to [$^2H_5$]-allyl palladium bis(triphenylphosphine) BAr'F, employing allyl ^{108}palladium chloride dimer. The crude material was crystallised by vapour diffusion with THF pentane to afford the title compound as off white needle crystals. **^{1}H NMR** (301 MHz, d_8-THF) δ 7.79 (t, *J* = 3 Hz, 8H, BAr'*H*F), 7.57 (s, 4H, BAr'*H*F), 7.54 – 7.20 (m, 28H, PPh_3), 6.10 – 5.91 (m, 0.65H, C(**1**)H), 4.11 – 3.99 (m, 1.45H, C(**2**)), 3.70 – 3.45 (m, C*H*H, obscured by THF); **^{31}P NMR** (122 MHz,) δ 22.20 (s), **MS (ESI)** *m/z* 673 (M^+)

4-iodo-6-oxabicyclo[3.2.1]octan-7-one

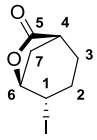

A solution of sodium hydrogen carbonate (1 g, 11.9 mmol) in H_2O (30 ml) was added dropwise to an ice cooled flask charged with 3-cyclohexene-1-carboxylic acid (0.5 g, 4.3 mmol). Following complete addition, a solution of iodine (1 g, 4.2 mmol) and potassium iodide (4 g, 24.1 mmol) in water (20 ml) was added dropwise. The resulting suspension was allowed to warm to room temperature and stirred overnight.

The suspension was filtered and the off white solid was recystallised from a minimum volume of hot ethanol to yield the title compound as colourless crystals (1.07 g, 99 %). ^{1}H NMR (601 MHz, $CDCl_3$) δ 4.84 (dd, *J* = 5.0 Hz, 1H, C(**6**)H), 4.52 (dd, *J* = 5.0, Hz, 1H, C(**1**)H), 2.81 (d, *J* = 12.0 Hz, 1H, (**7**)H), 2.68 (t, *J* = 5.0, 1H, C(**4**)H), 2.50 – 2.37 (m, 2H, C(**7**)H, C(**2**)H), 2.13 (dd, *J* = 17.0, 5.5 Hz, 1H, C(**2**)H), 1.92 (tdd, *J* = 12.0, 5.5, 1.5 Hz, 1H, C(**3**)H), 1.87 – 1.80 (m, 1H, C(**3**)H). ^{13}C NMR (151 MHz, $CDCl_3$) δ 177.74 C(**5**), 80.22 C(**6**), 38.61 C(4), 34.51 C(**7**), 29.73 C(**2**), 23.77 C(**1**), 23.13 C(**3**).

Consistent with the data published in the literature.[64]

7-oxa-bicyclo[3.2.1]oct-2-en-6-one

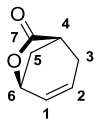

To a suspension of 4-iodo-6-oxabicyclo[3.2.1]octan-7-one (1.07 g, 4.2 mmol) in anhydrous toluene (20 ml) was added 1,8-diazabicyclo[5.4.0]undec-7-ene (630 µl, 0.64 g, 4.2 mmol) was added and the mixture heated to 80 °C for 8 h. The suspension was filtered and the volatiles removed *in vacuo* to yield the title compound as a colourless oil (0.5 g, 95 %). The crude material was used without purification in the next step. **^{1}H NMR** (601 MHz, $CDCl_3$) δ 6.34 – 6.15 (m, 1H, C(**1**)H), 5.94 – 5.79 (m, 1H, C(**2**)H), 4.76 (t, *J* = 5.5 Hz, 1H, C(**6**)H), 2.91 (d, *J* = 5.5 Hz, 1H, C(**4**)H), 2.62 – 2.37 (m, 3H, C(**3**)H, 2C(**5**)H), 2.10 (d, *J* = 11.0 Hz, 1H, C(**3**)H). **^{13}C NMR** (151 MHz, $CDCl_3$) δ 179.38 (1C(**7**)), 130.28 (1C(**2**)), 129.33 (1C(**1**)), 73.31 (1C(**6**)), 38.05 (1C(**4**)), 34.45 (1C(**3**)), 29.14 (1C(**5**)).

Consistent with data reported in the literature.[64]

Methyl cis-5-hydroxycyclohex-3-enecarboxylate

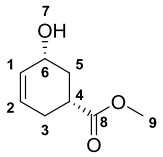

To a solution of 7-oxa-bicyclo[3.2.1]oct-2-en-6-one (0.7 g, 5.6 mmol) in anhydrous methanol (10 ml) was added potassium carbonate (390 mg, 2.8 mmol) at 0 °C. The suspension was allowed to warm to room temperature and stirred for 1 hr. The suspension was filtered through celite and the volatiles removed *in vacuo*. The residue was diluted with ether (30 ml) and washed with water (50 ml). The aqueous residue was extracted with ether (2 x 30 ml). The combined organic washes were dried over sodium sulfate and dried *in vacuo* to yield the title compound as a colourless residue, (440 mg, 51%). **^{1}H NMR** (601 MHz, C_6D_6) δ 5.60 (d, *J* = 10.5 Hz, 1H, C(**1**)H), 5.43 – 5.37 (m, 1H, C(**2**)H), 3.98 (s, 1H, C(**6**)H), 3.28 (s, 3H, 3C(**9**)H), 2.38 – 2.30 (m, 1H, C(**4**)H), 2.18 – 2.02 (m, 2H, C(**3**)H, C(**5**)H), 1.99 – 1.91 (m, 1H, C(**3**)H), 1.66 – 1.53 (m, 2H, C(**5**)H, OH). **^{13}C NMR** (151 MHz, C_6D_6) δ 174.65 1C(**8**), 131.51 1C(**1**), 125.90 1C(**2**), 65.78 1C(**6**), 50.93 1C(**9**), 37.76 1C(**4**), 34.41 1C(**5**), 27.33 1C(**3**).

***d*$_3$- *Methyl* cis-5-hydroxycyclohex-3-enecarboxylate**

^{1}H NMR (601 MHz, C_6D_6) δ 5.60 (d, *J* = 10.0, Hz, 1H, C(**1**)H), 5.45-5.35 (m, 1H, C(**2**)H), 3.98 (d, *J* = 7.5 Hz, 1H, C(**6**)H), 2.38-2.29 (m, 1H, C(**4**)H), 2.18 – 2.02 (m, 2H, C(**3**)H, C(**5**)H), 2.02 – 1.87 (m, 1H, C(**3**)H), 1.70 – 1.46 (m, 2H, C(**5**)H, OH). **^{13}C NMR** (151 MHz, C_6D_6) δ 174.65 1C(**8**), 131.51 1C(**1**), 125.90 1C(**2**), 65.78 1C(**6**), 37.76 1C(**4**), 34.41 1C(**5**), 27.33 1C(**3**).

Consistent with the data reported in the literature for the unlabelled compound.[64]

Methyl *cis* and *trans*-5-hydroxycyclohex-3-enecarboxylate

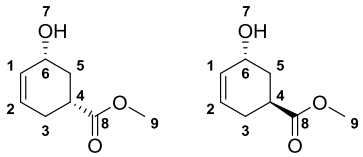

To a solution of methyl cis-5-hydroxycyclohex-3-enecarboxylate (20 mg, 0.13 mmol) in anhydrous methanol (1 ml) was added potassium carbonate (10 mg, 0.07 mmol). The suspension was heated to 35 °C for 24 h. The suspension was filtered through celite and the volatiles removed *in vacuo*. The residue was diluted with ether (10 ml) and washed with water (10 ml). The aqueous residue was extracted with ether (2 x 10 ml). The combined organic washes were dried over sodium sulfate and dried *in vacuo*. The residue was purified by flash chromatography (petroleum ether/ ethyl acetate, 7: 3) to yield a mixture of *cis*- and *trans*-**61** in a 2.8: 1 ratio (7 mg, 35%). **^{1}H NMR** (500 MHz, C_6D_6) δ 5.68 – 5.56 (m, 3.8H, C(**1**)H (*cis* and *trans*)), 5.55 – 5.49 (m, 1H, C(**2**)H (*trans*)), 5.45 – 5.38 (m, 2.8H, C(**2**)H (*cis*)), 4.02 (s, 2.8H, C(**6**)H (*cis*)), 3.95 (s, 1H, C(**6**)H (*trans*)), 3.32 (s, 3H, 3C(**9**)H, (*trans*)), 3.29 (s, 1.6 Hz, 8.6H, 3C(**9**)H, (*cis*)), 2.80 – 2.68 (m, 1H, C(**4**)H (*trans*)), 2.41 – 2.30 (m, 2.8H, C(**4**)H (*cis*)), 2.19 – 2.01 (m, 7.6H, C(**3**)H, C(**5**)H, (*cis* and *trans*)), 2.02 – 1.89 (m, 3.8H, C(**3**)H, (*cis* and *trans*)), 1.73 – 1.57 (m, 3.6H, C(**5**)H, (*cis* and *trans*)). ^{13}C NMR (126 MHz, C_6D_6) δ 175.15 1C(*trans*-**8**), 174.72 1C(*cis*-**8**), 131.55 1C(*cis*-**1**), 128.53 1C(*trans*-**1**) , 128.28 1C(*trans*-**2**), 125.91 1C(*cis*-**2**), 65.85 1C(*cis*-**6**), 62.80 1C(*trans*-**6**), 50.97 1C(*cis*-**9**), 50.87 1C(*trans*-**9**), 37.82 1C(*cis*-**4**), 34.52 (*trans*-**4**), 34.43 1C(*cis*-**5**), 33.95 1C(*trans*-**5**), 27.60 1C(*cis*-**3**), 27.34 1C(*trans*-**3**).

***Trans*-methyl 5-chlorocyclohex-3-enecarboxylate**

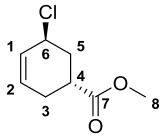

A solution of methyl cis-5-hydroxycyclohex-3-enecarboxylate (441 mg, 2.82 mmol) in diethylether (10 ml) was added dropwise to a solution of triphenylphosphine (740 mg, 2.82 mmol) and N-chlorosuccinimide (377 mg, 2.82 mmol) in DCM (10 ml) at 0 °C. The resulting mixture was allowed to warm to room temperature and stirred for 1 hour. The volatiles were removed *under reduced pressure* and the residue purified by flash chromatography (petroleum ether/ diethyl ether 8: 1) to yield the desired product as a colourless oil (205 mg, 42%). ^{1}H NMR (601 MHz, $CDCl_3$) δ 5.99 – 5.78 (m, 2H, C(**1**)H, C(**2**)H), 4.71 (ddd, *J* = 4.5, 2.4 Hz, 1H, C(**6**)H), 3.74 (s, 3H, 3C(**8**)H), 3.03 (dddd, *J* = 12.2, 11.1, 5.4, 2.9 Hz, 1H, C(**4**)H), 2.54 – 2.37 (m, 2H, C(**3**)H, C(**5**)H), 2.35 – 2.23 (m, 1H, C(**3**)H), 2.12 (ddd, *J* = 14.4, 12.4, 4.3 Hz, 1H, C(**5**)H). ^{13}C NMR (151 MHz, $CDCl_3$) δ 175.24, C(**7**), 129.30, C(**1**), 127.28, C(**2**), 53.84, C(**6**), 51.91, C(**8**), 34.45, C(**4)**, 34.13, C(**5**), 27.48, C(**3**).

***d_3-Trans*-methyl 5-chlorocyclohex-3-enecarboxylate**

^{1}H NMR (601 MHz, $CDCl_3$) δ 5.99 – 5.78 (m, 2H, C(**1**)H, C(**2**)H), 4.71 (ddd, *J* = 4.5, 2.4 Hz, 1H, C(**6**)H), 3.74 (s, 3H, 3C(**8**)H), 3.03 (dddd, *J* = 12.2, 11.1, 5.4, 2.9 Hz, 1H, C(**4**)H), 2.54 – 2.37 (m, 2H, C(**3**)H, C(**5**)H), 2.12 (ddd, *J* = 14.4, 12.4, 4.3 Hz, 1H, C(**5**)H). ^{13}C NMR (151 MHz, $CDCl_3$) δ 175.24, C(**7**), 129.30, C(**1**), 127.28, C(**2**), 53.84, C(**6**), 34.45, C(**4)**, 34.13, C(**5**), 27.48, C(**3**).

Consistent with the data reported in the literature for the unlabelled compound.[4a]

Cis-5-methylcarboxylate-1,2,3-cyclohexenylpalladium chloride dimer

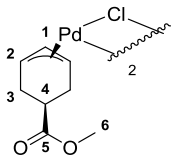

Lithium chloride (361 mg, 8.53 mmol) and palladium dichloride (189 mg, 1.06 mmol) stirred in water (10 ml, degassed) in a Schlenk tube under an atmosphere of nitrogen until dissolution was complete. In a separate round bottomed flask, t*rans*-methyl 5-chlorocyclohex-3-enecarboxylate (205 mg, 1.17 mmol) was dissolved in ethanol (10 ml, degassed) and THF (15 ml, degassed) under an atmosphere of nitrogen. A balloon of carbon monoxide was fitted to the flask via a long needle above the surface and septa, and the palladium dichloride solution was added in a single portion. A second needle was fitted to the flask and the solution was stirred until a colour change from orange to yellow was observed (approximately 10 min). Once the colour change was observed, the balloon was removed and the flask was purged with nitrogen and allowed to stir for a further 10 min. The mixture was diluted with water (30 ml) and chloroform (30 ml) and the layers separated. The aqueous extracts were washed with chloroform until no yellow colour was evident in the washings. The combined organic extracts were dried *in vacuo*. The residue was purified by column chromatography (petroleum ether/ chloroform/ methanol, 50: 50: 1) to yield the title compound as a yellow solid, and crystallised from a minimum volume of chloroform by layering with hexane (165 mg, 55%). ^{1}H NMR (601 MHz, $CDCl_3$) δ 5.57 (t, *J* = 6.0 Hz, 1H, C(**1**)H), 5.22 (t, *J* = 6.0 Hz, 2H, 2C(**2**)H), 3.70 (s, 3H, 3C(**6**)H), 2.27 (dt, *J* = 16.5, 8.0 Hz, 2H, 2C(**3**)H), 2.15 – 1.81 (m, 3H, 2C(**3**)H, C(**4**)H). ^{13}C NMR (151 MHz, $CDCl_3$) δ 173.84, C(**5**), 101.82, C(**1**), 75.84, C(**2**), 51.98, C(**6**), 35.78 C(**4**), 31.88 C(**3**).

Cis-5-d_3-methylcarboxylate-1,2,3-cyclohexenyl^{108}palladium chloride dimer

^{1}H NMR (601 MHz, $CDCl_3$) δ 5.57 (t, *J* = 6.5 Hz, 1H), 5.22 (t, *J* = 6.5 Hz, 2H), 2.28 (dd, *J* = 14.0, 7.0 Hz, 2H), 2.12 – 1.92 (m, 3H). ^{13}C NMR (151 MHz, $CDCl_3$) δ 173.86, C(**5**), 101.82, C(**1**), 75.85, C(**2**), 35.77, C(**4**), 31.88, C(**3**). Carbon at 35.78 ppm not observed. This carbon is quaternary and coupled to deuterium.

Consistent with the data reported in the literature for the unlabelled compound.[17b]

***Cis*-5-methylcarboxylate-1,2,3-cyclohexenylpalladium triflate**

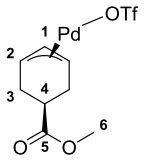

In the glovebox, cis-5-methylcarboxylate-1,2,3-cyclohexenylpalladium chloride dimer (20 mg, 0.035 mmol) and silver triflate (20 mg, 0.078 mmol) was stirred in THF (1 ml, anhydrous) for 1 hour. The mixture was filtered through glass filter paper and dried *in vacuo* to give the desired product as a pale yellow solid. The cis-5-methylcarboxylate-1,2,3-cyclohexenylpalladium triflate was unstable at room temperature and so used in the next step immediately. ^{1}H NMR (400 MHz, Benzene-d_6) δ 4.56 (t, *J* = 6.0 Hz, 1H, C(**1**)H), 4.22 (t, *J* = 6.0 Hz, 2H, 2C(**2**)H, 3.25 (s, 3H, 3C(**9**)H), 1.87 – 1.32 (m, 4H, 4C(**3**)H), 1.27 (dq, *J* = 10.8, 5.5 Hz, 1H, 1C(**4**)H).

Consistent with the data reported in the literature.[17b]

bis(triphenylphosphine) (5-carboxyl, 1,2,3-η^3-cyclohexenyl) palladium triflate

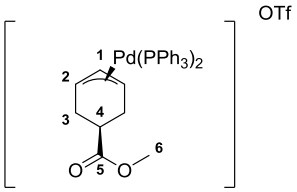

In the glovebox, *cis*-5-methylcarboxylate-1,2,3-cyclohexenylpalladium triflate was dissolved in toluene (2 ml, anhydrous). PPh_3 (35 mg, 0.13 mmol, 1.9 eq) was dissolved in toluene (2 ml, anhydrous) and added dropwise over 2 min, resulting in the precipitation of an off white solid. The solid was isolated by filtration and dried under vacuum, (0.48 mg, 73%).

Cis: ^{1}H NMR (500 MHz, C_6D_6) δ 7.45 – 6.81 (m, 30H, ArH), 4.93 (t, *J* = 6.5 Hz, 3H,), 3.13 (s, 3H), 1.56 – 1.30 (m, 4H), 1.27 – 0.90 (m, 2H). ^{31}P NMR (202 MHz, C_6D_6) δ 22.82.

Trans: ^{1}H NMR (500 MHz, Benzene-d_6) δ 7.45 – 6.81 (m, 30H, ArH), 4.93 (t, *J* = 6.5 Hz, 3H), 3.14 (s, 3H), 1.56 – 1.30 (m, 4H), 1.27 – 0.90 (m, 2H). ^{31}P NMR (202 MHz, C_6D_6) δ 22.01 . **MS (ESI)** *m/z* 769 (M^+ for major isotope (^{106}Pd))

***d*$_3$-bis(triphenylphosphine) (5-carboxyl, 1,2,3-η^3-cyclohexenyl) ^{108}palladium triflate**

Cis: ^{1}H NMR (500 MHz, C_6D_6) δ 7.45 – 6.81 (m, 30H, ArH), 4.93 (t, *J* = 6.5 Hz, 3H,), 1.56 – 1.30 (m, 4H), 1.27 – 0.90 (m, 2H). ^{31}P NMR (202 MHz, C_6D_6) δ 22.82.

Trans: ^{1}H NMR (500 MHz, Benzene-d_6) δ 7.45 – 6.81 (m, 30H, ArH), 4.93 (t, *J* = 6.5 Hz, 3H), 1.56 – 1.30 (m, 4H), 1.27 – 0.90 (m, 2H). ^{31}P NMR (202 MHz, C_6D_6) δ 22.01 . **MS (ESI)** *m/z* 774

7 References

1. Tsuji, J.; Takahashi, H.; Morikawa, M., *Tetrahedron Lett.* **1965,** *6* (49), 4387-4388.

2. Atkins, K. E.; Walker, W. E.; Manyik, R. M., *Tetrahedron Lett.* **1970,** *11* (43), 3821-3824.

3. Trost, B. M.; Dietsch, T. J., *J. Am. Chem. Soc.* **1973,** *95* (24), 8200-8201.

4. (a) Sheffy, F. K.; Godschalx, J. P.; Stille, J. K., *J. Am. Chem. Soc.* **1984,** *106* (17), 4833-4840; (b) Kurosawa, H.; Ogoshi, S.; Kawasaki, Y.; Murai, S.; Miyoshi, M.; Ikeda, I., *J. Am. Chem. Soc.* **1990,** *112* (7), 2813-2814; (c) Trost, B. M.; Verhoeven, T. R., *J. Am. Chem. Soc.* **1980,** *102* (14), 4730-4743; (d) Trost, B. M., *Org. Process Res. Dev.* **2012,** *16* (2), 185-194; (e) Wong, P. K.; Lau, K. S. Y.; Stille, J. K., *J. Am. Chem. Soc.* **1974,** *96* (18), 5956-5957.

5. (a) Trost, B. M.; Weber, L., *J. Am. Chem. Soc.* **1975,** *97* (6), 1611-1612; (b) Hayashi, T.; Konishi, M.; Kumada, M., *J. Chem. Soc., Chem. Commun.* **1984,** (2), 107-108; (c) Trost, B. M.; Verhoeven, T. R., *J. Am. Chem. Soc.* **1976,** *98* (2), 630-632.

6. (a) Bosnich, Pure Appl. Chem. **1982**; *54*, 189; (b) Auburn, P. R.; Mackenzie, P. B.; Bosnich, B., *J. Am. Chem. Soc.* **1985,** *107* (7), 2033-2046.

7. Mackenzie, P. B.; Whelan, J.; Bosnich, B., *J. Am. Chem. Soc.* **1985,** *107* (7), 2046-2054.

8. (a) Sprinz, J.; Kiefer, M.; Helmchen, G.; Reggelin, M.; Huttner, G.; Walter, O.; Zsolnai, L., *Tetrahedron Lett.* **1994,** *35* (10), 1523-1526; (b) Pregosin, P. S.; Salzmann, R.; Togni, A., *Organometallics* **1995,** *14* (2), 842-847.

9. Cesarotti, E.; Grassi, M.; Prati, L.; Demartin, F., *J. Chem. Soc., Dalton Trans.* **1991,** (8), 2073-2082.

10. Jones, M. D.; Almeida Paz, F. A.; Davies, J. E.; Johnson, B. F. G.; Klinowski, J., *Acta Crystallographica Section E* **2003,** *59* (7), m538-m540.

11. (a) Crociani, B.; di Bianca, F.; Giovenco, A.; Boschi, T., *Inorg. Chim. Acta.* **1987,** *127* (2), 169-182; (b) Sjoegren, M. P. T.; Hansson, S.; Aakermark, B.; Vitagliano, A., *Organometallics* **1994,** *13* (5), 1963-1971; (c) Burckhardt, U.; Baumann, M.; Togni, A., *Tetrahedron: Asymmetry* **1997,** *8* (1), 155-159.

12. Faller, J. W.; Thomsen, M. E.; Mattina, M. J., *J. Am. Chem. Soc.* **1971,** *93* (11), 2642-2653.

13. Kazmaier, U.; Zumpe, F. L., *Angew. Chem. Int. Ed.* **2000,** *39* (4), 802-804.

14. Gogoll, A.; Oernebro, J.; Grennberg, H.; Baeckvall, J.-E., *J. Am. Chem. Soc.* **1994,** *116* (8), 3631-3632.

15. Hansson, S.; Norrby, P. O.; Soegren, M. P. T.; Aakermark, B.; Cucciolito, M. E.; Giordano, F.; Vitagliano, A., *Organometallics* **1993,** *12* (12), 4940-4948.

16. Takahashi, T.; Jinbo, Y.; Kitamura, K.; Tsuji, J., *Tetrahedron Lett.* **1984,** *25* (51), 5921-5924.

17. (a) Granberg, K. L.; Baeckvall, J. E., *J. Am. Chem. Soc.* **1992,** *114* (17), 6858-6863; (b) Granberg, K.; Backvall, J.-E., *J. Am. Chem. Soc.* **1994,** *116* (23), 10853-10853.

18. (a) Fiaud, J. C.; Legros, J. Y., *The Journal of Organic Chemistry* **1990,** *55* (16), 4840-4846; (b) Legros, J.-Y.; Fiaud, J.-C., *Tetrahedron* **1994,** *50* (2), 465-474.

19. Matt, P. V.; Lloyd-Jones, G. C.; Minidis, A. B. E.; Pfaltz, A.; Macko, L.; Neuburger, M.; Zehnder, M.; Rüegger, H.; Pregosin, P. S., *Helv. Chim. Acta.* **1995,** *78* (2), 265-284.

20. (a) Trost, B. M.; Van Vranken, D. L., *Angewandte Chemie International Edition in English* **1992,** *31* (2), 228-230; (b) Trost, B. M., *Isr. J. Chem.* **1997,** *37* (1), 109-118.

21. Trost, B. M.; Patterson, D. E., *The Journal of Organic Chemistry* **1998,** *63* (4), 1339-1341.

22. Trost, B. M.; Murphy, D. J., *Organometallics* **1985,** *4* (6), 1143-1145.

23. Trost, B. M.; Van Vranken, D. L., *Chem. Rev.* **1996,** *96* (1), 395-422.

24. Ramdeehul, S.; Dierkes, P.; Aguado, R.; Kamer, P. C. J.; van Leeuwen, P. W. N. M.; Osborn, J. A., *Angew. Chem. Int. Ed.* **1998,** *37* (22), 3118-3121.

25. (a) Trost, B. M.; Krische, M. J.; Radinov, R.; Zanoni, G., *J. Am. Chem. Soc.* **1996,** *118* (26), 6297-6298; (b) Trost, B. M.; Van Vranken, D. L.; Bingel, C., *J. Am. Chem. Soc.* **1992,** *114* (24), 9327-9343.

26. Trost, B. M.; Frederiksen, M. U., *Angew. Chem. Int. Ed.* **2005,** *44* (2), 308-310.

27. Baldwin, I. C.; Williams, J. M. J.; Beckett, R. P., *Tetrahedron: Asymmetry* **1995,** *6* (3), 679-682.

28. Trost, B. M.; Thaisrivongs, D. A., *J. Am. Chem. Soc.* **2008,** *130* (43), 14092-14093.

29. Trost, B. M.; Schroeder, G. M., *J. Am. Chem. Soc.* **1999,** *121* (28), 6759-6760.

30. Trost, B. M.; Xu, J., *J. Am. Chem. Soc.* **2005,** *127* (9), 2846-2847.

31. Behenna, D. C.; Stoltz, B. M., *J. Am. Chem. Soc.* **2004,** *126* (46), 15044-15045.

32. Lloyd-Jones, G. C.; Stephen, S. C., *Chemistry – A European Journal* **1998,** *4* (12), 2539-2549.

33. Evans, L., *PhD Thesis* **2010**.

34. Trost, B. M.; Machacek, M. R.; Aponick, A., *Acc. Chem. Res.* **2006,** *39* (10), 747-760.

35. Fairlamb, I. J. S.; Lloyd-Jones, G. C., *Chem. Commun.* **2000,** (24), 2447-2448.

36. Butts, C. P.; Filali, E.; Lloyd-Jones, G. C.; Norrby, P.-O.; Sale, D. A.; Schramm, Y., *J. Am. Chem. Soc.* **2009,** *131* (29), 9945-9957.

37. (a) Eastoe, J.; Fairlamb, I. J. S.; Fernandez-Hernandez, J. M.; Filali, E.; Jeffery, J. C.; Lloyd-Jones, G. C.; Martorell, A.; Meadowcroft, A.; Norrby, P.-O.; Riis-Johannessen, T.; Sale, D. A.; Tomlin, P. M., *Faraday Discuss.* **2010,** *145* (0), 27-47; (b) Racys, D. T.; Eastoe, J.; Norrby, P.-O.; Grillo, I.; Rogers, S. E.; Lloyd-Jones, G. C., *Chemical Science* **2015**.

38. (a) Amatore, C.; Jutand, A.; Mensah, L.; Meyer, G.; Fiaud, J.-C.; Legros, J.-Y., *Eur. J. Org. Chem.* **2006,** *2006* (5), 1185-1192; (b) Amatore, C.; Gamez, S.; Jutand, A.; Meyer, G.; Moreno-Mañas, M.; Morral, L.; Pleixats, R., *Chemistry – A European Journal* **2000,** *6* (18), 3372-3376.

39. Ogoshi, S.; Kurosawa, H., *Organometallics* **1993,** *12* (7), 2869-2871.

40. Markert, C.; Neuburger, M.; Kulicke, K.; Meuwly, M.; Pfaltz, A., *Angew. Chem. Int. Ed.* **2007,** *46* (31), 5892-5895.

41. (a) Murahashi, T.; Kurosawa, H., *Coord. Chem. Rev.* **2002,** *231* (1–2), 207-228; (b) Kurosawa, H., *J. Organomet. Chem.* **2004,** *689* (24), 4511-4520.

42. (a) Becker, Y.; Stille, J. K., *J. Am. Chem. Soc.* **1978,** *100* (3), 838-844; (b) Lau, K. S. Y.; Wong, P. K.; Stille, J. K., *J. Am. Chem. Soc.* **1976,** *98* (19), 5832-5840.

43. Chock, P. B.; Halpern, J., *J. Am. Chem. Soc.* **1969,** *91* (3), 582-588.

44. Kramer, A. V.; Osborn, J. A., *J. Am. Chem. Soc.* **1974,** *96* (25), 7832-7833.

45. Hughes, E. D.; Juliusburger, F.; Masterman, S.; Topley, B.; Weiss, J., *J. Chem. Soc.* **1935,** 1525-1529.

46. Coplen Tyler, B.; Krouse, H. R.; Böhlke John, K., *Pure Appl. Chem.*, **1992**; *64*, 907.

47. Karlsson, R., *J. Chem. Eng. Data* **1973,** *18* (3), 290-292.

48. Dang, Y.; Qu, S.; Nelson, J. W.; Pham, H. D.; Wang, Z.-X.; Wang, X., *J. Am. Chem. Soc.* **2015,** *137* (5), 2006-2014.

49. Wolters, L. P.; Bickelhaupt, F. M., *ChemistryOpen* **2013,** *2* (3), 106-114.

50. Maki, T.; Iwasaki, F.; Matsumura, Y., *Tetrahedron Lett.* **1998,** *39* (31), 5601-5604.

51. Pangborn, A. B.; Giardello, M. A.; Grubbs, R. H.; Rosen, R. K.; Timmers, F. J., *Organometallics* **1996,** *15* (5), 1518-1520.

52. Herrmann, W. A.; Thiel, W. R.; Broißmer, C.; Öfele, K.; Priermeier, T.; Scherer, W., *J. Organomet. Chem.* **1993,** *461* (1–2), 51-60.

53. Faller, J. W.; Tully, M. T.; Laffey, K. J., *J. Organomet. Chem.* **1972,** *37* (1), 193-199.

54. Faller, J. W.; Mattina, M. J., *Inorg. Chem.* **1972,** *11* (6), 1296-1307.

55. (a) Keeler, J., Understanding NMR Spectroscopy. Second ed.; Wiley: 2010; (b) Claridge, T. D. W., *High-Resolution NMR Techniques in Organic Chemistry*. Elsevier Science: 2008.

56. La Mar, G. N., *J. Am. Chem. Soc.* **1971,** *93* (4), 1040-1041.

57. Freeman, R.; Hill, H. D. W.; Kaptein, R., *Journal of Magnetic Resonance (1969)* **1972,** *7* (3), 327-329.

58. Cookson, D. J.; Smith, B. E., *Journal of Magnetic Resonance (1969)* **1984,** *57* (3), 355-368.

59. Caporali, M.; Gonsalvi, L.; Kagirov, R.; Mirabello, V.; Peruzzini, M.; Sinyashin, O.; Stoppioni, P.; Yakhvarov, D., *J. Organomet. Chem.* **2012,** *714*, 67-73.

60. Amatore, C.; Jutand, A.; M′ Barki, Mohamed A.; Meyer, G.; Mottier, L., *Eur. J. Inorg. Chem.* **2001,** *2001* (3), 873-880.

61. Lee, D.; Williamson, C. L.; Chan, L.; Taylor, M. S., *J. Am. Chem. Soc.* **2012,** *134* (19), 8260-8267.

62. Kommreddy, A.; Bowsher, M. S.; Gunna, M. R.; Botha, K.; Vinod, T. K., *Tetrahedron Lett.* **2008,** *49* (28), 4378-4382.

63. Evans, L. A.; Fey, N.; Harvey, J. N.; Hose, D.; Lloyd-Jones, G. C.; Murray, P.; Orpen, A. G.; Osborne, R.; Owen-Smith, G. J. J.; Purdie, M., *J. Am. Chem. Soc.* **2008,** *130* (44), 14471-14473.

64. Watson, I. D. G.; Yudin, A. K., *J. Am. Chem. Soc.* **2005,** *127* (49), 17516-17529.